



UNIVERSITÀ  
DI TRENTO

Department of  
Cellular, Computational and Integrative Biology - CIBIO

**MASTER'S DEGREE IN QUANTITATIVE AND  
COMPUTATIONAL BIOLOGY**

**Exploring the integration of genomic data  
into stochastic modeling of Cell Cycle**

Supervisor:

Alessandro Romanel

Graduant:

Andrea Tonina

Signature:

A handwritten signature in black ink, appearing to read "A. Romanel".

Date of Discussion: 20 March 2025

*A mamma Annalisa e papa' Paolo, che mi hanno sempre sostenuto  
e hanno creduto in me prima che ci credessi io.  
Ai miei amici, la mia seconda famiglia, sempre pronti  
ad aiutarmi nei momenti di bisogno.  
A Gloria, fidanzata e compagna di questo percorso,  
senza di te non sarebbe stato lo stesso.  
Infine ai nonni Augusto, Bruno, Pia e Maria, che piu' di  
chiunque altro avreste voluto esserci, spero  
siate fieri del percorso che ho intrapreso.  
A voi tutti dedico questo giorno.*

*"All we have to decide is what to do with the time that is given us"  
- Gandalf in The Fellowship of the Ring, The Shadow of the Past*

# Contents

<b>Abstract</b>	<b>2</b>
<b>1 Introduction</b>	<b>3</b>
1.1 Cell cycle	3
1.2 Cell cycle regulations	4
1.3 Cell cycle checkpoints and transition	5
1.4 Genetic Variability	6
1.5 Cancer heterogeneity	7
1.6 Breast cancer heterogeneity	9
1.7 eQTLs	10
1.8 Models of Cell Cycle	12
<b>2 Aim</b>	<b>14</b>
<b>3 Materials and Methods</b>	<b>15</b>
3.1 BlenX	15
3.2 Sensitivity Analysis	16
3.3 Dataset description	16
3.4 RNA-seq data normalization	17
3.5 SCNA and patient-specific data analyses	17
3.6 eQTLs data analysis	17
3.7 Survival analysis	19
<b>4 Results and discussion</b>	<b>20</b>
4.1 General model of cell cycle transition	20
4.1.1 Explanation of the general cell cycle transition model	20
4.1.2 Simulations of GO and STOP transcriptional regulations	23
4.2 Sensitivity analysis of the general model	24
4.3 Human specific cell-cycle model G2/M	36
4.4 Integration of eQTLs data in human specific model of various tissues	40
4.5 Integration in human specific model of breast cancer copy number data	43
4.6 Patient-specific data into human-specific model and survival analysis	46
<b>5 Conclusion</b>	<b>50</b>
5.1 Future Perspectives	50
<b>Bibliography</b>	<b>52</b>
<b>Appendix</b>	<b>67</b>

# Abstract

This study presents the characterization of a generic stochastic model of cell cycle transition and investigates the impact of germline expression quantitative trait loci (eQTLs) and somatic copy number alterations (SCNAs) on cell cycle dynamics. The research aims to elucidate how genetic variation influences cell cycle transitions in both healthy and cancerous contexts and to explore the utility of mathematical modeling for gaining insights into cancer biology. A key objective is to develop a model that integrates the role of eQTLs in cell cycle regulation across various healthy tissues and accounts for the effects of SCNAs in breast cancer. Patient-specific breast cancer models incorporating copy number data were generated to assess their potential in understanding tumor biology and predicting clinical outcomes.

The study employed a computational approach using BlenX and the Beta Workbench to implement and analyze a stochastic model of cell cycle transitions. The influence of model parameters and species was first evaluated through sensitivity analysis. The general cell cycle transition model, based on prior literature, was then adapted to the human G2/M transition by assuming periodic transcription of either the inhibitor or the activator.

The impact of eQTLs on switch time and switch percentage was analyzed across different tissues, with a particular focus on breast tissue and genes involved in the G2/M transition. Furthermore, the study explored the effects of SCNAs on cell cycle transition dynamics in breast cancer patient-specific models. Preliminary survival analysis suggested a correlation between delayed cell cycle transitions and improved overall survival probability.

In conclusion, this research demonstrates the potential of utilizing stochastic mathematical models to represent and investigate cell cycle transitions and the influence of both germline and somatic genetic variations. The findings highlight the importance of integrating multi-omics data with mathematical modeling to gain insights into cancer aggressiveness and patient prognosis.

# 1 Introduction

## 1.1 Cell cycle

The term cell cycle refers to the various events that take place in a cell, enabling an accurate duplication of its contents and generating two genetically identical daughter cells by segregation<sup>1</sup>. It is a highly regulated and orchestrated process driving growth, development, tissue repair, and reproduction in all living organisms<sup>2</sup>.

The cell cycle is composed of two basic parts: Mitosis and Interphase. During Interphase, a cell typically doubles in size with a consistent rate between cell divisions. This phase can be subdivided into three stages: phase G1, where the cell prepares for DNA synthesis, phase S, where DNA replication takes place and finally, phase G2, when the cell prepares for the mitotic event<sup>1,3</sup>.

The mitotic phase (M) encompasses cell division and usually the subsequent Cytokinesis (cytoplasmic division)<sup>4</sup>. Subsequently, during the G1 phase, the daughter cells undertake their original physiological role and undergo a period of growth, reaching the mature state<sup>3</sup>.

Cells that permanently stop dividing, like red blood cells and neurons, enter a resting state called G0 (G "zero") after differentiation. Some cells, such as liver cells that typically reside in G0, can re-enter the G1 phase to facilitate tissue repair<sup>5</sup>.

After G1 comes the S phase (synthesis), where the genome is duplicated (from the normal 2n to 4n) and most of the DNA repair activity occurs in preparation for the mitotic event<sup>4,6</sup>.

Finally, after the S phase, the cell enters the G2 step (gap 2), where the cell continues to grow and produces proteins necessary for mitosis<sup>4</sup>.

Also, Mitosis can be divided into five steps: Prophase, Prometaphase, Metaphase, Anaphase and Telophase<sup>7</sup>. Cytokinesis, occurring concurrently with the latter stages of mitosis, divides the cytoplasm, completing the cell division<sup>8</sup>.

During mitotic prophase, chromatin condenses by making individual chromosomes visible<sup>7</sup>. This stage is also characterized by a shift in microtubule dynamics involving the disassembly of interphase microtubules (long and less dynamic) and the assembly of short, highly dynamic mitotic microtubules<sup>9</sup>. Centrosomes, replicated during the S-phase of the cell cycle and serving as microtubule-organizing centers in most animal cells, move apart during prophase<sup>10</sup>. As they separate, an aster structure forms around each centrosome, with microtubules extending outwards from the centrosome with their plus ends. This process initiates the assembly of the mitotic spindle, a dynamic macromolecular machine essential for chromosome segregation<sup>11</sup>.

The breakdown of the nuclear envelope signifies the start of prometaphase. During this phase, a bipolar spindle assembles as microtubule plus ends emanating from opposite asters overlap and form bundles, facilitated by the coordinated action of various microtubule-based motors and microtubule-associated proteins (MAPs)<sup>12</sup>. Within the nuclear region, dynamic microtubule plus ends undergo cycles of polymerization and depolymerization<sup>13</sup>. These microtubules may encounter kinetochores, specialized protein structures on chromosomes that mediate chromosome-microtubule attachment. While initial interactions between kinetochores and microtubules may be lateral<sup>14,15</sup>, they are typically converted into end-on attachments, believed to enhance microtubule stability<sup>16</sup>.

In most model organisms, kinetochore fibers are formed, which are multiple parallel microtubules bundling together and binding each kinetochore<sup>17</sup>.

Typically, chromosomes initially establish a monotelic attachment where only one sister kinetochore is bound to microtubules<sup>18</sup>. These monotelic chromosomes can either directly transition to amphitelic attachment, where both sister kinetochores are bound to microtubules originating from opposite spindle poles and then migrate towards the spindle equator<sup>19</sup>. Alternatively, they can first migrate towards the spindle equator through lateral kinetochore-microtubule interactions and subsequently establish amphitelic attachment<sup>20</sup>. Throughout prometaphase, chromosomes undergo a process called congression, where they gradually

achieve amphitelic attachment and align at the spindle equator<sup>21</sup>.

Metaphase begins when all chromosomes are aligned at the spindle equator, forming the metaphase plate<sup>22</sup>. Characteristically, in many cell types, chromosomes at this stage exhibit dynamic behavior, oscillating back and forth around the spindle equator<sup>19</sup>.

The beginning of anaphase is characterized by the abrupt and synchronous separation of sister chromatids, a process driven by the degradation of cohesin complexes<sup>23</sup>, indeed, the two sister chromatids separate and move to the spindle poles as their respective k-fibers shorten. Anaphase comprises two distinct phases: anaphase A and anaphase B<sup>24</sup>. During anaphase A, chromosomes are pulled towards the poles of the cell as kinetochore fiber microtubules shorten, whereas, in anaphase B, the spindle poles move further apart due to the elongation and sliding of interpolar microtubules past each other<sup>24,25</sup>. Importantly, in most organisms, anaphase A and B occur concurrently, with some degree of temporal overlap<sup>26</sup>.

In telophase, chromosomes arrive at the spindle poles and begin to decondense<sup>7</sup>. At the same time, the nuclear envelope reforms around these decondensed chromosomes, giving rise to two distinct daughter interphase nuclei<sup>19</sup>.

Cytokinesis, which is the final stage of cell division, involves the physical partitioning of the cytoplasm<sup>8</sup>. This process typically commences during late anaphase or telophase of mitosis, characterized by the formation of an actomyosin contractile ring at the spindle equator<sup>27</sup>. This ring constricts the cell membrane, ultimately dividing the cytoplasm into two distinct daughter cells, each containing a complete set of chromosomes<sup>28</sup>.

## 1.2 Cell cycle regulations

A complex regulatory network controls the cell cycle to ensure the proper order and transitioning of the various phases such as DNA replication, mitosis and cell division<sup>29</sup>. This network determines when the cycle can proceed to the next phase based on environmental signals and by monitoring DNA integrity<sup>30</sup>. This intricate orchestration relies on a set of key regulatory elements, most notably the cyclins and Cyclin-dependent kinases (CDKs)<sup>31</sup>. Cyclins are a family of proteins whose cellular concentrations oscillate throughout all the phases of the cell cycle, exhibiting a periodic pattern of synthesis-degradation<sup>32</sup>. This cyclical expression is crucial for the cyclins' regulatory role, which works by binding to and activating CDKs, a family of serine/threonine protein kinases<sup>33</sup>.

CDKs are present at relatively constant levels, but their activity strictly depends on cyclin binding<sup>34</sup>. The complex cyclin-CDK is the functional unit that drives cell cycle progression by phosphorylating a variety of target proteins that can be either activated or inhibited, modulating their activity and influencing downstream events<sup>35</sup>. Different cyclins associate with different CDKs to form distinct complexes that work at different cell cycle phases, this ensures the execution of phase-specific events at the opportune time<sup>36</sup>. Some important examples are present during the G1 cell cycle phase, where cyclins (like Cyclin D in mammalian cells) activate CDKs that promote entry into the S phase<sup>37</sup>, while mitotic cyclins (like Cyclin B) activate CDKs necessary for mitosis<sup>38</sup>. This intricate interplay between cyclins, CDKs and their complex is part of the system behind the cell cycle control, driving the transitions between phases and ensuring the proper timing of cellular events<sup>32</sup>.

Beyond these regulations, the cell cycle is subject to other regulatory mechanisms that control its progression and ensure fidelity. One of them is the ubiquitin-proteasome system (UPS), which is the primary machinery for protein degradation in eukaryotic cells and plays a crucial role in cell cycle regulation by selectively targeting proteins<sup>39</sup>. UPS is essential for the timely progression through different cell cycle phases, and without it, it would be impossible to exit from one phase and enter the next one<sup>40</sup>.

An important component of the UPS system is the anaphase-promoting complex/cyclosome (APC/C), a ubiquitin ligase that orchestrates the degradation of several cell cycle regulators, including mitotic cyclins, allowing the cell to exit mitosis<sup>41,42</sup>. Similarly, other ubiquitin ligases target specific proteins for degradation at different cell cycle phases, ensuring the proper timing of events<sup>39</sup>.

Another important layer of regulation involves transcriptional control, so the regulation at the transcriptional level of genes encoding cell cycle regulators, including cyclins, CDKs and checkpoint proteins<sup>43</sup>. With this

regulation, the cell ensures that the necessary proteins are available at the correct concentrations and at the appropriate time. The expression of genes can be regulated by multiple players like transcription factors, which bind to specific DNA sequences and regulate gene expression, or also growth factors, which are related to extracellular signals and link cell cycle progression to the cellular environment<sup>44,45</sup>.

Beyond the core mechanisms of cell cycle regulation already discussed, protein-protein interactions and subcellular localization play crucial roles in modulating phase transitions<sup>46,47</sup>. Subcellular localization dynamically regulates the access and activity of key proteins<sup>48</sup>, such as through nuclear-cytoplasmic shuttling, which can determine a protein's interaction with nuclear targets or its susceptibility to degradation<sup>49</sup>. Furthermore, protein-protein interactions beyond cyclin-CDK binding are essential because they influence the activity and stability of many cell cycle regulators, indeed inhibitor proteins can bind to cyclin-CDK complexes, providing another layer of control over cell cycle progression<sup>50</sup>.

## 1.3 Cell cycle checkpoints and transition

Cell cycle progression is not a continuous flow but rather a regulated series of transitions governed by a complex network of checkpoints and molecular mechanisms<sup>51</sup>. These transitions are regulated processes driven by a complex interplay of molecular events, acting as surveillance mechanisms that ensure the fidelity and accuracy of cell division, and represent cell cycle checkpoints<sup>52</sup>.

Checkpoints monitor critical events and trigger appropriate cellular responses based on the situations, ranging from cell cycle arrest and DNA repair to apoptosis<sup>53,54</sup>. There are three major checkpoints: the G1 checkpoint, the G2 checkpoint and the metaphase checkpoint<sup>3</sup>.

The G1 checkpoint, which occurs in the late G1 phase, determines whether the cell is ready to undergo DNA replication and proceed through the rest of the cell cycle<sup>55</sup>. This checkpoint aims to assess the integrity of the DNA by checking for damages caused by radiation, chemicals or other environmental factors. It also evaluates the availability of essential growth factors and nutrients, ensuring that the cell has the necessary resources for the division process, and verifies if the cell has reached an appropriate size and if the DNA is ready for replication<sup>56</sup>. A main player in the G1 checkpoint is the p53 protein, which is activated in case of DNA damage and, if activated, induces the expression of p21, the inhibitor protein that influences the activity of the complex cyclin-CDK and halts the cell cycle, providing time for DNA repair mechanisms to operate<sup>32,57</sup>. In cases where the DNA damage is too extensive to be repaired, p53 can trigger apoptosis and eliminate the potentially harmful cells<sup>58</sup>.

The G2 checkpoint, which is positioned between G2 and M phases, whose main function is to ensure that DNA replication is completed and no DNA damage is incurred during replication or at any other point in the cell cycle, is repaired before the cell proceeds to the complex and potentially error-prone process of mitosis<sup>59</sup>. This checkpoint acts as a final gatekeeper, preventing the cell from entering mitosis with damaged or incompletely replicated DNA, which could lead to chromosomal abnormalities and genomic instability<sup>60</sup>. Key players during G2 checkpoints include ATM and ATR kinases, which are activated when DNA damage occurs. This causes the activation of downstream signaling pathways, which triggers Chk1 and Chk2 kinases<sup>61,62</sup>. These kinases inhibit CDK1, which plays a key role in cell cycle progression<sup>63</sup>.

Finally, the metaphase checkpoint, also known as the spindle checkpoint, occurs during mitosis and is crucial for ensuring the proper segregation of chromosomes<sup>64</sup>. It checks that each chromosome is correctly attached to a spindle fiber and that there is tension on the kinetochores, the protein structures on chromosomes where spindle fibers attach<sup>64,65</sup>. If one or more kinetochores are unattached, they activate the spindle assembly checkpoint (SAC) pathway, which generates a "wait-anaphase" signal, preventing the cell from prematurely separating its chromosomes<sup>66,67</sup>. Only when all chromosomes are correctly attached and under tension is the SAC signal silenced, allowing the cell to proceed with anaphase and complete mitosis<sup>67</sup>.

These checkpoints are fundamental for normal cellular function and development. They maintain genomic stability and prevent the formation of daughter cells with chromosomal abnormalities by preventing the propagation of errors<sup>68</sup>. The possible dysfunction of these checkpoints can lead to severe consequences, including uncontrolled cell proliferation and the development of cancer<sup>69</sup>.

## 1.4 Genetic Variability

Genetic variability in humans can be described as the inherent difference in DNA sequences within our genomes among individuals<sup>70</sup>. This variability underlies the vast array of traits that make each of us unique, influences our susceptibility to a wide range of diseases, and provides insight into our evolutionary history and population dynamics, which is crucial for fields ranging from medicine and forensics to anthropology and evolutionary biology<sup>71-73</sup>.

Mutations are the ultimate source of new genetic variants in DNA, which are permanent alterations in the DNA sequence<sup>74</sup>. These changes can occur spontaneously due to inherent errors in DNA replication or be induced by environmental factors, known as mutagens, such as radiation, chemicals and even some viruses<sup>75</sup>. A crucial distinction among mutations is whether they are heritable, meaning capable of passing down to offspring. The characteristic of heritability depends on the cell type in which the mutation occurs. Indeed, germline mutations are heritable because they arise in germ cells involved in the fertilization process<sup>76</sup>. An offspring inheriting a germline mutation will carry the variant in all their cells, including their germ cells, ensuring the transmission of the mutation to the next generation<sup>77</sup>.

Germline mutations are the source of genetic diversity both within and across species. Some can cause genetic diseases, whereas others may be neutral or even beneficial in certain environments<sup>78</sup>. Due to their heritability, germline mutations tend to persist in a population for many generations<sup>78</sup>.

Conversely, somatic mutations can arise during an individual's lifetime in any cell of the body except germ cells because these variants are not heritable<sup>79</sup>.

A somatic mutation occurs in a single cell and is then propagated to its descendants through cell division, creating cell clones carrying the mutation<sup>80</sup>. While some somatic mutations have negligible effects, others can contribute to a variety of conditions<sup>81</sup>. Cancer is a prime example developed from the accumulation of multiple somatic mutations within a single-cell lineage, which leads to disruptions of cellular processes, resulting in uncontrolled cell growth and tumor formation<sup>82</sup>. Because somatic mutations affect only the individual in which they occur and are not transmitted to offspring, they do not play a direct role in the long-term evolution of the species<sup>79</sup>.

The spectrum of mutation is quite broad and diverse. Indeed, it can range from changes in a single DNA base to a large-scale chromosomal rearrangement<sup>83</sup>. Among the most common types are point mutations, which affect a single base pair<sup>84</sup>. Examples of this mutation type are single nucleotide polymorphisms (SNPs), defined as variants at a single locus with a minor allelic frequency of at least 1% in a given population<sup>85</sup>, and somatic single nucleotide variants (SNVs), which are variants that are not as common as SNPs in any given population. Though seemingly minor, these variants can have a significant impact on protein structure or gene regulation<sup>86,87</sup>.

Another important source of variation is small insertions or deletions (INDELS), where a few to a hundred bases are added or removed from the genome, this type of variant can potentially be associated with human disease<sup>88</sup>.

Copy number variants (CNVs) represent larger-scale changes that involve duplications or deletions of DNA stretches spanning hundreds of thousands to millions of bases and even entire genes<sup>89,90</sup>. This type of mutation can alter gene dosage, so a change in the number of copies of a gene present in the genome can influence the amount of protein produced and contribute to phenotypic changes and disease susceptibility<sup>91</sup>. Structural variants (SVs) include a broad spectrum of large-scale genomic rearrangements, like inversion, translocation and large deletions or insertions<sup>92</sup>. These variants can alter gene regulation and have consequences for chromosome stability and cell function<sup>93</sup>.

Beyond what is already explained, another characteristic of mutations is based on whether the variant occurs within coding regions or non-coding regions, that is, DNA regions that do or do not code for proteins<sup>94</sup>. Coding region mutations occur within a protein-coding sequence of a gene, affecting a portion of DNA that specifies the amino acid sequence of a protein and leading to a range of effects<sup>75</sup>. Missense mutations, which are variations where a single base change results in a different amino acid, can have various effects, from no

change in the protein's function to a complete loss of function. This depends on the specific amino acid change and its location within the protein<sup>95</sup>.

Nonsense mutations, which are also point mutations that, through a single base change, introduce a stop codon, resulting in a protein that is often non-functional<sup>96</sup>.

Frameshift mutations, caused by insertions or deletions of nucleotides in numbers that are not a multiple of three, disrupt the reading frame of a gene. This leads to the addition of incorrect amino acids and usually results in a non-functional protein<sup>75</sup>. As explained above, in-frame insertions or deletions may add or remove amino acids from the protein, potentially affecting its function<sup>97</sup>. Overall, coding region mutations can alter protein structure and function, leading to a variety of phenotypic effects, such as genetic diseases, influencing disease susceptibility or contributing to normal phenotypic variations<sup>98</sup>.

On the other hand, non-coding region mutations occur in DNA regions that do not code for proteins<sup>99</sup>. These regions comprise a vast amount of DNA, such as introns, promoter regions, enhancers and silencers, untranslated regions at the ends of mRNA (UTRs) and intergenic regions<sup>100,101</sup>. Many mutations in non-coding regions have no apparent effect on the phenotype, however, mutation in regulatory regions can alter gene expression levels, thus affecting protein production<sup>99,102</sup>. For example, a mutation in a promoter region might increase the expression of an oncogene, contributing to cancer<sup>103</sup>. Traditionally, these types of mutations were considered less important than coding region mutations. However, they are now recognized as having significant impacts on gene regulation and phenotype, contributing to disease, influencing complex traits and playing a role in evolution<sup>104</sup>.

Beyond these changes to the DNA sequence itself, it is important to consider the role of recombination during meiosis<sup>105</sup>. This process, where homologous chromosomes exchange genetic material, creates new combinations of alleles on chromosomes, further enhancing genetic diversity<sup>106</sup>. An independent assortment of chromosomes during meiosis is also a contribution, as each gamete receives a unique mix of maternal and paternal chromosomes<sup>106</sup>. Finally, gene flow, the movement of individuals and their genes between populations introduces new genetic variants into a population or alters the frequencies of existing variants, further shaping the genetic landscape of human populations<sup>107</sup>.

## 1.5 Cancer heterogeneity

Cancer is a disease driven by the accumulation of genetic alterations that cause disruption in cellular processes and lead to uncontrolled proliferation<sup>108</sup>. These genetic variabilities arise from a complex interplay of inherited and acquired changes that contribute to cancer development<sup>109</sup>.

Germline mutations often occur in genes involved in DNA repair processes, cell cycle control or other critical functions that can lead individuals to a predisposition for some type of cancer<sup>110,111</sup>. However, accumulations of somatic mutations, genetic changes that occur during an individual's lifetime in specific cells of the body, in driver genes can disrupt key cellular pathways and contribute to cancer<sup>112,113</sup>. Indeed, these mutations can affect both proto-oncogenes and tumor suppressor genes<sup>113</sup>. The former are genes that present the ability to transform normal cells into cancerous cells, whereas the latter are genes that regulate cellular functions like apoptosis and proliferation<sup>113</sup>. The interplay of activated oncogenes and inactivated tumor suppressor genes can lead to carcinogenesis<sup>113</sup>.

As a consequence of the evolutionary forces of variation and selection, genetic and phenotypic variations exist not only across cancers (inter-tumor heterogeneity) but also within individual tumors (intra-tumor heterogeneity)<sup>114</sup>. Tumors that originate from different tissues and cell types vary in terms of their genomic landscape, prognosis and response to treatments<sup>115</sup>. Mutational frequencies of oncogenes and tumor suppressors vary between tumors of different tissues, reflecting the importance of distinct tissue-dependent signaling pathways<sup>116</sup>.

Within tumors, genetically distinct subclonal populations of cells arise through intercellular genetic variation, followed by selective outgrowth of clones with a phenotypic advantage within a given tumor environmental context<sup>117,118</sup>. If a new clone takes over the entire population by replacing ancestral ones, this will result in a homogeneous cell population<sup>119</sup>. Otherwise, if during linear evolution a new clone fails to outcompete its predecessors, a degree of heterogeneity will be observed<sup>119</sup>. If distinct subclones evolve in parallel, this will result in extensive subclonal diversity<sup>119</sup>.

In addition to the heterogeneity of cancer genes, there is considerable diversity in the nature, number, and distribution of mutations within and across different cancer histologies<sup>120</sup>. Studies have revealed that the degree of intra-tumor heterogeneity can be highly variable, with thousands of coding mutations found to be heterogeneous within primary, metastatic, or recurrent sites<sup>121</sup>. Genomic copy number heterogeneity can also be extensive within tumors. Large-scale chromosomal alterations may have a profound impact on the genome architecture, disrupting hundreds of genes that can contribute to tumor progression<sup>122–124</sup>.

Dysregulation of cell cycle is a fundamental characteristic of cancer cells, contributing significantly to uncontrolled cell proliferation and the accumulation of genomic instability<sup>125,126</sup>. The observed dysregulation arises from a complex interplay of alterations in numerous components, including cell cycle regulators, checkpoint proteins, and their associated signaling pathways. Cyclin-dependent kinases (CDKs) and cyclins, key positive regulators of the cell cycle, are frequently overexpressed in cancer cells, leading to unrestrained cell division<sup>127</sup>. Cyclin-dependent kinase complexes, comprising a cyclin and CDK, drive cell cycle progression. While CDKs are constitutively expressed, cyclin levels are tightly regulated by transcriptional mechanisms and ubiquitin-mediated degradation<sup>128</sup>. CDK activation necessitates cyclin binding and site-specific phosphorylation. Specific complexes, such as Cyclin D-CDK4/6, regulate the G1 to S phase transition through retinoblastoma protein (pRB) phosphorylation, with approximately 50% of invasive breast cancers exhibiting elevated cyclin D expression<sup>129</sup>.

Conversely, CDK inhibitors (CDKIs), such as INK4 and CIP/KIP family members, which normally inhibit CDK activity, often exhibit loss of function in cancer cells<sup>130,131</sup>. For instance, p27 is aberrantly expressed in breast cancers, with low concentrations correlating with aggressive tumor phenotypes<sup>128</sup>. Decreased p57 expression is observed in bladder cancers, and deletion or inactivation of p15 and p16 via methylation is associated with various malignancies, including melanomas, lymphomas, mesotheliomas, and pancreatic cancers<sup>128</sup>. Retinoblastoma protein (pRB), a target of cyclin-CDK complexes in the G1-S transition and inhibitor of cell cycle progression<sup>132</sup>, is also subject to alterations<sup>133</sup>. In tumors with a functional pRB gene, dysregulation of upstream signaling pathways, such as increased cyclin D and cyclin E levels, is frequently observed<sup>128</sup>.

Checkpoint proteins, critical regulators of cell cycle transitions, are also commonly altered in cancer<sup>127</sup>. An important example is p53, which as a transcription factor orchestrates a broad range of cellular processes like cell cycle arrest<sup>134</sup> and notably mutations of p53 represent the most frequently observed genetic lesion in human tumors<sup>127</sup>. Mutations in important genes of DNA damage signaling pathways, like ATM, ATR, CHK1 and CHK2, arise in human cancer<sup>128,135,136</sup>. Various studies suggest that Cdc25 phosphatases, which activate CDKs by removing inhibitory phosphorylation, are overexpressed in many human tumors and are associated with poor clinical prognosis<sup>137</sup>. The mitotic spindle checkpoint, which monitors chromosome attachments, is also implicated in cancer pathogenesis. An important example is BUB1, whose functions are related to the organization of the spindle assembly checkpoint (SAC) during mitosis and monitoring the stability of spindle-microtubule-kinetochore attachment, and its mutation has been identified in human colon carcinoma cells and also taken into consideration as prognostic biomarker in neuroblastoma<sup>138,139</sup>. The frequent loss of checkpoint integrity propagates DNA lesions and permanent genomic alterations, contributing to genomic instability.

The cumulative effect of these alterations, including the overexpression of positive regulators (CDKs and cyclins) and the inactivation of negative ones (CDKIs), leads to unlimited replication potential in cancer cells<sup>140</sup>. This dysregulation, coupled with the frequent loss of checkpoint integrity, results in the propagation of DNA lesions and permanent genomic alterations, ultimately driving cancer development and progression<sup>141</sup>. It is possible to observe the various genes mutated that cause the dysregulation of the cell cycle across different types of cancers in Figure 1.

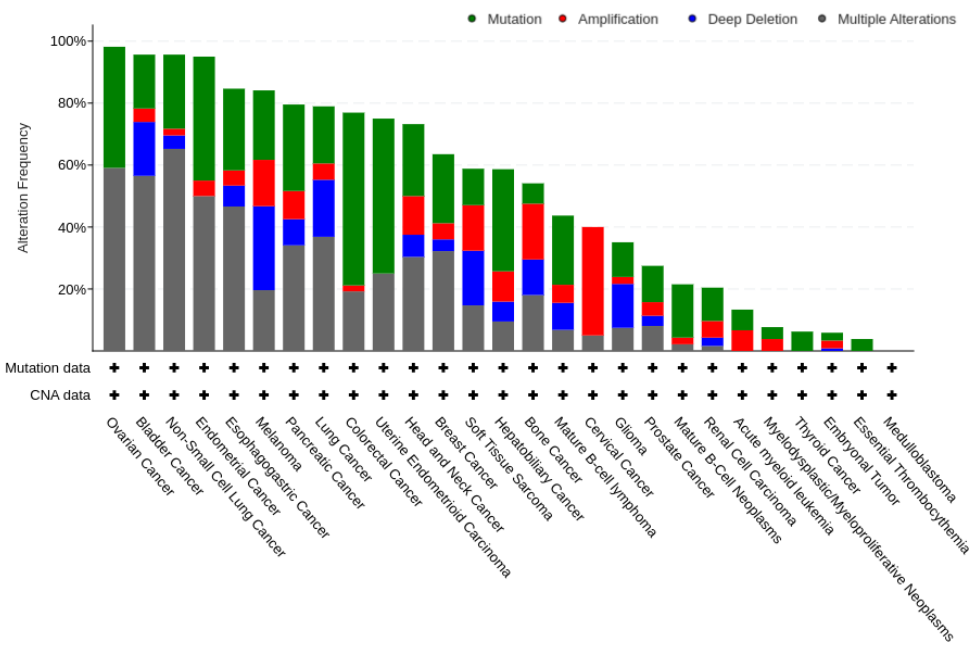


**Figure 1. Mutations summary over various cancer types of the cited mutated genes impacting cell cycle.** This plot has been retrieved from cBioPortal<sup>142</sup> using the Pan-cancer analysis of whole genomes (ICGC/TCGA, Nature 2020)<sup>143</sup> dataset.

## 1.6 Breast cancer heterogeneity

Breast cancer has emerged as the second most common type of cancer<sup>144</sup>. Accounting for nearly 25% of all cancer diagnoses, with an incidence that has been rising with an annual increase of 3.1% starting with 641.000 cases in 1980, to more than 1.6 million in 2010, this trend is likely to continue<sup>145</sup>.

Over the past decade, breast cancer treatment has evolved significantly, largely due to the recognition of its molecular heterogeneity. This shift in understanding began with the groundbreaking classification proposed by Perou and Sorlie in 2000, which has been refined and updated over the years, ultimately leading to the identification of five distinct molecular subtypes: Luminal A, Luminal B, Triple negative (basal-like), HER-2 type and normal-like<sup>146,147</sup>.

Unfortunately, the mechanism by which breast cancer begins is still unknown, nevertheless, much effort has been made to molecularly characterize this disease<sup>148</sup>. While hereditary factors account for only 5 to 10% of all breast cancer cases, carrying a BRCA1 or BRCA2 inherited mutation increases significantly the lifetime risk<sup>149</sup>. Recent estimation indicates that 55 to 65% of women with inherited BRCA1 mutation and approximately 45% of those with inherited BRCA2 mutation will develop breast cancer at the age of 70<sup>150</sup>, indeed germline mutations in BRCA1 and BRCA2 genes are the primary hereditary risk factors for breast and ovarian cancers<sup>151</sup>.

Some studies suggest also other genes with moderate penetrance that can be part of the hereditary genes that can lead to breast cancer, often related to the functionality of BRCA<sup>152</sup>. An example is the gene CHEK2, which encodes a cell cycle checkpoint kinase related to the DNA repair pathway<sup>153</sup>. When the pathogenic variant is present, it leads to a two-fold increase in the risk of developing breast cancer, even though this does not confer risk in BRCA mutation carriers<sup>154</sup>.

In early-stage breast cancer, genes reported as the most frequently mutated by somatic point mutations or copy number amplification are TP53 (41% of tumors), PIK3CA (30%), MYC (20%), PTEN (16%), CCND1 (16%), ERBB2 (13%), FGFR1 (13%) and GATA3 (10%)<sup>155</sup>. All genes that encode for cell-cycle modulators, which can be repressed or activated, are important for the proliferation and inhibition of the apoptosis process, inhibition of oncogene pathways or inhibitors of elements that are no longer repressed. The majority of breast cancers are caused by multiple, cumulated low penetrance mutations. Luminal A tumors present a high prevalence of PIK3CA mutated, whereas TP53 mutations are a hallmark of basal-like tumors<sup>156</sup>.

Most of the driver alterations present in primary breast cancer are also found in metastatic sites<sup>157</sup>. However, different metastatic sites may present private aberrations including new drivers, which are alterations appearing later in cancer progression that can be triggered by treatment measures, resulting in intra-tumor heterogeneity<sup>158,159</sup>. For instance, the mutation of ESR1 can appear in women with breast cancer after undergoing successful therapies of aromatase inhibitors in 23-40% of cases<sup>160</sup>.

Differences in ER, PR and HER2 expression between primary and metastatic breast tumors are likely a consequence of subclonal diversification<sup>161</sup>. These molecular targets are more commonly lost during metastasis than gained<sup>162</sup>; indeed, for HER2-positive primary tumors 13% generate HER2-negative metastases but only 5% of HER2-negative primary tumors generate positive metastases<sup>163</sup>.

Cell cycle dysregulation is a hallmark of breast cancer, contributing to uncontrolled proliferation and genomic instability<sup>164</sup>. This dysregulation arises from diverse molecular alterations, varying significantly across breast cancer subtypes<sup>164</sup>. Luminal A tumors, characterized by estrogen receptor (ER) expression, exhibit fewer TP53 and GATA3 mutations, which are responsible for cell cycle arrest and cell death<sup>165,166</sup>, but a higher frequency of PIK3CA mutations compared to Luminal B tumors, an important factor of the pathways PI3K/AKT/mTOR (PAM) which is important for the promotion of cell cycle progression<sup>167</sup>.

Also luminal-like breast cancer subtypes that present to be estrogen-receptor positive frequently exhibit cyclin D1 amplification<sup>168</sup>, with elevated ESR1 and PIK3CA expression contributing to cell cycle progression, however, this type of breast cancer demonstrates genomic stability with functional RB tumor suppressor<sup>169</sup>.

The HER2-enriched subtype is characterized by prevalent CDK4 copy gains, concomitant with frequent APOBEC3B-associated mutations, which is a protagonist of p53 pathways and its overexpression seems to be related with progression of cell cycle and cell proliferation<sup>170</sup>. Furthermore, elevated levels of CDK4, ErbB2, p53, PIK3CA and cyclin D1 are observed within this subtype<sup>164</sup>.

Triple-negative breast cancer (TNBC) is characterized by RB1 reduced expression due to deletion or mutation, cyclin E1 overexpression, elevated CDKN2A expression and frequent alterations in DNA damage response genes such as tumor suppressor BRCA1<sup>169</sup>. TNBC also displays stimulated BRAF, PIK3CA, KRAS proto-oncogen and PTEN deletions, leading to aberrant PI3K/Akt/mTOR or Raf/MAPK/ERK signaling impacting cell cycle and enhancing survival, growth and metabolism of tumor cells<sup>171</sup>.

It is possible to observe the various mutated genes that cause the dysregulation of the cell cycle across the different subtypes of breast cancers in Figure 2.

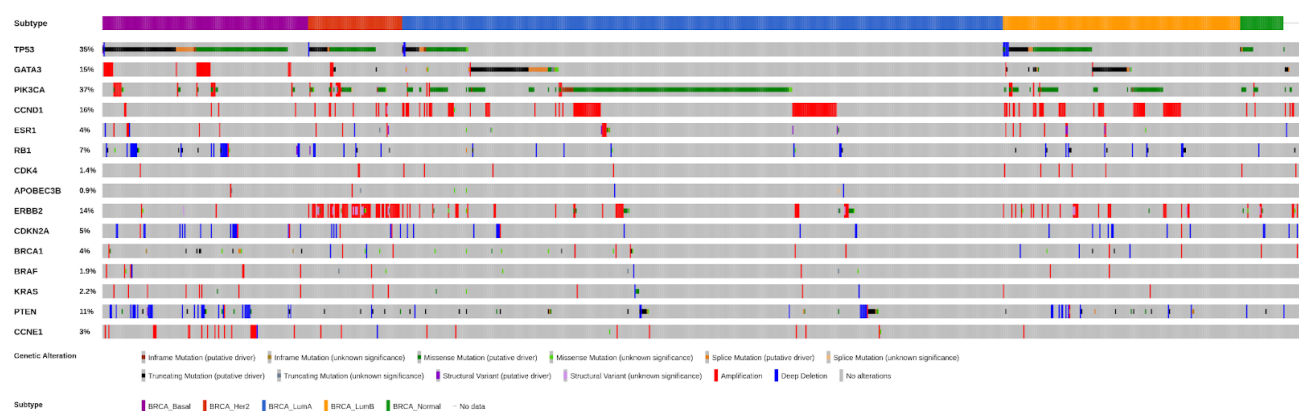


**Figure 2. Oncoprint containing the cited mutated genes that impact cell cycle in breast cancer across the different subtypes.** This plot has been retrieved from cBioPortal<sup>142</sup> using the Breast Invasive Carcinoma (TCGA, PanCancer Atlas)<sup>172</sup> dataset.

## 1.7 eQTLs

Expression quantitative trait loci (eQTLs) are genomic regions that contain one or more DNA sequence variants that influence the expression level of a gene. Indeed, eQTLs are similar to other quantitative trait loci (QTLs) that can influence any given trait of interest (height, growth rate and disease risk) but the trait under study is gene expression<sup>173</sup>.

Individuals in most species differ from each other by thousands to millions of DNA sequence variants, some of these variations contribute to observable phenotypic differences in traits ranging from morphology, physiology and behavior to predisposition to many human diseases<sup>174</sup>.

Usually, eQTLs are identified by measuring gene expression in panels of genetically different, genotyped individuals and by comparing the genotypes with the expression levels using association in outbred populations, so populations that exhibit considerable genetic and phenotypic variability, or linkage analysis in pedigrees or designed crosses<sup>175</sup>.

eQTLs are often classified according to their locations relative to the genes they influence and the mechanism through which expression is affected. Studies have characterized these regulatory variants as local or distant based on the physical distance from the gene they regulate, indeed variants within 1Mb on either side of the transcription start site of the gene are classified as local, whereas those with at least 5Mb downstream or upstream or even on a completely different chromosome are classified as distant eQTLs in humans<sup>176</sup>.

Local eQTLs can influence gene expression by two different mechanisms, they can act in cis and affect expression in an allele-specific manner<sup>174</sup>. So each allele of such eQTLs affects only the expression of the copy of the gene located on the same physical chromosome and not the expression of the copy on the homologous chromosome, cis-eQTLs can be detected in heterozygous individuals by quantifying the relative expression levels of the two alleles and if it is possible to see an imbalance in the expression levels then the target gene is altered by a cis-eQTL<sup>177,178</sup>. However, local eQTLs can also act in trans<sup>179,180</sup>, where trans-eQTLs are a result of polymorphisms that change the structure, function or expression of a proximal diffusible factor like transcription factor, RNA-binding, signal factor, chromatin modifier or possible non-coding RNA. The diffusible factors are equally available to both alleles of a target gene, due to this, trans-eQTLs do not lead to allele-biased expression in heterozygous individuals, meaning that one allele is more expressed than the other, which usually happens when a cis-eQTL affects only one allele<sup>181</sup>.

Local eQTLs are abundant in humans. In a survey of 1,000 individuals, nearly 80% of expressed genes in whole blood had a local eQTL<sup>182</sup>. Distant eQTLs are loci located further away from the genes they influence and they usually act in trans<sup>183</sup>.

Regulatory variation can intervene in the steps along the gene expression cascade, from DNA to protein, and affect the organism, indeed it has been shown that eQTLs take important roles in influencing traits, from yeast growth to fitness to human disease<sup>174</sup>.

In recent years, several examples have been found of causal links between diseases and human regulatory variants, an important example is an SNP situated at the region 1p13, rs646776, sitting at the 3' untranslated region (UTR) of the CELSR2 gene. The common SNP is known to be associated with myocardial infarction, also known as “heart attack”, indeed it has been shown to be associated with an increase in LDL-C (low-density lipoprotein cholesterol) levels, especially in very small lipoprotein subclass LDL-VS, of patients being homozygous major for this SNP compared to patients being heterozygous or homozygous minor<sup>184</sup>.

The minor allele SNP, on the other hand, was correlated with an increased expression 12-fold higher for SORT1 and PSRC1 in the case of minor allele homozygotes compared to major allele homozygotes, where also in the case of heterozygotes the quantity of SORT1 expression was higher compared to major allele homozygotes. This is possible because the minor variant creates a binding site for a transcription factor CCAAT/enhancer-binding protein (C/EBP), the binding of this TF leads to an increase in the expression of the sortilin1 gene in liver cells which, at least in mice, reduce the levels of low-density lipoprotein cholesterol which is a well-known risk factor for the myocardial infarction<sup>184</sup>.

## 1.8 Models of Cell Cycle

Biological systems, such as those governing the cell cycle, rely on efficient mechanisms to respond to environmental changes where the signal process often leads to switch-like activation of downstream pathways. These biological switches are commonly derived from molecular interactions that create positive feedback loops<sup>185</sup>. Computational algorithms share similarities with these biological switches, particularly in their structure and dynamic features<sup>186</sup>.

Feedback loops are responsible for complex dynamic behaviors in biological contexts<sup>187</sup>. They come in two primary forms: negative and positive<sup>187</sup>. Negative feedback loops contain an odd number of negative interactions, so interactions that diminish or inhibit the activity or production of a molecule<sup>188,189</sup>. The latter is critical for the loop's function, as it ensures that the loop's ultimate effect is to counteract any deviation from the set point, thereby promoting stability or homeostasis. However, longer negative feedback loops can induce oscillation by delays, causing the system to overshoot its set point, leading to a cyclical pattern of overcorrection and undercorrection<sup>188,189</sup>.

Positive feedback loops, conversely, contain only positive interactions, enhancing or amplifying the activity or production of a molecule. However, they can also contain an even number of negative interactions which can lead to multistability. Therefore, the system can exist in multiple stable states given a specific level of input or conditions and its history, determining its current state<sup>190,191</sup>.

Biological switches utilize this architecture to convert gradual input changes into on/off signals when an input signal reaches a certain critical threshold<sup>187</sup>.

A well-studied example of biological switches is the transition from interphase to mitosis ( $G2 \Rightarrow M$ ) in the cell cycle, based on the activity of the mitotic cyclin-dependent kinase complex<sup>187,192</sup>. In the context of this transition, two positive feedback loops are present<sup>193</sup>, one is a pure positive, corresponding to the activation of Cdc25 by Cdk<sup>194,195</sup>, while the other one is an antagonist feedback loop, where the inhibitory effect of Cdk to Wee1 has a net effect of promoting itself, resulting in a positive feedback loop (Fig. 3)<sup>196</sup>.

The G2/M transition exemplifies an important biological switch, but other cell cycle transitions and biological switches share similarly structured regulatory networks with multiple positive feedback loops<sup>187</sup>.

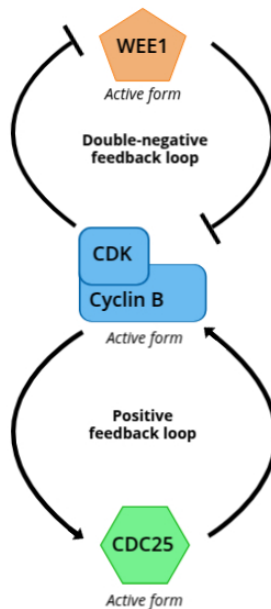


**Figure 3. Positive feedback loops G2/M.** Figure adapted from Zámborszky *et al*<sup>197</sup>.

The irreversibility of cell cycle transition is commonly attributed to the irreversible degradation of certain regulatory proteins. However, it has been argued that in the cell cycle, irreversible transitions are derived from feedback signals in reaction networks<sup>198</sup>. Although protein hydrolysis is thermodynamically irreversible, protein degradation on the other hand is counteracted by de novo synthesis, which is also an irreversible chemical reaction due to the large demand of ATP hydrolysis<sup>198</sup>. Despite being

thermodynamically irreversible, the chemical reactions governing protein levels involve dynamically reversible processes: protein accumulation and degradation. These opposing processes maintain a steady-state equilibrium for most proteins throughout the cell cycle.

However, for some proteins like cyclins, synthesis and/or degradation rates are repeatedly switched to upset this balance<sup>198</sup>.

As already stated, cell cycle transitions are driven by cyclin-dependent kinases, which are regulated by binding to CDK inhibitors (CKI), cyclins and inhibitory tyrosine phosphorylation<sup>199,200</sup>. At each irreversible cell-cycle transition (G1-S, G2-M and M-G1), one of these regulators is degraded by the proteasome. Irreversibility in a molecular regulatory system differs from an irreversible chemical reaction, indeed, it relies on feedback signals in the control network, making proteolysis an optional component but feedback an essential one<sup>201,202</sup>.

Paul Nurse proposed a universal control mechanism for the regulation of mitotic entry in which Cdk helps its activation through two positive feedback loops<sup>203</sup>. This idea can be extended to other cell cycle transitions, suggesting a universal control system with transcriptional and post-translational positive feedback for the regulation of all cell cycle transitions<sup>187</sup>. Computational modeling has been used to analyze transition dynamics in various combinations of transcriptional and post-translational regulations<sup>204,205</sup>. The latter revealed that some combinations lead to imprecise transitions, while others provide very precise control<sup>187</sup>. Although only one transition regulator (TR), either the activator or the inhibitor, is (periodically) expressed during the cell cycle, the precise periodic transcriptional regulation of the chosen TR leads to radically different dynamics<sup>187</sup>.

Mathematical modeling of dynamic systems employs two primary approaches: deterministic and stochastic<sup>206</sup>.

Deterministic models represent biochemical processes as inherently deterministic, positing that a fixed set of inputs will invariably yield an identical output<sup>207</sup>. Typically, these models employ ordinary differential equations (ODEs) to describe the dynamics of biochemical systems, operating under the assumption that variables can assume continuous values<sup>206,207</sup>. This approach, while computationally advantageous, constitutes a simplification, as molecular entities are fundamentally discrete. Furthermore, ODE-based models provide an aggregated representation of system dynamics, obscuring the underlying logical structure of molecular fluxes by consolidating them into mathematical equations. A representative example of a deterministic model applied to the cell cycle is the translation of molecular interaction networks into a system of ODEs<sup>206</sup>. An example is presented in *Adler et al*<sup>208</sup>, in which the aim of the studies was the creation of a deterministic model to model the yeast cell cycle integrating external stimuli like mating pheromones, osmotic pressure changes and nutrient to demonstrate how this introduction of this stimuli can perturb the dynamics of cell cycle and how it resumes after adapting to the stimuli<sup>208</sup>.

Stochastic models address the limitations of deterministic approaches by explicitly representing interactions between individual entities and calculating the temporal evolution of molecular counts for participating species<sup>209</sup>. This approach accommodates random fluctuations, which are absent in differential equation-based models, and proves particularly significant in small systems. In a discrete-stochastic framework, variables represent integer molecular counts, and interactions are modeled as reactions with integer stoichiometry, occurring at stochastic intervals<sup>210</sup>. Stochastic models offer valuable insights when molecular noise plays a crucial role in shaping the emergent behavior of oscillatory systems<sup>206</sup>. The Gillespie algorithm, a widely employed method for the stochastic simulation of chemical systems, is recognized as an exact method, yielding results equivalent to those obtained from the master equation<sup>211</sup>. The significance of the Gillespie algorithm lies in its capacity to accurately simulate the time evolution of chemical systems by capturing the inherent randomness of chemical reactions. This capability facilitates the stochastic characterization of reaction times as negatively exponentially distributed random variables<sup>210</sup>. An example of the utilization of a stochastic model in the cell cycle is presented in *Barik et al*<sup>212</sup>, the aim of the project was the development of a stochastic model of the cell cycle in budding yeast and through the utilization of Gillespie's algorithm investigate how molecular noise affects its regulation and variability. Building upon deterministic models, it aims to demonstrate the stability of the cell cycle under noise, validate the model against experimental data, predict mutant phenotypes, and serve as a foundation for more complex models of feedback mechanisms<sup>212</sup>. The model, based on elementary chemical reactions and experimentally derived molecular counts, seeks to provide an accurate representation of cell cycle variability and generate testable hypotheses<sup>212</sup>.

## 2 Aim

This work aims to characterize a generic stochastic model of cell cycle transition and explore the impact of germline and somatic cancer variants on its dynamics. A key objective is to create a model that elucidates how genetic variables in both healthy and cancerous tissues influence cell cycle models, and to explore whether mathematical models can provide insights into cancer. This includes investigating the role of eQTLs in cell cycle transitions by looking at various healthy tissues. Additionally, the work will control for how somatic copy number variations in breast cancer could impact and dysregulate cell cycle transition. Finally, breast cancer patient-specific models incorporating copy number data will be generated to explore their utility for patient stratification.

By adapting a generic stochastic model of cell cycle transitions to a human-specific one and identifying key regulators (checkpoints) in human cell cycle progression, the dynamics of genes involved in the cell cycle can be investigated. This research also aims to address model robustness through sensitivity analysis, identifying parameters that cause significant perturbations in the model when modified.

Understanding the impact of specific eQTLs on cell cycle transitions, whether promoting or inhibiting them, could provide insights into the broader role of eQTLs in non-cancerous contexts. Furthermore, determining whether a tumor-specific model can be derived from this generic stochastic cell cycle transition model would enable analyses to evaluate the utility of these models in understanding tumor biology, encompassing diverse aspects of tumor growth and behavior.

Stochastic models are valuable in understanding tumor biology, as they can capture tumor growth phases and explore how tumor growth responds to therapy. Given that limitless replicative potential, a hallmark of cancer, is acquired through various mechanisms, including mutations in cell cycle checkpoints, this study aims to further investigate the role of copy number aberrations in cell cycle transitions, specifically in breast cancer and within patient-specific models. This will also explore if mathematical models incorporating copy number variations in the tumor environment can provide patient-specific information.

# 3 Materials and Methods

## 3.1 BlenX

BlenX and the Beta Workbench in this project are used to reimplement the general dynamic cell cycle transition model implemented in *Romanel et al.*<sup>187</sup> and to adapt the general model to the G2/M transition in humans, taking into consideration specific genes of interest.

BlenX is a stochastic programming language crafted to model the interactions of biological entities, including proteins. The system specifications allow for the retrieval of information about the probability and speed of actions, which is the meaning of stochastic<sup>213</sup>.

A BlenX program comprises three key components: the program file, the interfaces file and optionally a declaration file. The program file is responsible for defining the program's architecture by delineating all the 'boxes' (biological entities) active within the model, refined by the keyword *bproc*<sup>213</sup>. The interfaces file provides quantitative details about the system and the declaration file, which permits the specification of constants, variables and functions<sup>213</sup>.

BlenX uses 'boxes' as an abstraction to represent a biological entity as a computational device. Each box is defined by a set of interfaces and an internal program. Interfaces, serving as interaction points between entities, possess an associated type that mirrors the structure. The internal program dictates how interactions translate into an entity's conformational changes, potentially altering other interface types.

Actions such as input, output, change, delay, hide and expose are used in the internal program to describe the behaviour of a box<sup>213</sup>.

Within BlenX, reactions are classified as monomolecular, bimolecular and events. Monomolecular reactions involve the transformation of individual units, where each unit's evolution is independent of others (Fig. 4(a)). Bimolecular reactions illustrate how two boxes interact through composition or communication, contingent on compatible interfaces (Fig. 4(b)). Events facilitate the programming of system disturbances triggered by specific simulation conditions, enabling observation of their broader effects<sup>213</sup>.

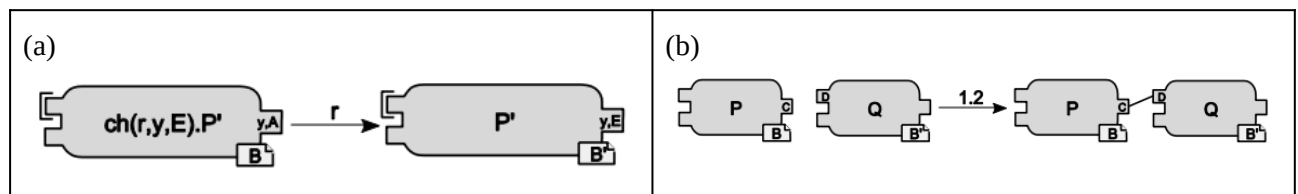


**Figure 4. Graphical representation of monomolecular and bimolecular reactions.** Figure adapted from *Demattè et al.*<sup>213</sup>. Panel (a) represents the transformation of a monomolecular reaction via action *change*, which changes the type of an interface, here from  $y_A$  to  $y_E$ . On the left of the arrows, the structure of the box before the execution of the action is represented; the action is indicated with the arrow, which is associated to  $r$ , the stochastic rate of the reaction; on the right of the arrows we have the box after the execution of the action.

Panel (b) represents the example of a bimolecular reaction via interaction between two compatible boxes possessing interfaces with types "C" and "D", respectively. These boxes can therefore bind with a rate equal to 1.2 to form a complex.

The Beta Workbench (BWB) provides tools for building, simulating, and analyzing BlenX models. At its heart is CoreBWB, a command-line application that combines BWB simulation, CTMC generation and BWB reaction generation. These tools work together, sharing the BlenX compiler and the BlenX runtime environment<sup>214</sup>.

Core BWB serves as the central processing unit, accepting BlenX program files as input. It then employs the compiler to translate these files into a runtime representation, which is subsequently sorted within the runtime environment. The BWB simulator then takes over as a stochastic simulator engine. The runtime environment equips this engine with the necessary primitives to monitor and modify the system's current state, including species populations and variable values. The simulator is responsible for driving the simulation and managing the time evolution in a stochastic manner while preserving the dynamics inherent to

BlenX<sup>213</sup>. Notably, the stochastic simulation engine within the BWB simulator implements an efficient variant of Gillespie's algorithm<sup>211</sup>.

In scenarios where the model is in finite-state, so when the number of species and complexes that the model can create is finite, the population of species and complexes is finite and no continuous variables are used, a BlenX program gives rise to a continuous-time Markov (CTMC) process. In such a case, the BWB CTMC generation steps in, interacting through species, complexes, and actions to traverse the entire state space of the BlenX program comprehensively while labeling transitions between states with their corresponding exponential rate<sup>214</sup>.

The BWB reactions generator offers a different perspective, identifying all complexes and species that could potentially be generated through the execution of a BlenX program, without the need for actual execution or simulation (also, in this case, it is required that the model needs to be finite). This tool provides a description of the system, presenting it as a list of 'boxes' of species and reactions, which are then abstracted into a graph where nodes represent species and edges represent reactions. Ultimately, the DWB reactions generator produces an SBML description of the original BlenX program<sup>214</sup>.

To further facilitate the model writing and interpretation of the results, a suite of tools has been developed around CoreBWB. These tools include: BetaPlotter for initial analysis of simulation result; Grapfen for visualizing and analyzing large graphs; ComplexViewer for classifying and visualizing complexes and BlenXDesigner, a graphical tool for authoring BlenX program<sup>213</sup>.

## 3.2 Sensitivity Analysis

During the construction of mathematical models, sensitivity analysis is a fundamental tool for evaluating the influence of input parameters on model outputs<sup>215</sup>. Specifically, model species and parameters are crucial components of sensitivity analysis, as it helps us understand how fluctuations in model outputs relate to variations in parameter and species values<sup>216,216</sup>. In our study, a sensitivity analysis is essential for characterizing the proposed model, identifying parameters that cause significant output fluctuations, and ultimately adapting the model to human and breast cancer patient-specific conditions.

In this study, sensitivity analysis was conducted by generating perturbed input values for all species and parameters within each general model. The models represented various combinations of feedback loops (on the activator or inhibitor), checkpoint regulations (on the activator or inhibitor), and expression patterns (activator periodically expressed with inhibitor constantly expressed, or vice versa).

In the sensitivity analysis, species input values were varied from 0 to 1000, in increments of 50. For parameters, a different approach was employed. Initially, values ranged from 10% to 100% of the parameter's initial value, with 10% increments. Subsequently, values were extended from two times the initial parameter value up to ten times the initial value, with unit increments. For each model, only one parameter or species value was varied at a time, with 100 simulations performed for each value before proceeding to the next.

## 3.3 Dataset description

The Invasive Breast Carcinoma (TCGA, PanCancer Atlas) dataset was selected as a reference to extract gene expression levels from a total of 1256 samples, including both breast cancer patients (BRCA) and healthy controls. This dataset is part of a bigger study in which the researchers performed a comprehensive integrative molecular analysis on a complete set of tumors within The Cancer Genome Atlas (TCGA), which includes approximately 10,000 specimens and 33 cancer types<sup>172</sup>. This dataset was selected based on several factors: the clinical relevance of breast cancer, the high availability of data, and its representativeness of the various breast subtypes.

Among the data available from this dataset, the batch-corrected RNA-seq data (generated using the Illumina HiSeq RNA-seq V2 platform) and the somatic copy number variation data were of particular interest for this analysis. The somatic copy number variation data were available for a subset of 938 BRCA patients, rather than the full cohort.

The batch-corrected RNA-seq data were obtained from the publicly available *recount3* resource, which contains over 750,000 uniformly processed human and mouse RNA-seq samples<sup>215</sup>, using the R library *recount3*<sup>217</sup>. The somatic copy number variations were acquired from the cBioPortal<sup>142</sup> online resource (<https://www.cbioportal.org>).

The Adult Genotype-Tissue Expression (GTEx) project (<https://gtexportal.org/home>), a publicly available resource, was utilized to extract eQTLs information. GTEx provides comprehensive genetic variants and gene expression data (WGS, WES, and RNA-seq) from up to 54 non-diseased tissue sites<sup>218</sup> across about 950 deceased individuals of local and *cis* expression quantitative trait loci (eQTLs)<sup>219</sup>.

Specifically, the database was used to extract median gene-levels in TPM for each tissue (GTEx\_Analysis\_v10\_RNASeQCv2.4.2\_gene\_median\_tpm.gct) and extract eQTLs information for each gene of interest involved in the cell cycle G2/M transition. This was achieved by performing a query through the web interface and extracting several information, including the normalized effect size (NES) and SNP ID data for each eQTL.

### 3.4 RNA-seq data normalization

The batch-corrected RNA-seq data were analyzed in R. The expression data was initially filtered through the utilization of the library *dplyr*<sup>220</sup>, retaining only primary breast cancer samples and one sample for each oncological patient.

The data were then utilized to make a gene expression comparison across samples. Two other computational methods were used to analyze the data. Firstly, the TPM method for quantification and normalization<sup>221</sup> was used. TPM, defined as transcript per million, normalizes gene expression data in a way that the total expression across all genes is constant in every sample, allowing for direct comparison of relative gene expression levels between samples<sup>221,222</sup>.

$$TPM = 10^6 * \frac{\text{reads mapped to transcript / transcript length}}{\sum (\text{reads mapped to transcript / transcript length})}$$

Secondly, quantile normalization was applied. As the name suggests, it normalizes the data by computing for each quantile the mean value across samples and substituting it to the gene's value, ensuring that the distribution of the data of each sample is the same<sup>218</sup>.

### 3.5 SCNA and patient-specific data analyses

For each gene of interest, a linear regression was performed to highlight correlation between normalized gene expression data and somatic copy number status. Linear regression was chosen because it is the simplest type of regression and several studies, spanning multiple cancers, revealed a predominantly linear correlation between copy number variations and expression levels<sup>219</sup>. Indeed, it has been demonstrated that gene amplification typically results in increased gene expression, while deletions lead to decreased expression<sup>219</sup>.

For the genes following a linear correlation between the two variables (gene expression and copy number status), the fitted regression formulas were retrieved and subsequently used to scale variables of the transition cell cycle model G2/M.

Furthermore, information on the copy number of the genes for each patient was used to create a patient-specific dataset. The latter was used, in combination with the various fitted regression formulas, to test how the cell cycle transition model G2/M responds by adapting it to the patient-specific information.

### 3.6 eQTLs data analysis

Within the median gene-levels dataset, 44 tissue sites were identified in which at least one gene demonstrated expression influenced by an eQTL. For each identified eQTL, information about biotype, associated dbSNP

identifiers, allelic fold change and additional relevant information are present. However, corresponding gene expression data were not available. To address this limitation, median bulk RNA-seq data, normalized in TPM, were obtained for each tissue from GTEx.

To address the absence of information on genotype-specific gene expression data, median bulk RNA-seq data and allelic fold change were utilized. In the GTEx project, allelic fold change (aFC) was determined following the methodology outlined by Mohammadi et al<sup>223</sup>. This approach employs an additive model of gene expression, wherein the total expression within a given genotype group is represented as the sum of contributions from the two haplotypes. Specifically, for reference homozygotes, heterozygotes and alternate homozygotes, the total expression, denoted as  $e(\text{genotype})$  is modeled as  $2e_r$ ,  $e_r + e_a$  and  $2e_a$  respectively. Here,  $e_r$  represents the expression of the haplotype carrying the reference allele and  $e_a$  represents the expression of the haplotype carrying the alternate allele<sup>223</sup>. The allelic fold change, which in the following equation is denoted as  $k$ , is defined by the relationship  $e_a = k * e_r$ , where  $k$  is a positive number. For analytical purposes, the allelic fold change in GTEx is represented on a log<sub>2</sub> scale<sup>224</sup>.

Having this information, it was hypothesized that the median expression of each gene of interest could be approximated by considering the expression of each allele, weighted by the minor allele frequency (MAF), which is the frequency of the less common allele<sup>225</sup>. MAFs were obtained using SNPnexus, a web-based tool for annotation, analysis and interpretation of genetic variance<sup>226</sup>.

A system of two equations was constructed (Fig 5). The first equation represents the median gene expression for a specific tissue. The value is retrievable from the bulk median RNA-seq data as the sum of the expression of the reference and alternative allele weighted by MAF. The second equation utilizes the allelic fold change (aFC) data retrieved from GTEx for each eQTL.

### First part

$$\begin{cases} e_{tot} = (1 - MAF)e_r + (MAF)e_a \\ aFC = \log_2\left(\frac{e_a}{e_r}\right) \end{cases}$$

$$\begin{cases} e_{tot} = (1 - MAF)e_r + (MAF)e_a \\ 2^{aFC} * e_r = e_a \end{cases}$$

$$\begin{cases} e_{tot} = e_r * (1 - MAF + MAF * 2^{aFC}) \\ 2^{aFC} * e_r = e_a \end{cases}$$

$$\begin{cases} e_r = \frac{e_{tot}}{(1 - MAF + MAF * 2^{aFC})} \\ 2^{aFC} * e_r = e_a \end{cases}$$

### Second part Calculate $e_a$ and $e_r$

$$\begin{cases} e_r = \frac{e_{tot}}{(1 - MAF + MAF * 2^{aFC})} \\ e_a = \frac{2^{aFC} * e_{tot}}{(1 - MAF + MAF * 2^{aFC})} \end{cases}$$

**Figure 5. Resolution of the two equation system.** In the first equation of the system,  $e_{tot}$  stands for the median expression value of the gene.  $MAF$  is the minor allele frequency  $e_a$  and  $e_r$  represents the expression of the alternative allele and the expression of the reference allele. The second equation also contains the variables  $e_a$  and  $e_r$ , with another variable  $aFC$ , which is the value of the allelic fold change.

By solving the system, it was possible to retrieve, as solutions, the median expression for the reference and alternative allele. By having this information, it was possible to compute the median expression per genotype by computing  $2e_r$ ,  $e_r + e_a$  and  $2e_a$ , respectively. Later, this data was utilized inside the transition cell cycle model G2/M.

Minor allele frequencies (MAFs) were subsequently used to define genotype status for each gene of interest. Specifically, for observed MAFs < 0.25, a homozygous reference status was assigned as the normal state, with the gene quantity fixed at 500 (previously selected as the normal value to generate cell cycle transition models). For MAFs > 0.25, the normal state was designated as heterozygous, again with the gene quantity fixed at 500. This information was then used to derive initial values for the other two genotypes (heterozygous and homozygous alternative, or homozygous reference and homozygous alternative). Specifically, a simple proportion was calculated between median expression values and the initial gene quantity. In this way, for each gene in each tissue, each genotype was associated with a quantity value for model simulation. Each model was run 100 times, varying only one gene quantity at a time before proceeding to the next gene quantity and then to a different gene. This procedure was performed to observe how genotype information alters switch time and switch percentage in the cell cycle model.

### 3.7 Survival analysis

Survival analysis was performed in R using the *survival*<sup>227</sup> and *survminer*<sup>228</sup> packages. The survival package provides core functions for survival analysis<sup>227</sup>, while survminer facilitates the visualization of survival curves<sup>228</sup>. In this study, survival analysis was used to analyze the relationship between mean switch time and switch percentage, derived from cell cycle transition simulations, and patient survival. Overall survival was determined using patient status (dead or alive) and survival time (time from diagnosis to death or last follow-up).

For each patient, cell cycle transition simulations under breast cancer conditions were repeated 100 times. The mean switch time represents the average time at which a checkpoint switch, indicating transition between cell cycle phases, was observed for each patient. The switch percentage indicates the proportion of simulations in which a checkpoint switch was observed for each patient.

K-means clustering was performed to identify two distinct patient groups based on average switch time and switch percentage. Specifically, the *kmeans* function from the *stats*<sup>229</sup> package in R was used.

The *survfit* and *Surv* functions were used to create a survival object, defining patient status and survival time, and to fit survival curves<sup>227</sup>. Kaplan-Meier curves were generated to assess whether significant differences in survival existed between patient groups defined by mean switch time or switch percentage.

The *coxph* and *Surv* functions were then used to perform multivariate Cox regression (including age at diagnosis and cancer subtype as covariate) and extract regression coefficients and hazard ratios. The sign of the regression coefficient indicates whether the hazard (risk of death) is higher (worse prognosis) or lower (better prognosis) in one group with respect to the other. The hazard ratio, calculated as  $e^{(\text{coeff})}$ , quantifies the effect of the hazard on one group with respect to the other<sup>227</sup>.

# 4 Results and discussion

## 4.1 General model of cell cycle transition

### 4.1.1 Explanation of the general cell cycle transition model

Romanel et al.<sup>187</sup> present the creation of a general cell cycle transition model to investigate in silico the findings of multiple studies, in which the idea that the transitions control and dynamics of the cell cycle are universal among eukaryotes<sup>93,198,203,226–228</sup>. For the creation of this model, an overview of the literature about eukaryotic cell cycle was performed to find common features to create the model.

Aligned with Paul Nurse's theory of G2/M transition universality in eukaryotes, research confirms that CDK/cyclins function as pivotal transition regulators, operating within an activator-inhibitor framework. Analogous regulatory models, characterized by the presence of one or more positive feedback loops, have been proposed for G1/S and M/G1 transitions. This model specifically examines cell cycle transitions governed by post-translational positive feedback loops, a commonly observed feature across diverse organisms.

A comprehensive literature review, as conducted by Romanel et al., reveals that the G2/M transition is distinguished by the presence of two positive feedback loops across various organisms. However, for other cell cycle transitions, studies suggest the existence of a single positive feedback loop, with no discernible preference for feedback acting through either the inhibitor or the activator. Similar observations can be made regarding checkpoint regulation, wherein checkpoints can affect both the activator and inhibitor, or only one of these components, depending on the organism.

Furthermore, a major finding from Romanel et al.'s research is that periodic transcription predominantly affects only one of the regulators, either the activator or the inhibitor, without a consistent preference observed across organisms or cell cycle transitions. This indicates that while positive feedback loops and checkpoint mechanisms are critical, the specific targets of transcriptional regulation exhibit significant variability.

The general cell cycle transition model is characterized by an activator and an inhibitor, which jointly regulate the activity of a transition regulator protein<sup>187</sup>. The transition regulator in its active form (TR\*) is capable of inducing its activator and/or repressing its inhibitor, establishing one or two feedback loops (PFB). Transcriptional regulation of the inhibitor and activator components of the network is achieved through transcriptional factors (TFs, as described in Fig.6)<sup>187</sup>. Cell cycle checkpoints (Chp) provide an additional layer of control, ensuring the transitions occur only upon successful completion of preceding cell cycle events<sup>233,234</sup>. Checkpoint signals halt the transitions though either activator inhibition or inhibitor activation, making it more difficult for the active transcription regulator to engage its positive feedback loops.

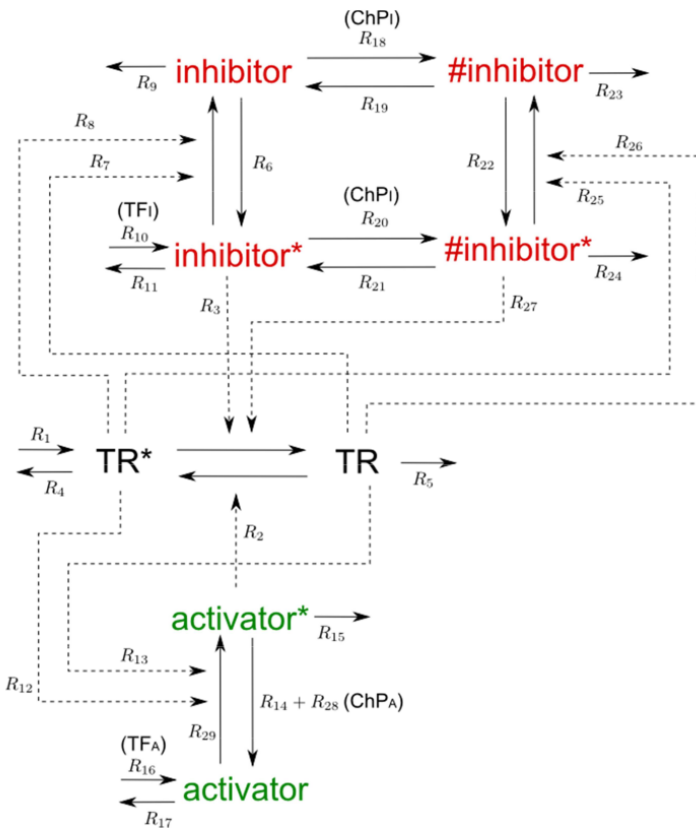


**Figure 6. Map of the interactions of the generic transition model.** Figure adapted from Romanel *et al*<sup>187</sup>.

Kinetic laws were defined as follows: synthesis and degradation reactions follow the law of mass action, which means that reaction rates are proportional to the concentrations of reactants; other reactions follow Michaelis-Menten kinetics (Table 1).

The model's notational framework employs  $TR^*$  and  $TR$  to represent the active and inactive states of the transition regulator, respectively. Similarly,  $activator^*$  and  $activator$  designate the active and inactive states of the activator, while  $inhibitor^*$  and  $inhibitor$  denote the corresponding states for the inhibitor. Specifically,  $TR^*$  activates  $activator$  and inhibits  $inhibitor^*$ . Although  $TR$ , the inactive form of the transition regulator, interacts with both  $activator$  and  $inhibitor$ , its functional efficacy is diminished by two orders of magnitude based on prior theoretical and experimental findings<sup>235,236</sup>. Furthermore, the interactions of  $TR^*$  (and  $TR$ ) with  $activator$  and  $inhibitor^*$  constitute positive feedback loops (PFB);  $activator^*$  enhances  $TR^*$  activation, whereas  $inhibitor$  exerts an inhibitory influence. The checkpoint mechanism ( $ChPi$ ) triggers a hyperactive state in the inhibitor, denoted as  $\# \text{inhibitor}$ , which demonstrates a four-fold increase in inhibitory potency towards  $TR^*$  relative to the unmodified  $inhibitor^*$  state. This implementation of checkpoint activation is adapted from a model of the morphogenetic checkpoint in budding yeast cells<sup>237</sup>.

Some molecular species not present in Figure 6 of the model present constant populations and represent the activities of kinases and phosphatases, always in background.  $E1$  and  $E2$  exert regulatory control over the  $inhibitor$  and  $activator^*$ , respectively.  $E1$  activates the  $inhibitor$ , encompassing the hyperactive state  $\# \text{inhibitor}$ , while  $E2$  inhibits  $activator^*$ . These regulatory interactions establish a threshold for  $TR^*$ -mediated autocatalysis, set as 150 quantity of the species. Additionally,  $S$  represents a constitutive signal that activates  $activator$  when positive feedback on the activator is absent.  $ChP_A$  and  $ChP_I$ , representing checkpoints acting on activator and inhibitor, respectively.  $ChP_A$  mediates activator inhibition, and  $ChP_I$  facilitates the transition of inhibitor to its hyperactive state,  $\# \text{inhibitor}$ . In this model, a transcriptional factor ( $TF$ ) influences either the inhibitor or the activator, which initiates corresponding synthesis and degradation reactions. Conversely, when transcriptional regulation of the activator, inhibitor, or both is absent, synthesis and degradation parameters are set to zero, and the respective species are maintained at a constant level of 500 molecules (normal status level).

$R_1 = \frac{kms}{\alpha}$	$R_{16} = kcs \times TF$
$R_2 = \frac{kma \times \alpha \times activator^* \times TR}{jma + (\alpha \times TR)}$	$R_{17} = kcd_1 \times activator$
$R_3 = \frac{kmi \times \alpha \times inhibitor^* \times TR^*}{jmi + (\alpha \times TR^*)}$	$R_{18} = \frac{kcp_7 \times \alpha \times ChPI \times inhibitor}{jcp_7 + (\alpha \times inhibitor)}$
$R_4 = kmd \times TR^*$	$R_{19} = \frac{kcp_6 \times \alpha \times Pho \times \#inhibitor}{jcp_6 + (\alpha \times \#inhibitor)}$
$R_5 = kmd_1 \times TR$	$R_{20} = \frac{kcp_1 \times \alpha \times ChPI \times inhibitor^*}{jcp_1 + (\alpha \times inhibitor^*)}$
$R_6 = \frac{kwa \times \alpha \times E_1 \times inhibitor}{jwa + (\alpha \times inhibitor)}$	$R_{21} = \frac{kcp_2 \times \alpha \times Pho \times \#inhibitor^*}{jcp_2 + (\alpha \times \#inhibitor^*)}$
$R_7 = \frac{kwi \times \alpha \times TR^* \times inhibitor^*}{jwi + (\alpha \times inhibitor^*)}$	$R_{22} = \frac{kcp_5 \times \alpha \times E_1 \times \#inhibitor}{jcp_5 + (\alpha \times \#inhibitor)}$
$R_8 = \frac{kwi \times \alpha \times perc \times TR \times inhibitor^*}{jwi + (\alpha \times inhibitor^*)}$	$R_{23} = kwd_1 \times \#inhibitor$
$R_9 = kwd_1 \times inhibitor$	$R_{24} = kwd \times \#inhibitor^*$
$R_{10} = kws \times TF$	$R_{25} = \frac{kcp_3 \times \alpha \times TR^* \times \#inhibitor^*}{jcp_3 + (\alpha \times \#inhibitor^*)}$
$R_{11} = kwd \times inhibitor^*$	$R_{26} = \frac{kcp_4 \times \alpha \times perc \times TR \times \#inhibitor^*}{jcp_4 + (\alpha \times \#inhibitor^*)}$
$R_{12} = \frac{kca \times \alpha \times TR^* \times activator}{jca + (\alpha \times activator)}$	$R_{27} = \frac{kmi_1 \times \alpha \times \#inhibitor^* \times TR^*}{jmi_1 + (\alpha \times TR^*)}$
$R_{13} = \frac{kca \times \alpha \times perc \times TR \times activator}{jca + (\alpha \times activator)}$	$R_{28} = \frac{kcp_8 \times \alpha \times ChPA \times activator^*}{jcp_8 + (\alpha \times activator^*)}$
$R_{14} = \frac{kci \times \alpha \times E_2 \times activator^*}{jci + (\alpha \times activator^*)}$	$R_{29} = \frac{kca \times \alpha \times S \times activator}{jca + (\alpha \times activator)}$
$R_{15} = kcd \times activator^*$	

**Table 1 . Kinetic laws associated to model reactions.** Table adapted from *Romanel et al*<sup>187</sup>. Parameters with letter *k* are catalytic constants with dimension 1/min, whereas the ones starting with letter *j* are Michaelis constants as dimensionless.

Something to highlight is that the system is described in terms of explicit molecule count instead of concentrations, to make this transition a scaling factor  $\alpha$  applied in the kinetic laws formulas. This parameter is computed as  $\alpha = (N_A * 10^{-6} * V)^{-1}$ ,  $N_A$  represents Avogadro's number and  $V$  is the average volume of the cell, as explained in *Mura et al*<sup>209</sup>. The arbitrary basal parameters, which have been chosen to get a sharp threshold for  $TR^*$  from which its quantity keeps increasing and transition happens, for the constants present in the kinetic laws of the reactions are described in Table 2 and retrieved from *Romanel et al*<sup>187</sup>.

$kms = 0.004$	$kca = 2$	$kcd = 0.01$	$kcp_1 = 0.1$
$kma = 0.5$	$jca = 0.1$	$kcd_1 = 0.01$	$kcp_2 = 0.2$
$jma = 1$	$kci = 0.2$	$jcp_1 = 2$	$kcp_3 = 2$
$kmi = 0.5$	$jci = 0.1$	$jcp_2 = 0.1$	$kcp_4 = 2$
$jmi = 1$	$kmi_1 = 2$	$jcp_3 = 0.1$	$kcp_5 = 0.2$
$kmd = 0.002$	$kws = 0.5$	$jcp_4 = 0.1$	$kcp_6 = 0.2$
$kmd_1 = 0.002$	$kwd = 0.5$	$jcp_5 = 0.1$	$kcp_7 = 0.2$
$kwa = 0.2$	$kwd_1 = 2$	$jcp_6 = 0.1$	$kcp_8 = 0.1$
$jwa = 0.1$	$jwi = 0.1$	$jcp_7 = 0.1$	$perc = 0.01$
$kwi = 2$	$kcs = 0.01$	$jcp_8 = 0.1$	$\alpha = 1/500$

**Table 2. Basal parameters set.** Table adapted from *Romanel et al*<sup>187</sup>.

The model was implemented using the BlenX programming language, a framework that facilitates modular modeling and stochastic simulation<sup>213</sup>. Stochastic simulations were performed using an efficient variant of the Gillespie algorithm<sup>211</sup> (github link: [https://github.com/iamandreatonina/master-s\\_thesis?tab=readme-ov-file](https://github.com/iamandreatonina/master-s_thesis?tab=readme-ov-file)).

#### 4.1.2 Simulations of GO and STOP transcriptional regulations

A series of computational models were constructed to elucidate the regulatory mechanism governing cell cycle transitions. These models systematically explored the combinatorial effects of three key regulatory processes: transcriptional control, post-transcriptional positive feedback and checkpoint activation. To represent variations in transcriptional regulation, the models were constructed to simulate a transcription regulator influencing either the activator or the inhibitor, forming two distinct sub-model types. Moreover, the positive feedback loops were represented by three sub-model types, allowing for feedback mechanisms to operate on the activator, inhibitor or both.

Checkpoint activation was modeled through four distinct sub-model types, representing the absence of checkpoint activation, checkpoint activation affecting activator, inhibitor or both. The combinatorial integration of these regulatory effects resulted in the creation of 24 unique models, each representing the distinct configuration of transcriptional control, post-translational positive feedback and checkpoint activation.

Modeling various configurations revealed a distinct pattern present in most models related to transcriptional regulator influence on either the activator or the inhibitor, particularly concerning the impact of a tenfold reduction in transcription levels compared to normal quantity (500). Two distinct modes of transcriptional regulation were observed, classified as "GO" and "STOP" systems.

The "GO" system, characterized by transcriptional factor (TF) influence on the inhibitor, simulates scenarios where the inhibitor is periodically transcribed while the activator remains constitutively present. In this system, failure of inhibitor transcription permits cell cycle progression through the transition (Fig. 7 lower part). Notably, even with the incorporation of diverse combinations of checkpoint activation and post-transcriptional feedback loops, the transition cannot be completely arrested. This regulatory strategy is exemplified by the G1/ transition in budding yeast<sup>238</sup>.

Conversely, the "STOP" system is defined by the periodic expression of the activator and the static expression of the inhibitor. In this configuration, failure of periodic activator transcription, or even a significant reduction in its transcription level, prevents the transition from occurring (Fig. 7, upper part). Indeed, even with the integration of positive feedback loops, the transition regulator cannot be activated due to the persistent inhibitory activity, effectively precluding transition progression. This mode of control is likely prevalent in cell cycle transitions of critical importance to cellular viability, providing a more stringent checkpoint mechanism compared to the "GO" control system. Specifically, the G2/M control in fission yeast cells is an example of this "STOP" system, wherein the absence of activators results in the complete blockage of cell cycle transition<sup>239</sup>.

These results confirm the findings presented in *Romanel et al*<sup>187</sup> (Appendix Fig S1 - S22), although the models that present the transcription factor influencing the activator with the positive feedback loop impacting the inhibitor, models that should be categorized as "STOP" system, do not produce any switches in both reduced and normal transcription level scenarios. Furthermore, in the model where the positive feedback loop is present on the inhibitor, with the transcription factor influencing the inhibitor and checkpoint activation impacting the activator, switching occurred exclusively under reduced transcription factor levels, whereas with normal transcription factor levels no switch is observed. Although the models depicted in *Romanel et al.*<sup>187</sup> are conceptually the same as those used in this study and are based on the same formalism, distinct implementation approaches were employed using BlenX. Specifically, one of the key features of BlenX is the ability to construct models using different implementation approaches. In our implementation we fully exploited BlenX events. While not directly affecting the work in this thesis, future investigations will be performed to explore the source of the observed discrepancies to better understand if they originate from implementation differences, model limitations, or inherent biological mechanisms of cell cycle regulation.

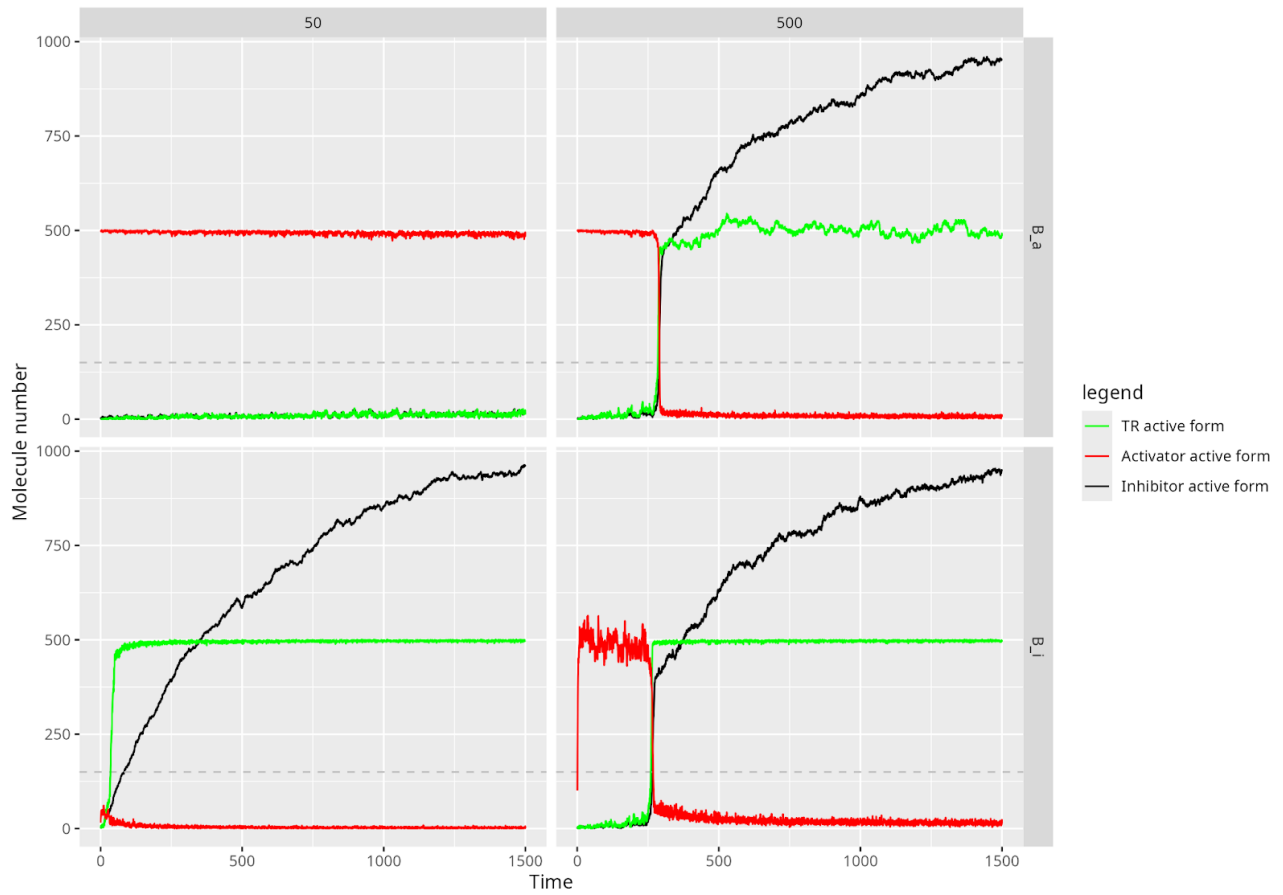


**Figure 7. Transcriptional control modes of cell cycle transitions.** Simulations of models  $B_A$  and  $B_I$  are characterized by the periodic transcription applied to either the activator or inhibitor, the absence of checkpoint regulations and positive feedback on both the inhibitor and activator. Simulations were initiated (time = 0) by activating the transcription of either the activator or inhibitor, utilizing assumed normal (right column) or reduced (left column) activity levels of  $TF_A$  or  $TF_I$ . The dynamics of active species, including *activator* (green), *inhibitor* (red), and  $TR^*$  (black), were then analyzed. Under conditions of relative normal TF abundance (right column), the transitions showed qualitatively analogous patterns, with the  $TR^*$  threshold of 150 being attained within a similar timeframe. However, when TF levels were low (left column), the models diverged significantly in their behavior.

## 4.2 Sensitivity analysis of the general model

For each model, sensitivity analysis was performed and generated a series of plots illustrating the relationship between parameter input values and the resulting fluctuations in average switch time and switch percentage. Only the most significant fluctuations were discussed in detail. For models with constitutive activator expression and transcriptional inhibitor regulation, we analyze results based on the presence of feedback loops for both or either the activator and inhibitor.

To facilitate a clearer understanding of the model under consideration, a specific nomenclature has been adopted, as detailed in Figure 8.

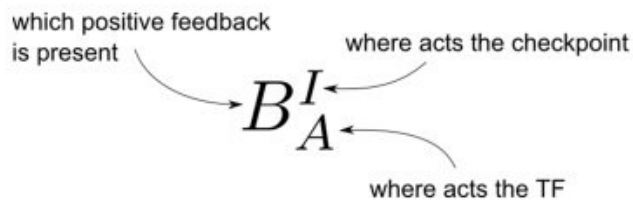


**Figure 8. Nomenclature used to describe the models defined in this analysis.** Figure adapted from Romanel et al<sup>187</sup>.

## **I<sub>i</sub><sup>B</sup> model**

The average switch time for  $TF_I$  (transcriptional control of inhibitor quantity) exhibits significant variation compared to the normal  $TF_I$  state, which has a switch time of 987.2, as shown in Figure 9 (a). Specifically, at high initial values of  $TF_I$  ( $> 700$ ), the average switch time is substantially delayed, reaching approximately 6000. This delay in the G2/M transition is expected, as we are increasing inhibitor levels in the model while maintaining activator levels constant at 500 (normal level). Furthermore, despite the presence of a positive feedback loop that reduces inhibitor levels, these levels remain sufficiently high to induce a delay in cell cycle transition.

$Chp_A$ , the checkpoint inhibitor that inactivates the active form of the activator, exhibits a similar behavior. Specifically, at high  $Chp_A$  levels ( $> 700$ ), a delay in the G2/M transition is observed, as indicated by the increased average switch time. Notably, even small variations in  $Chp_A$  levels, including those near the normal level (500), result in significant fluctuations in switch time. This behavior is expected, as  $Chp_A$  inhibits the active form of the activator, thereby reducing the amount of active activator which is required for cell cycle transition.

Finally, among the species,  $E2$  can be highlighted.  $E2$  is the enzyme that regulates the reaction from the active to the inactive form of the activator. Its overall average switch time deviates slightly from the normal state, and at high levels ( $> 700$ ), a behavior similar to that observed for  $TF_I$  and  $Chp_A$  is evident, with increased average switch times. Indeed, elevated levels of  $E2$  impact the activator similarly to  $Chp_A$ , reducing the amount of active activator.

Analysis of the switch percentage for these species in Figure 9 (b) reveals similar trends. Specifically, we observe that at high levels ( $> 700$ ) of  $TF_I$ ,  $Chp_A$ , and  $E2$ , the switch percentage rapidly decreases, reaching 0, which indicates the absence of cell cycle transition. This finding strengthens the results previously presented regarding the average switch time.

Among the parameters analyzed (Figure 9(c)) that impact the average switch time,  $jcp_8$  is one of the most significant. Specifically, the average switch time oscillates from the normal state (987.17) for both values near the original parameter value and substantially different values.  $jcp_8$  influences the reaction rate  $R_{28}$ , which governs the transition from the active to the inactive form of the activator. At the reaction level,  $jcp_8$  appears in the denominator, indicating that higher  $jcp_8$  values result in a lower  $R_{28}$  rate. This implies that  $R_{28}$  is effectively 'inhibited' by higher  $jcp_8$  values. Consequently, higher  $jcp_8$  values are associated with a slower conversion of active activator to its inactive form, resulting in a lower average switch time. Conversely, low  $jcp_8$  values increase  $R_{28}$  activity, leading to enhanced inactivation of the active activator and thus, a delay in cell cycle transition.

At the switch percentage level (Figure 9(d)), high  $jcp_8$  values correlate with a 100% switch percentage, supporting the hypothesis that  $R_{28}$  is downregulated at high  $jcp_8$  levels, leading to less stringent activator deactivation. Conversely, low  $jcp_8$  levels enhance  $R_{28}$ , causing strong activator deactivation and a decreased probability of cell cycle transition.

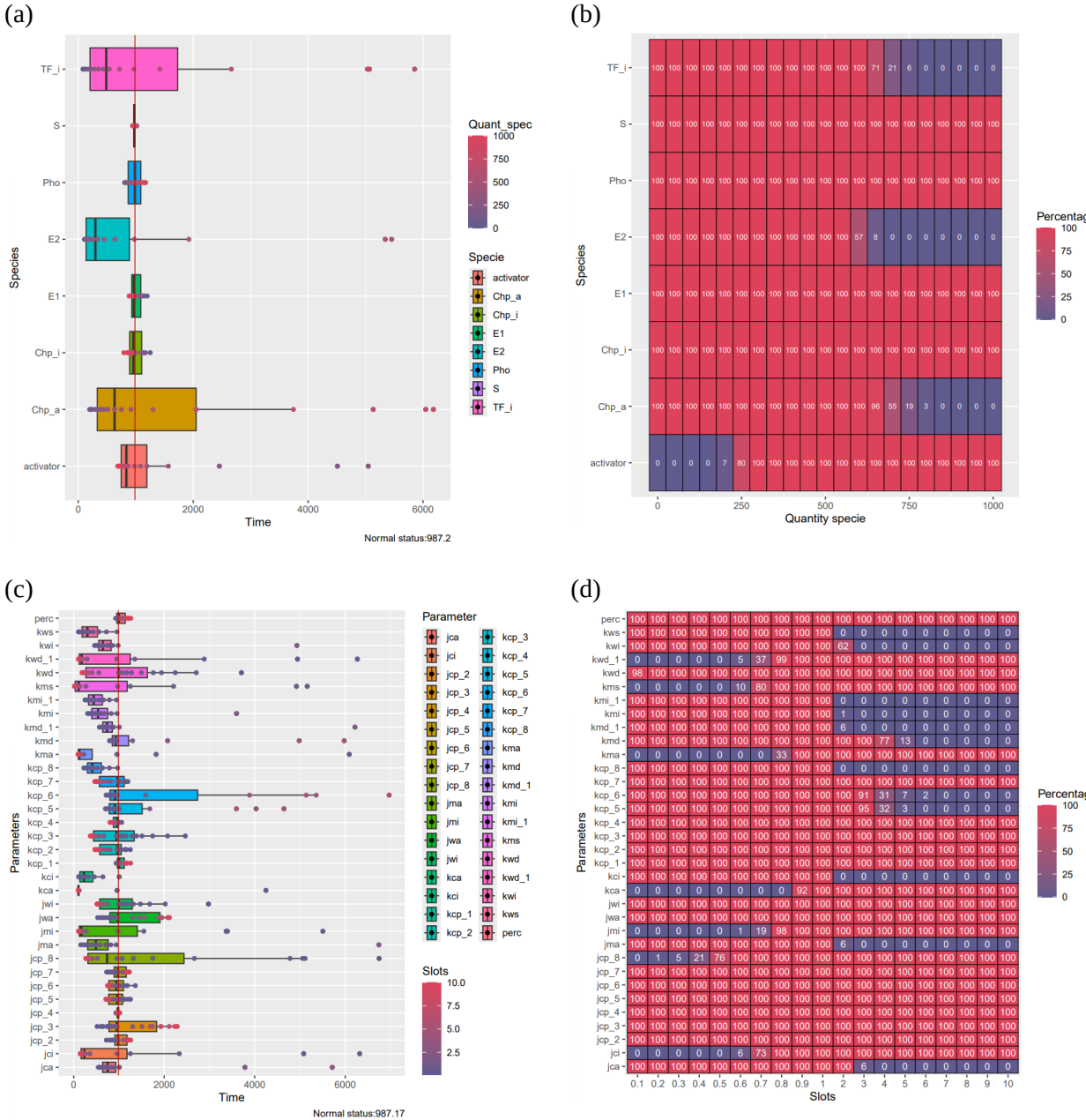


**Figure 9. Sensitivity analysis plots for the  $I_I^B$  model.** Panel (a) and (b) represent the sensitivity plot for the species while panels (c) and (d) represent the parameters' behaviour. Panels (a) and (c) display the average switch time on the x-axis and the corresponding species or parameter on the y-axis. For each species or parameter, a boxplot illustrates the fluctuations in switch time based on the selected initial values. Colored dots represent specific initial value-switch time pairs, facilitating a clearer understanding of the sensitivity analysis. Panels (b) and (d) present the species or parameter quantities on the x-axis and the corresponding species or parameters on the y-axis. A heatmap is used to visualize the switch percentage for each species or parameter at each analyzed quantity. Low switch percentages are indicated in violet, while high switch percentages are indicated in red.

## $I_I$ model

Overall, trends similar to those observed for the  $I_I^B$  model are evident. Specifically, the average switch times for  $TF_I$  (transcriptional control of inhibitor quantity) and  $E2$  exhibit significant variation compared to the normal switch time of 399.6, as shown in Figure 10(a). Again, at high initial values of  $TF_I$  and  $E2$  ( $> 700$ ), the average switch time is substantially delayed. Furthermore, the switch percentage for these species in Figure 10(b) reinforces the observed trends. Specifically, we observe that at high levels of  $TF_I$  and  $E2$ , the switch percentage rapidly decreases, reaching 0. This confirms the absence of cell cycle transition, further

strengthening the previously presented results.

In the parameter sensitivity analysis,  $kms$  and  $kmd$  exhibited significant fluctuations in average switch time (Figure 10(c)).  $kms$  is associated with reaction  $R_1$ , which regulates the amount of active transition regulator, essential for the transition switch. The active transition regulator inhibits the active form of the inhibitor. In this study, high  $kms$  values correlate with a lower average switch time, indicating a strong downregulation of the active inhibitor form. Conversely, low  $kms$  values are associated with a higher cell cycle transition time. The opposite behaviour is observed for  $kmd$ .  $kmd$  influences reaction  $R_4$ , the reverse of  $R_1$ , which is influenced by  $kms$ . As expected, high  $kmd$  values correlate with higher average transition times, and low  $kmd$  values correlate with lower average switch times. Complementary results are highlighted in the switch percentage plot (Figure 10(d)). High  $kms$  values correlate with a 100% switch percentage, signifying a strong downregulation of the active inhibitor. Conversely, low  $kms$  values cause strong inhibitor activation, decreasing the cell cycle transition rate. The opposite effect is observed for  $kmd$ .

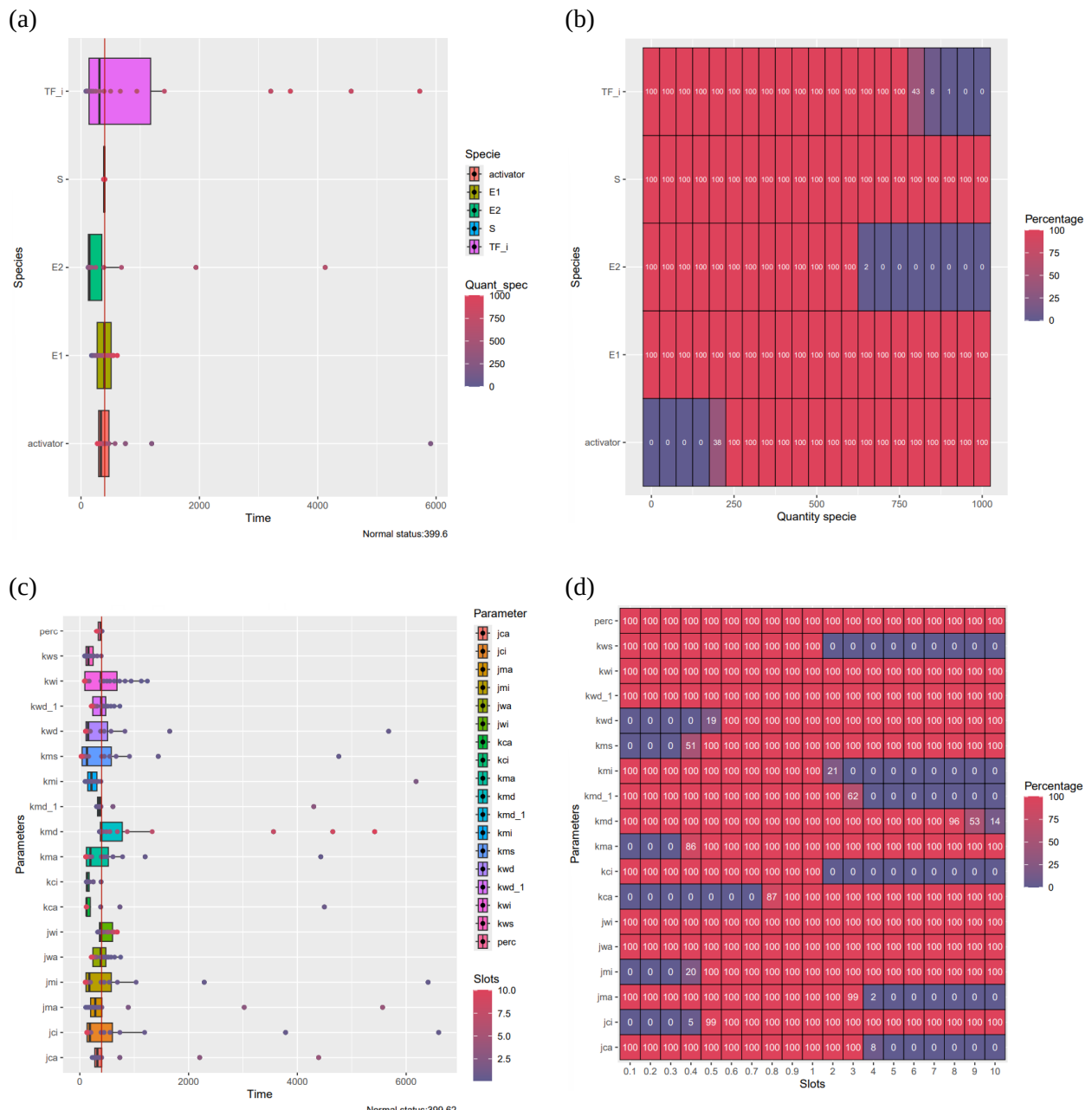


**Figure 10. Sensitivity analysis plots for the  $I_1$  model.** Panel (a) and (b) represent the sensitivity plot for the species while panels (c) and (d) represent the parameters' behaviour.

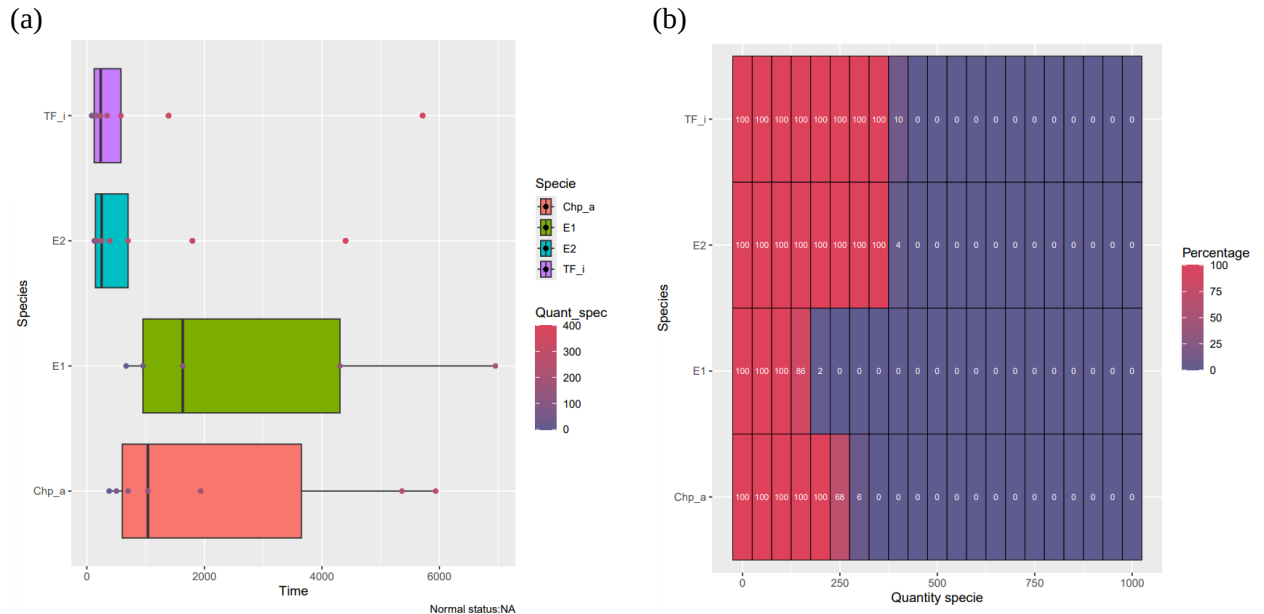
## $I_{I^A}$ model

The observed trends (Figure 11(a)) slightly differ from those observed in the two previous models. While similar trends for  $TF_I$ ,  $Chp_A$ , and  $E2$  are observed at high species levels,  $E1$  requires particular consideration.  $E1$  is the enzyme that activates the inhibitor. In this analysis, it is evident that low  $E1$  levels correlate with a lower average switch time. This is expected, as lower  $E1$  levels result in less active inhibitor. Conversely, high  $E1$  levels correlate with a higher average switch time.

Furthermore, the switch percentage for these species in Figure 11(b) reinforces the observed trends. Specifically, focusing on  $E1$ , the switch percentage rapidly decreases at high  $E1$  levels. The plot confirms the absence of cell cycle transition at high levels of  $E1$ ,  $E2$ ,  $Chp_A$ , and  $TF_I$ , further strengthening the previously presented results.

In the parameter sensitivity analysis (Figure 11(c)),  $jcp_8$  and  $jwa$  exhibited significant fluctuations.  $jcp_8$ , previously highlighted in the  $I_{I^B}$  model, demonstrates identical fluctuations here.  $jwa$  is a parameter associated with reaction  $R_6$ , which regulates the conversion of inactive inhibitor to its active form, effectively the degradation of inactive inhibitor. In this analysis, high  $jwa$  values result in a lower average switch time. Specifically,  $jwa$  appears in the denominator of the reaction rate equation, meaning that higher  $jwa$  values lead to a lower reaction rate, resulting in less active inhibitor and consequently, lower transition times.

Similar results are highlighted in the switch percentage plot (Figure 11(d)). The behavior of  $jcp_8$  is consistent with previous observations. High  $jwa$  values result in a higher switch percentage, reinforcing the observed trend in average switch time.



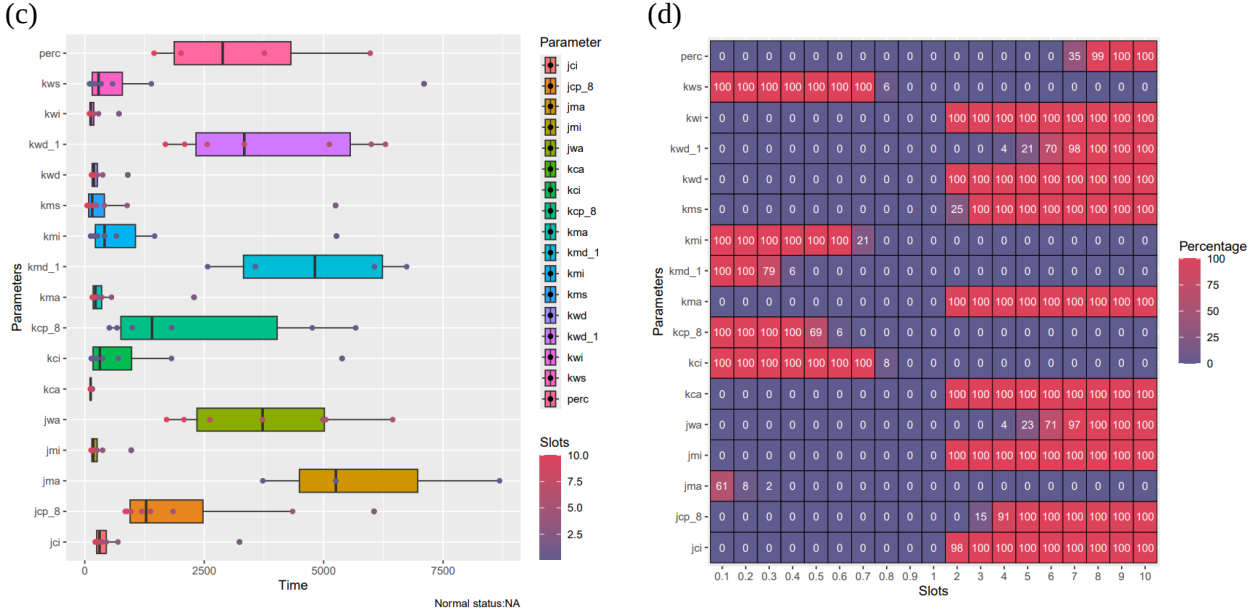


**Figure 11. Sensitivity analysis plots for the  $I_i^B$  model.** Panel (a) and (b) represent the sensitivity plot for the species while panels (c) and (d) represent the parameters' behaviour.

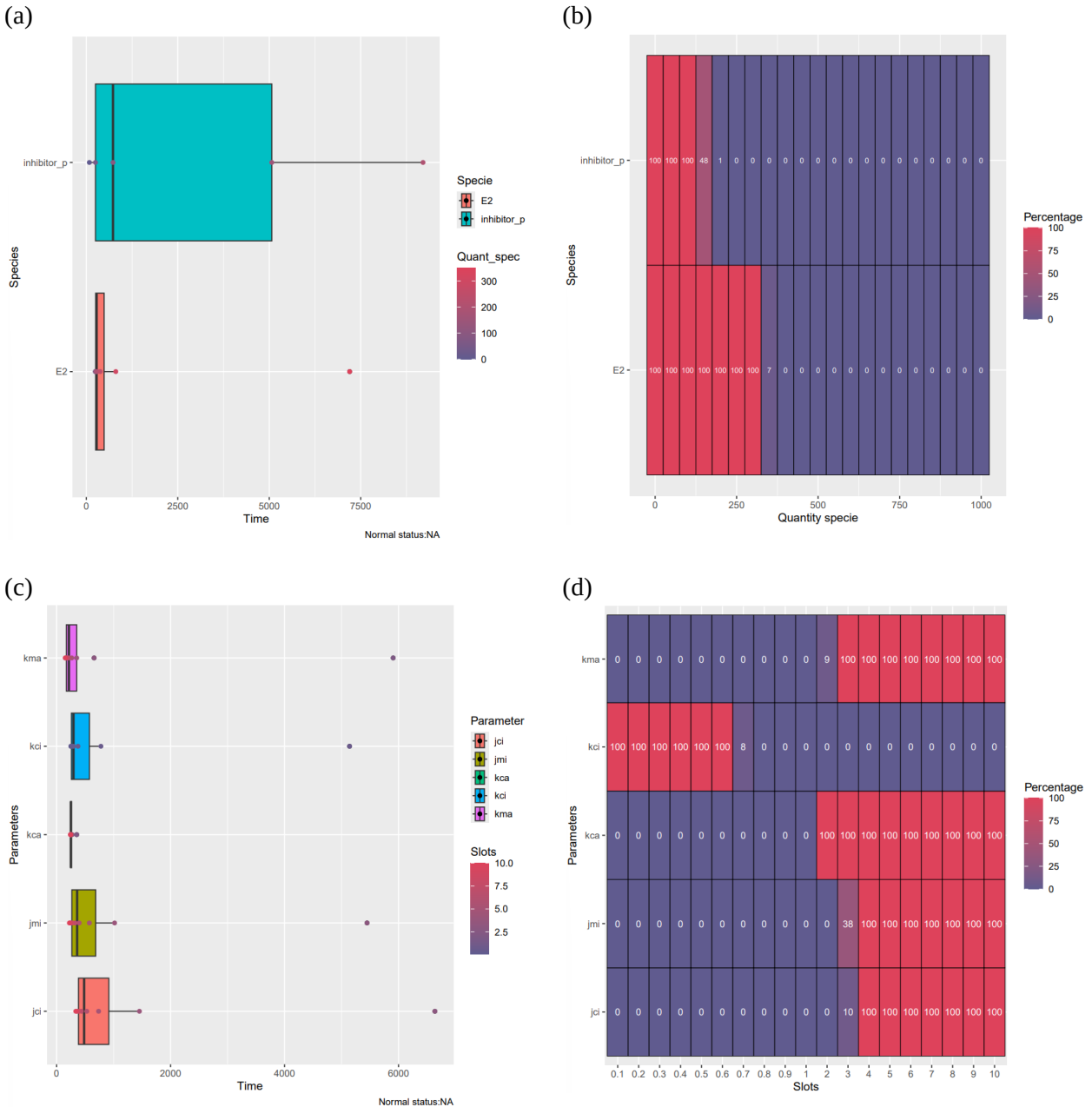
### $I_A^I$ model

Figure 12(a) presents two species,  $E2$  and  $inhibitor\_p$ , whose input significantly impacts the average switch time.  $E2$ , as previously explained, is the enzyme that regulates the transition from active to inactive activator. Its overall average switch time deviates slightly from the normal state, and at high levels ( $> 700$ ), increased average switch times are observed. Indeed, elevated  $E2$  levels reduce the amount of active activator required for the G2/M transition, thereby impacting the average switch time. A similar behavior is observed for  $inhibitor\_p$ , the active form of the inhibitor. Higher active inhibitor levels result in higher average switch times, as expected.

The switch percentage for these species, presented in Figure 12(b), reinforces the observed trends. Higher levels of  $inhibitor\_p$  and  $E2$  are associated with a lower switch percentage, indicating that the G2/M transition is impaired in these cases.

In the parameter sensitivity analysis (Figure 12(c)),  $jci$  and  $kma$  are worth noting.  $jci$  influences reaction  $R_{14}$ , inversely regulating the effect of  $E2$  on the transition from active to inactive activator. As expected, higher  $jci$  values result in a lower  $R_{14}$  rate, leading to reduced deactivation of active activator and consequently, lower average switch times.  $kma$  exhibits a similar behavior.  $kma$  regulates the transition from inactive to active transition regulator, which is required to activate the transition switch. As expected, higher  $kma$  values result in lower average transition times.

Consistent results are highlighted in the switch percentage plot (Figure 12(d)). The behaviors of  $kma$  and  $jci$  align with previous observations. High  $kma$  and  $jci$  values result in a higher switch percentage, reinforcing the observed trend in average switch time.



**Figure 12. Sensitivity analysis plots for the  $I_A^1$  model.** Panel (a) and (b) represent the sensitivity plot for the species while panels (c) and (d) represent the parameters' behaviour.

## **I<sub>A</sub><sup>A</sup> model**

The sensitivity analysis presented in Figure 13(a) shares similarities with what is observed in the  $I_A^1$  model. Once again  $E2$  and *inhibitor\_p*, are highlighted and follow a similar trend to what was previously observed. Furthermore,  $E1$  can be highlighted, whose input significantly impacts the average switch time.  $E1$  activates the inhibitor and, as seen for the  $I_A^1$  model, low  $E1$  levels correlate with a lower average switch time.

These results are highly concordant with what was observed in the switch percentage plot, presented in Figure 13(b). Indeed, higher levels of *inhibitor\_p*, *E2* and *E1* are associated with a lower switch percentage, indicating that the G2/M transition is impaired in these cases.

Among the parameters highlighted in the sensitivity analysis (Figure 13(c)), several previously discussed parameters are present, specifically  $kma$ ,  $jci$  (from the  $I_A^I$  model), and  $jwa$  (from the  $I_A^A$  model), which exhibit

their previously observed behaviors. Additionally,  $kms$ , a parameter involved in reaction  $R_1$ , which participates in the production of active transition regulator, is observed. Indeed, increased  $kms$  values result in a lower average switch time, as higher transition regulator levels are present, which are necessary to activate the G2/M transition. Conversely, lower  $kms$  values diminish the regulator levels, complicating the switch.

Consistent results are highlighted in the switch percentage plot (Figure 13(d)). High  $kms$  values result in a higher switch percentage, reinforcing the observed trend in average switch time.

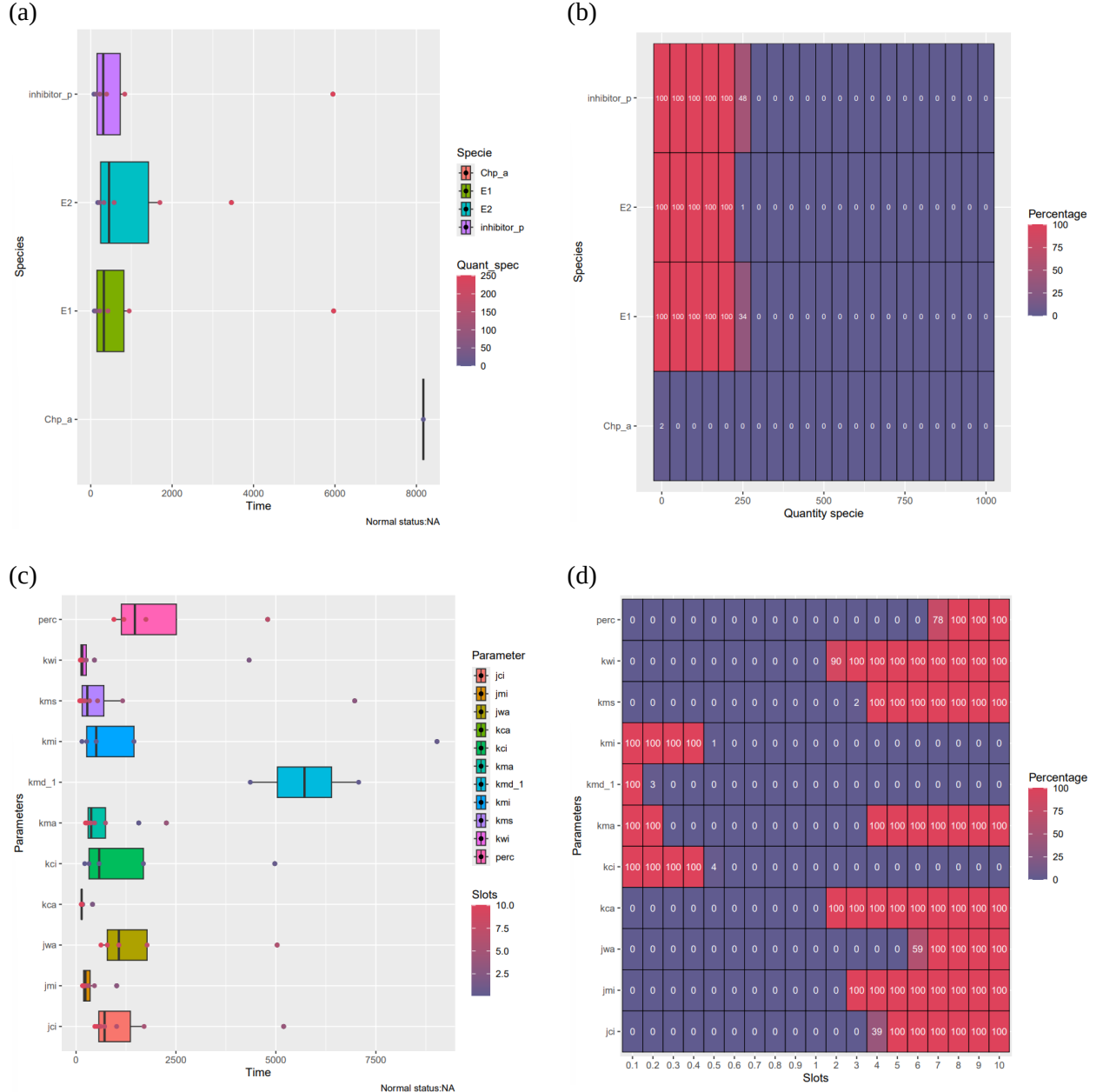


**Figure 13. Sensitivity analysis plots for the  $I_A^A$  model.** Panel (a) and (b) represent the sensitivity plot for the species while panels (c) and (d) represent the parameters' behaviour.

### $I_A^B$ model

The species behavior in the sensitivity analysis presented in Figure 14(a) shares similarities with that observed in the  $I_A^I$  model.  $E2$  and  $inhibitor\_p$  are again highlighted, exhibiting trends similar to those previously observed. Specifically,  $E2$  shows higher variability compared to  $inhibitor\_p$ . As previously discussed,  $E2$  regulates the transition from active to inactive activator. Significant fluctuations in the average

switch time are observed in this model when  $E2$  input values vary. As before, at elevated  $E2$  levels, the amount of active activator is reduced, impacting the average switch time. The switch percentage plot (Figure 14(b)) is highly consistent with the average switch time plots. High levels of  $inhibitor\_p$  and  $E2$  are associated with a lower switch percentage, indicating that the G2/M transition is impaired.

Among the parameters highlighted in the average switch time sensitivity analysis (Figure 14(c)), previously discussed parameters are present, specifically  $kma$ , observed in models  $I_A^1$  and  $I_A^A$ , which exhibit their previously observed behaviors. Additionally,  $jmi$  needs attention, as it regulates the transition from active to inactive transition regulator. Specifically,  $jmi$  is located in the denominator of the reaction rate equation, and higher  $jmi$  levels slow down the reaction. As observed, high  $jmi$  levels are associated with lower average switch times, as the transition regulator remains predominantly activated, increasing the switch probability.

This is highly consistent with the switch percentage plot (Figure 14(d)). High  $jmi$  levels are associated with a higher switch percentage, as the transition regulator remains in the active form and is not deactivated. Conversely, low  $jmi$  levels lead to strong deactivation of the transition regulator, preventing the switch.

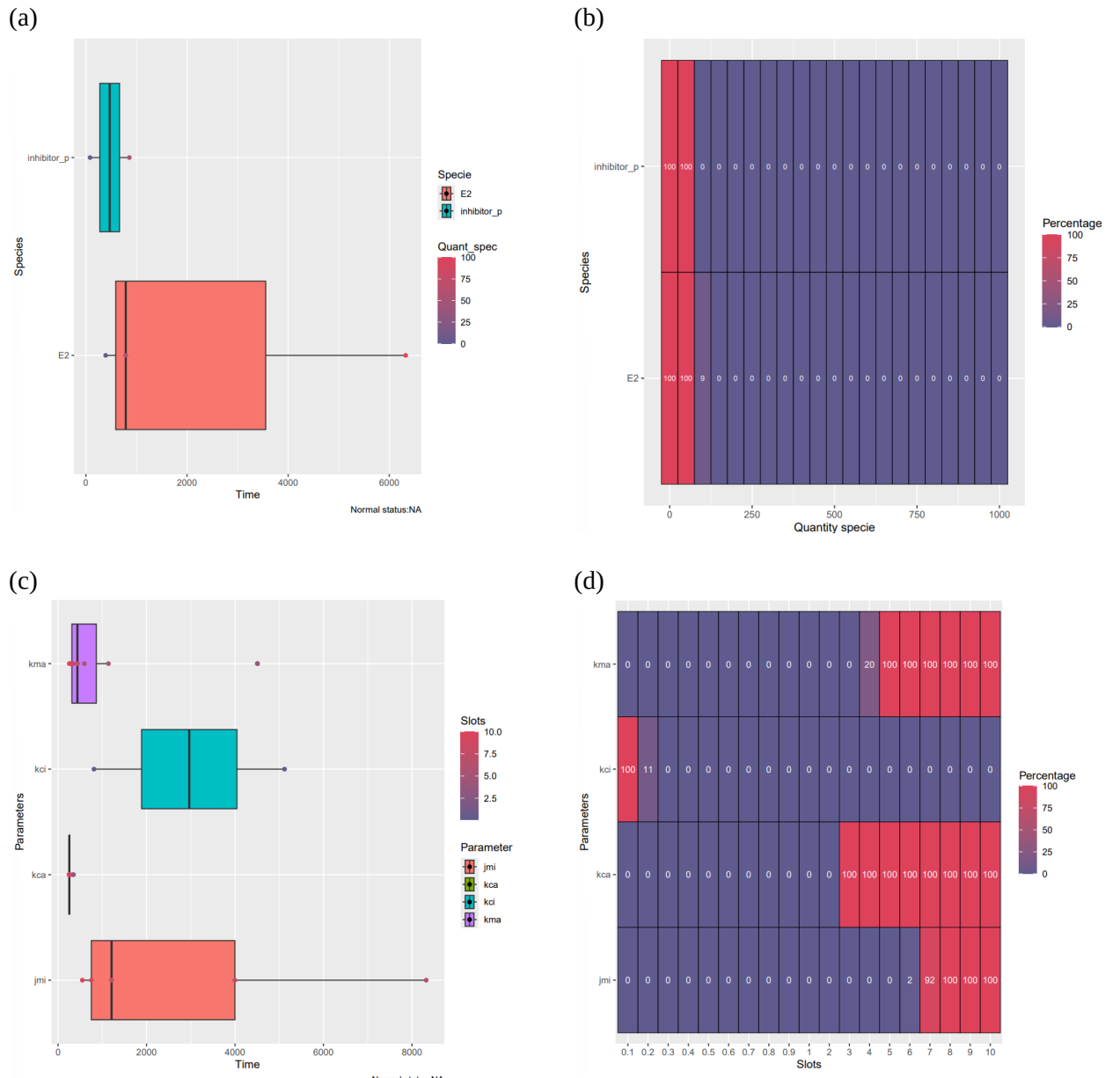


**Figure 14. Sensitivity analysis plots for the  $I_A^B$  model.** Panel (a) and (b) represent the sensitivity plot for the species while panels (c) and (d) represent the parameters' behaviour.

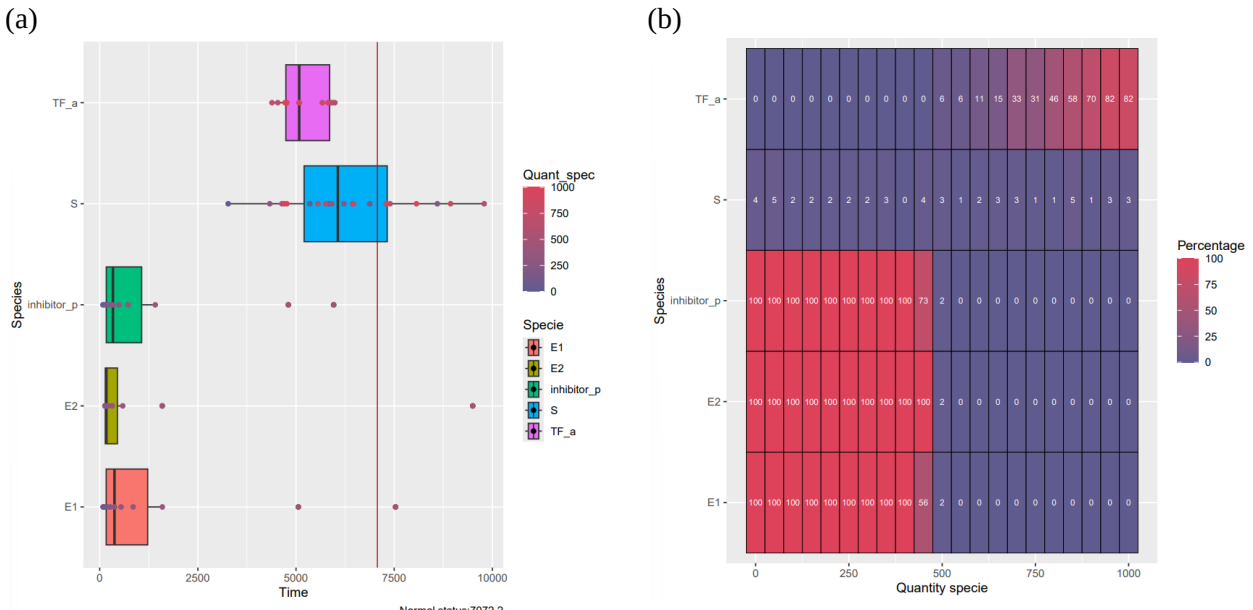
## I<sub>A</sub> model

Figure 15(a) presents the average switch time plots for the sensitivity analysis, revealing similarities to previously observed models. *E2*, *inhibitor\_p*, *E1*, and *TF\_a* are again highlighted, exhibiting their previously described behaviors. Notably, species *S*, representing a signal capable of activating the activator, displays highly variable behavior. It is difficult to determine precisely whether its impact on switch time is dependent on high or low *S* levels. Further investigation of *S* is needed to elucidate its role in switch time fluctuations.

The switch percentage plot (Figure 15(b)) exhibits a similar pattern. Indeed, the role of *S* fluctuations in switch percentage is unclear, and for most observed *S* levels, the switch percentage remains low, near the model's normal switch percentage state (6%).

In the average switch time sensitivity analysis (Figure 15(c)), previously discussed parameters *kma*, *jmi*, *jci*, and *jwa* are present, exhibiting their extensively explained behaviors. Additionally, *kcs* and *perc* are highlighted. *kcs* influences reaction  $R_{16}$ , controlling and positively influencing activator production. As expected, higher *kcs* levels are associated with higher activator levels, resulting in a lower average switch time. *perc* influences reaction  $R_7$ , which accelerates the transition from active to inactive inhibitor. As expected, higher *perc* levels, associated with higher inactive inhibitor levels, result in lower average switch times. The G2/M transition is favored when inhibitor levels are low.

This is highly consistent with the switch percentage plot (Figure 15(d)). High *kcs* and *perc* levels are associated with a higher switch percentage, as higher activator and lower inhibitor quantities are present, respectively.



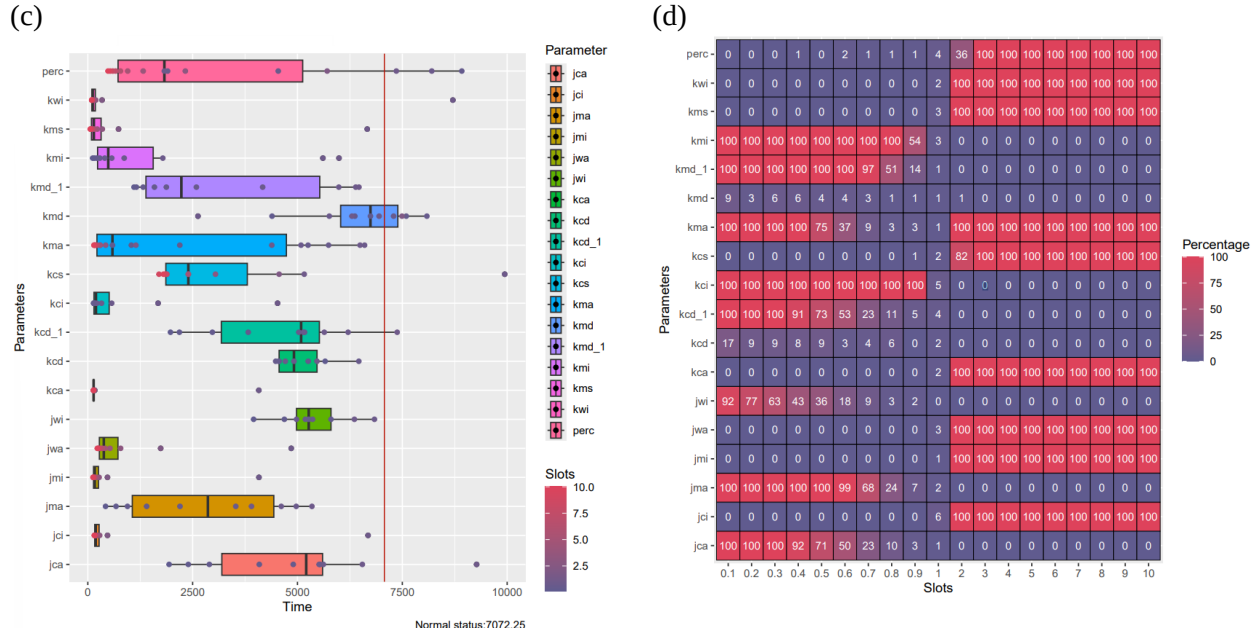


**Figure 15. Sensitivity analysis plots for the  $I_A$  model.** Panel (a) and (b) represent the sensitivity plot for the species while panels (c) and (d) represent the parameters' behaviour.

### $I_I^I$ model

The sensitivity analysis for the average switch time, presented in Figure 16(a), highlights  $E2$  as highly influential for switch time fluctuations. Consistent with previous models,  $E2$  regulates the transition from active to inactive activator. As expected, high  $E2$  levels, which correlate with lower active activator levels, result in a higher average switch time, delaying the G2/M transition.

The switch percentage plot (Figure 16(b)) exhibits a similar pattern, reinforcing the observations regarding  $E2$ . Specifically, high  $E2$  levels are associated with a delay and impairment of the G2/M transition.

In the average switch time sensitivity analysis (Figure 16(c)), previously discussed parameters, such as  $kma$  and  $kms$ , exhibit their expected behaviors. Additionally,  $jma$  and  $jca$  are highlighted.  $jma$  influences reaction  $R_2$ , which regulates the transition from inactive to active transition regulator. Specifically,  $jma$  inversely regulates this transition, with higher  $jma$  levels leading to lower active transition regulator levels. As observed in the sensitivity analysis, high  $jma$  levels are associated with higher average switch times. Similarly,  $jca$  regulates the form of the activator. High  $jca$  levels correlate with increased inactive activator, while low  $jca$  levels result in high active activator levels. This is consistent with the sensitivity analysis, where high  $jca$  levels are associated with higher transition times, as less active activator is available for the G2/M transition.

This is highly consistent with the switch percentage plot (Figure 16(d)), where high  $jca$  and  $jma$  levels are associated with a lower switch percentage, as lower active transition regulator and active activator quantities are present, respectively.

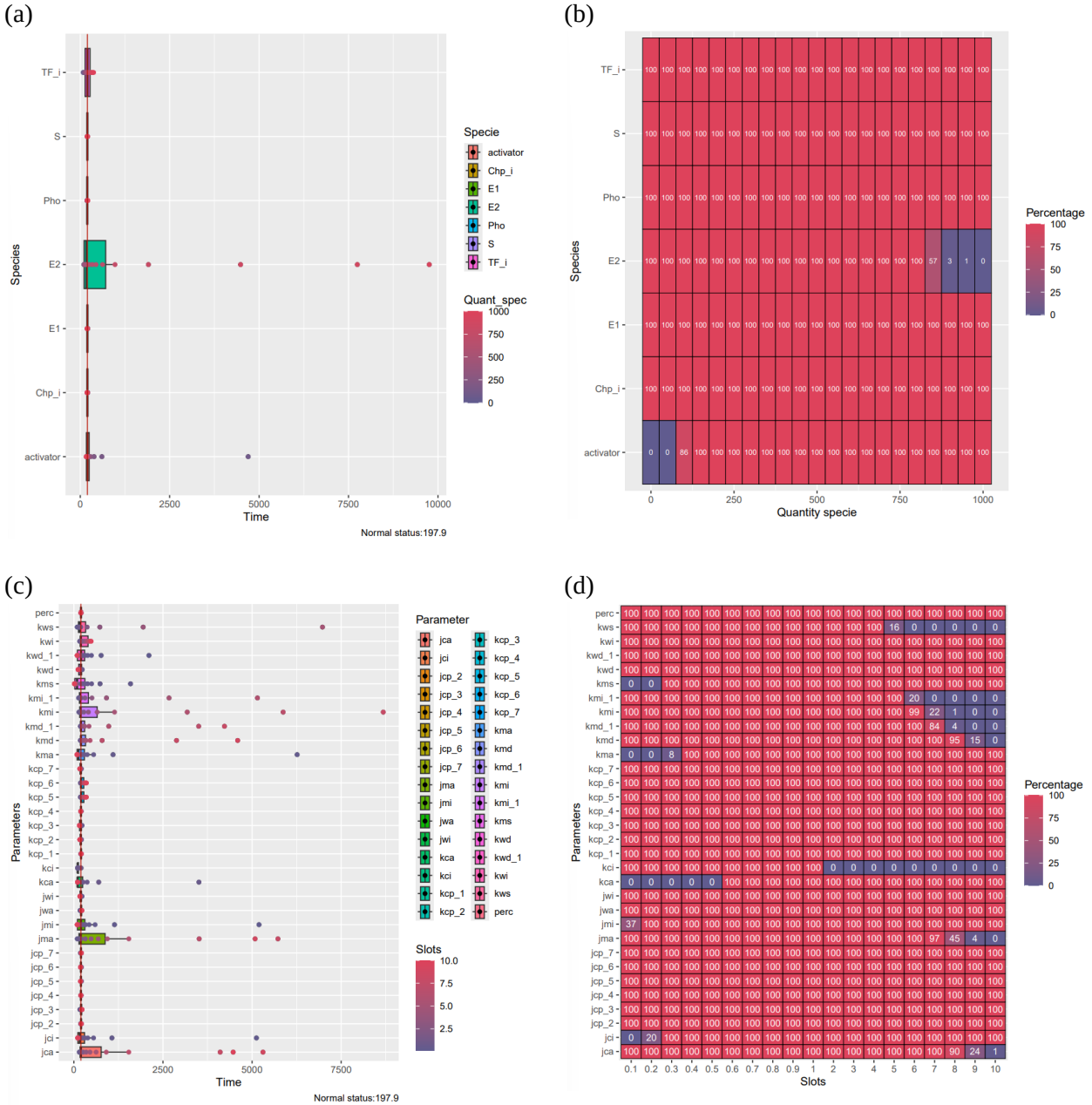


**Figure 16. Sensitivity analysis plots for the  $I_1^I$  model.** Panel (a) and (b) represent the sensitivity plot for the species while panels (c) and (d) represent the parameters' behaviour.

Subsequent models will be analyzed using a broader approach, focusing on species that induce significant fluctuations in both average switch time and switch percentage. This analysis will categorize models into two primary groups: those featuring a positive feedback loop on the activator, and those featuring positive feedback loops on both the activator and the inhibitor

### Positive feedback loop on the activator models

The sensitivity analyses (Appendix Fig. S23) for the average switch time highlight three main species significantly impacting model output fluctuations (switch time):  $E_2$ ,  $inhibitor\_p$ , and  $activator$ .  $E_2$  regulates the transition from active to inactive activator. Consistent with observations from positive feedback loop inhibitor models, high  $E_2$  levels, which correlate with lower active activator levels, result in a higher average switch time, delaying the G2/M transition. A similar behavior is observed for  $inhibitor\_p$ , the active form of the inhibitor. As expected, higher levels of active inhibitor correlate with higher average switch times, as the

inhibitor acts by inhibiting the G2/M transition. Conversely, higher *activator* levels correlate with lower average switch times. This is expected, as the *activator* is essential for transforming the inactive transition regulator to its active form, enabling the G2/M transition.

These results are highly consistent with the findings from the switch percentage sensitivity analysis. High *E2* and *inhibitor\_p* levels correlate with a lower switch percentage, while high *activator* levels correlate with a higher switch percentage, as expected.

Regarding the parameters, several key factors significantly impact the fluctuations of average switch time and switch percentage. Firstly, *kms* is notable. This parameter influences the reaction generating active transition regulator (*TR\_p*), which is essential for the switch and G2/M transition. As observed, high *kms* levels correlate with lower switch times and higher switch percentages. The same behavior is observed for *kca*, *jmi*, and *jci*. *kca* influences the transition from inactive to active activator. As expected, high *kca* levels correlate with lower switch times and higher switch percentages, as higher activator levels enable transition regulator activation. *jmi* influences the transition from active transition regulator (*TR\_p*) to its inactive form (*TR*). *jmi* inversely regulates this transition, thus high *jmi* levels correlate with higher active transition regulator levels. As observed in the sensitivity analysis, high *jmi* levels correlate with lower switch times and higher switch percentages, as *TR\_p* is essential for the G2/M transition. *jci* influences the transition from active to inactive activator. *jci* inversely regulates this transition, thus high *jci* levels correlate with higher active activator levels. The sensitivity analysis confirms that high *jci* levels correlate with lower transition times and higher switch percentages, as active activator is essential for transition regulator activation and the G2/M transition. Furthermore, *jma*, influencing the transition from inactive to active transition regulator, significantly impacts model fluctuations. *jma* inversely regulates this transition, thus high *jma* levels correlate with lower *TR\_p* levels, causing a delay in average switch time, as observed in the sensitivity analysis. Additionally, high *jma* levels correlate with lower switch percentages.

### **Positive feedback loop on both the activator and the inhibitor models**

Results similar to those observed in previous models are evident. Specifically, the species sensitivity analysis (Appendix Fig. S24) highlights previously observed behaviors. *E2* and *inhibitor\_p* are again highlighted for their significant impact on switch time and switch percentage fluctuations. Furthermore, *TF\_A* is highlighted. *TF\_A* represents the transcription factor of the activator, and as expected, high *TF\_A* levels are associated with higher activator levels, as the transcription factor contributes to activator production. The sensitivity analysis demonstrates that high *TF\_A* levels correlate with lower average switch times and higher switch percentages. This is expected, as the activator is essential for activating the transition regulator, enabling the G2/M transition.

Regarding the parameters, previously observed parameters are again highlighted. Specifically, *kms*, *jmi*, *jma*, and *jci* exhibit their previously described behaviors. Additionally, the parameter sensitivity analysis highlights *kma*, which influences the transition from inactive to active transition regulator, essential for the G2/M transition. Indeed, the sensitivity analysis demonstrates that higher *kma* levels correlate with lower average switch times and higher switch percentages, as expected.

### **General considerations**

A generalization of the sensitivity analysis results, focusing on the impact of various species on mean switch time and switch percentage, reveals that *E2* consistently exerts a significant influence across all models, irrespective of transcriptional control, post-transcriptional positive feedback, and checkpoint activation. This observation aligns with *E2*'s role as the agent responsible for inactivating the activator. Furthermore, the analysis elucidates the impact of transcriptional control on transition dynamics. In models featuring transcriptional control of the activator, the transcription factor's quantity predominantly affects the transition when present at lower levels. Conversely, models with transcriptional control of the inhibitor exhibit a distinct pattern. Specifically, transcriptional control of the inhibitor is more impactful at lower quantities, to the extent that the switch is abolished.

Checkpoint activation demonstrates a selective influence on switch dynamics. Overall, checkpoint activation

appears to inhibit transitions primarily in models where feedback loops are exclusive to the inhibitor or present on both the inhibitor and activator. Notably, checkpoint actions on inhibitors are less impactful than anticipated. This is unexpected, as the model's structure suggests that checkpoint activation should lead to a hyperactive formation of the inhibitor, resulting in a more pronounced effect compared to its absence.

A general analysis of parameter impact across the models reveals that *kma* consistently exerts a significant influence on switch time and switch percentage, independent of transcriptional control, post-transcriptional positive feedback, and checkpoint activation. This is consistent with *kma*'s direct role in regulating the transition from the inactive to the active form of the transition regulator. As expected, elevated *kma* levels correlate with reduced average switch times and increased switch percentages, indicating an active G2/M transition. Conversely, diminished *kma* levels are associated with delayed, and in some instances, impaired or halted G2/M transitions.

Regarding the influence of transcriptional control, models with transcriptional control of the activator exhibit significant fluctuations in response to variations in *kma* and *jci*. *Jci*, which regulates the transition from the active to the inactive form of the activator, appears to be particularly influential. This behavior may stem from the activator's non-constitutive expression, rendering the model highly sensitive to reductions in the transition rate to its active form. Models featuring transcriptional control of the inhibitor do not display distinct patterns, aside from *kma*-related fluctuations.

Finally, concerning checkpoint effects, models with checkpoints on the activator or on both the activator and inhibitor show no specific patterns and exhibit overall fluctuations. In contrast, models with checkpoints solely on the inhibitor demonstrate fewer fluctuations; in approximately 50% of these models, most parameters show no fluctuations at all.

## 4.3 Human specific cell-cycle model G2/M

The generic cell cycle transition model underwent adaptation to create a human-specific version of it as much as possible, correct and functional. The G2/M transition, known for its critical role in cancer development and progression when malfunctioning, was chosen as the reference for human cell cycle model adaptation. This adaptation was informed by a comprehensive literature review to accurately represent the involved genes (Figure 17).

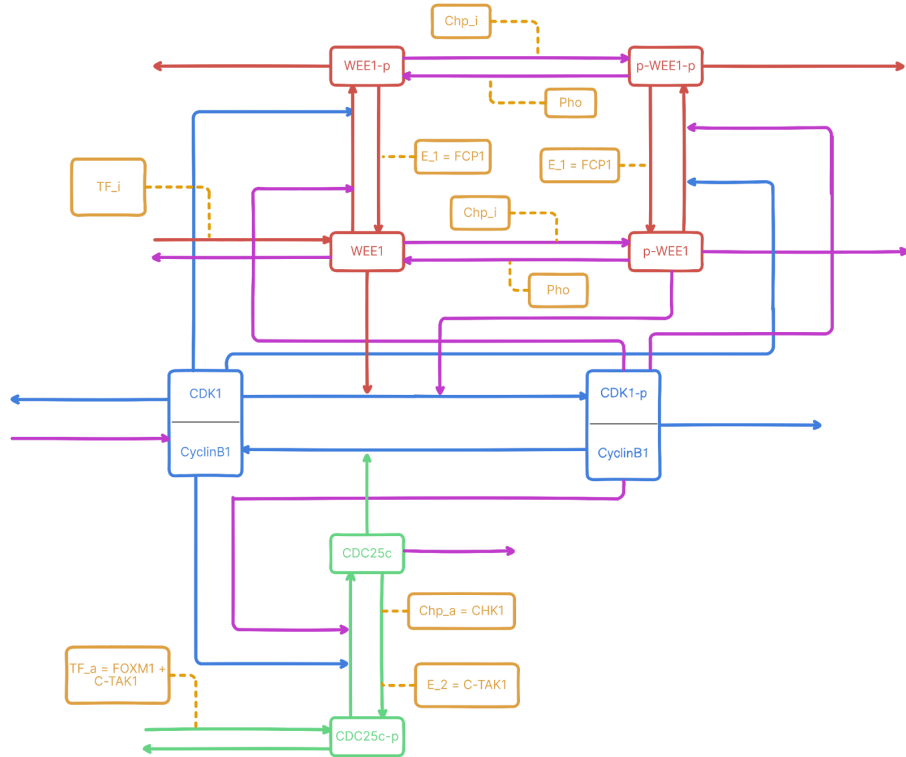


**Figure 17. Adapted cell cycle model to G2/M cell cycle transition in human.** General adapted to the information retrieved by the literature research on G2/M cell cycle transition. The basal parameters and the kinetic laws associated with the reactions are the same as the general model. In the figure are represented with color orange are the TFs, checkpoints agents, kinase and phosphatases linked to reactions they impact, whereas in green are the activator forms and its reactions, in red the inhibitor forms at the associated reactions and in blue the translational protein (which in this case is a complex) and the related reactions. It is noteworthy that the figure includes purple arrows representing interactions for which there is a lack of supporting literature. These interactions, while not empirically validated, have been introduced as necessary assumptions to ensure the model's operational integrity.

The G2/M transition constitutes a critical phase in the cell cycle, wherein the cell prepares for division<sup>240</sup>. This transition is rigorously controlled by a delicate balance of activators and inhibitors, ensuring that mitosis commences only upon completion of DNA replication and the successful repair of any DNA damage<sup>240</sup>. Key regulatory components include the Cdk1/cyclin B1 complex, Cdc25C phosphatase, and Wee1 kinase<sup>240</sup>. The process initiates with the gradual accumulation of cyclin B1 during the late G2 phase, leading to the formation of a complex with Cdk1<sup>241</sup>. This complex is maintained in an inactive state within the cytoplasm through the phosphorylation of Cdk1 on Tyr15 and Thr14, mediated by Wee1 and Myt1 kinases, respectively<sup>240</sup>. This mechanism prevents premature entry into mitosis, allowing cells to verify DNA replication fidelity via the G2/M checkpoint<sup>241</sup>. At the culmination of the G2 phase, the Cdk1/cyclin B1 complex is activated through the dephosphorylation of Tyr15 and Thr14 residues by Cdc25C phosphatases<sup>240</sup>.

Cdc25 phosphatases, particularly Cdc25C, play a pivotal role in activating the Cdk1/cyclin B1 complex by removing inhibitory phosphate groups<sup>242</sup>. Conversely, Wee1 kinase counteracts this activation by phosphorylating and inactivating the cyclin/Cdk complexes<sup>243</sup>. Specifically, Wee1 inhibits Cdk1 through phosphorylation on tyrosine 15<sup>243</sup>. These regulatory proteins are also subject to feedback loops involving the Cdk1/cyclin B1 complex, further modulating their activity<sup>244</sup>.

Wee1 regulation involves multiple mechanisms. Cdk1/cyclin B1 complexes can directly inactivate Wee1<sup>244</sup>. Cdk1-mediated phosphorylation in vitro does not directly inhibit Wee1 kinase activity<sup>244</sup>; however, T239 phosphorylation in vivo facilitates the binding of peptidyl-prolyl isomerase Pin1, which appears to inactivate the Wee box function<sup>244</sup>. Cdc25 regulation also involves intricate mechanisms. The phosphatase activity of Cdc25C increases upon phosphorylation during mitotic entry<sup>245</sup>. This phosphorylation is mediated by the Cdk1/cyclin B1 complex<sup>245</sup>. In vitro, Cdk1/cyclin B1 directly phosphorylates and activates Cdc25C. This phosphorylation and activation of Cdc25C by its substrate allows for signal amplification, contributing to the surge of Cdk1/cyclin B1 activity that propels mitosis<sup>245</sup>. Fcp1 dephosphorylates and activates Wee1<sup>246</sup>. At the conclusion of mitosis, Wee1 inhibits Cdk1 through phosphorylation of its Tyr15 residue, a process dependent on the activation of the CTD phosphatase subunit 1 (Fcp1)<sup>246</sup>. Cdk phosphorylation of S123 triggers a phosphorylation cascade involving Plk1 and CK2, leading to the creation of phosphodegrons that promote Wee1 degradation, and hyperphosphorylation can lead to decreased Wee1 activity and subsequent degradation at M phase<sup>247</sup>. Furthermore, Wee1 regulation is also subject to modulation through the DNA damage checkpoint response, as documented by *Romanel et al*<sup>187</sup>. However, unlike certain organisms, such as budding yeast, there is no literature supporting the existence of a hyperactive form of Wee1 in this context.

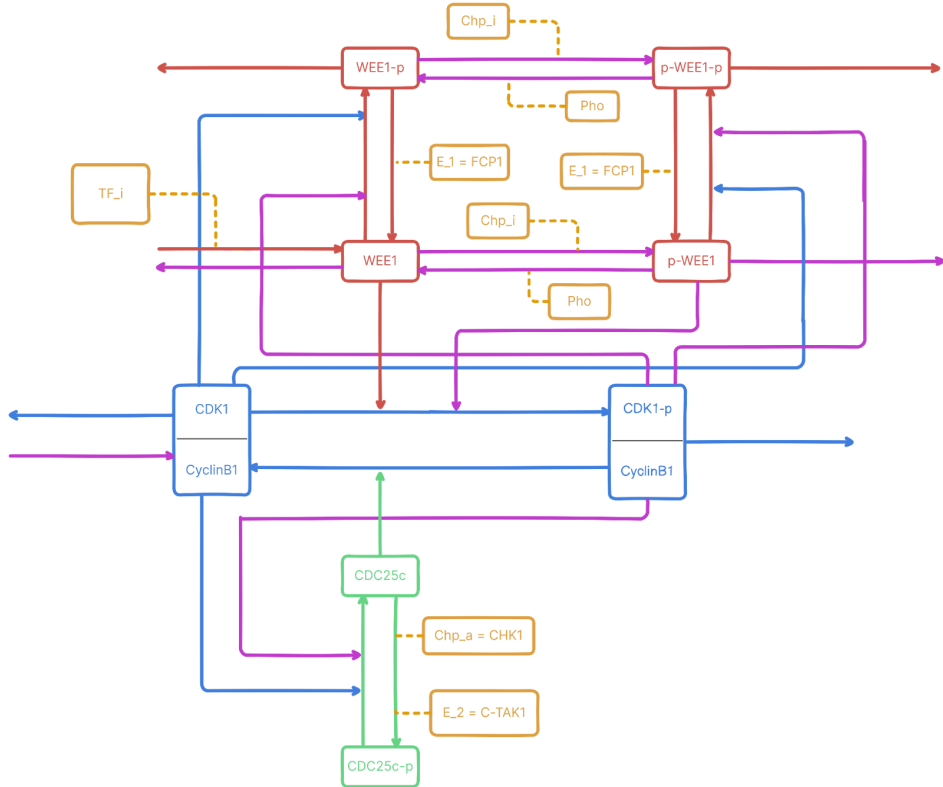
A key component of the DNA damage response pathway is Chk1 (Checkpoint Kinase 1)<sup>248</sup>. Upon DNA damage, Chk1 can phosphorylate Cdc25C, leading to its inactivation. Chk1 exerts its phosphorylation function at the Cdc25C Ser287 residue, which induces Cdc25C degradation<sup>242</sup>. Chk1-mediated phosphorylation of Cdc25C creates a binding site for 14-3-3 proteins<sup>249</sup>. This binding can sequester Cdc25C in the cytoplasm, preventing it from activating Cdk1/cyclin B1 complexes in the nucleus. This sequestration inhibits Cdk1 dephosphorylation and activation<sup>250</sup>. While Chk1-mediated phosphorylation inactivates Cdc25C as part of the DNA damage checkpoint, mechanisms involving phosphatases like PP1 and PP2A, as well as proteins like Pin1, can reverse this inactivation, restoring Cdc25C's ability to promote cell cycle progression<sup>242</sup>.

FoxM1 regulates the transcription of Cdc25C, ensuring proper progression through the G2 phase of the cell cycle<sup>251</sup>. FoxM1 directly activates the expression of Cdc25C. FoxM1 binds to cell cycle-regulated genes with peak expression in the G2/M phases. By upregulating Cdc25C, FoxM1 ensures proper progression through the G2 phase<sup>251</sup>.

It is noteworthy that imbalances in Cdc25 and Wee1 regulation have implications in tumorigenesis, indicating the clinical relevance of these regulatory mechanisms<sup>242</sup>.

As saw in the previous part and with the integration of the literature knowledge about the various regulatory mechanism governing the G2/M transition in human cell cycle but without informations on the selected genes if are periodically expressed, two sub-models were created assuming that the inhibitor or the activator are periodically transcribed (Fig. 18). These two models were then used for the downstream data integrations and analyses. The model is designed based on a conservative implementation of the transition model presented in *Romanel et al*<sup>187</sup>, providing a solid foundation for comparing our results to those reported in that study. Our model focuses on cell cycle transitions, with the G2/M transition chosen as a primary focus. A reliable reference is essential, as no definitive reference model exists in the literature. Indeed, several cell cycle models are available, each employing diverse approaches and varying levels of detail. An example is presented by the work of *Bouhaddou et al*<sup>252</sup>, which developed a sophisticated stochastic-deterministic model to simulate cell fate in response to drugs within a tumor microenvironment. This model integrates multi-omics data and comprises several sub-models, including a detailed cell cycle model. The cell cycle sub-model, derived from *Gérard et al*<sup>253</sup>, was expanded to incorporate a broader range of control pathways that regulate cell cycle progression. It is also important to note that this model can be expanded and further developed, potentially by integrating information from additional studies and integrating further levels of definition and details into the representation of cell cycle transitions.

(a)



(b)

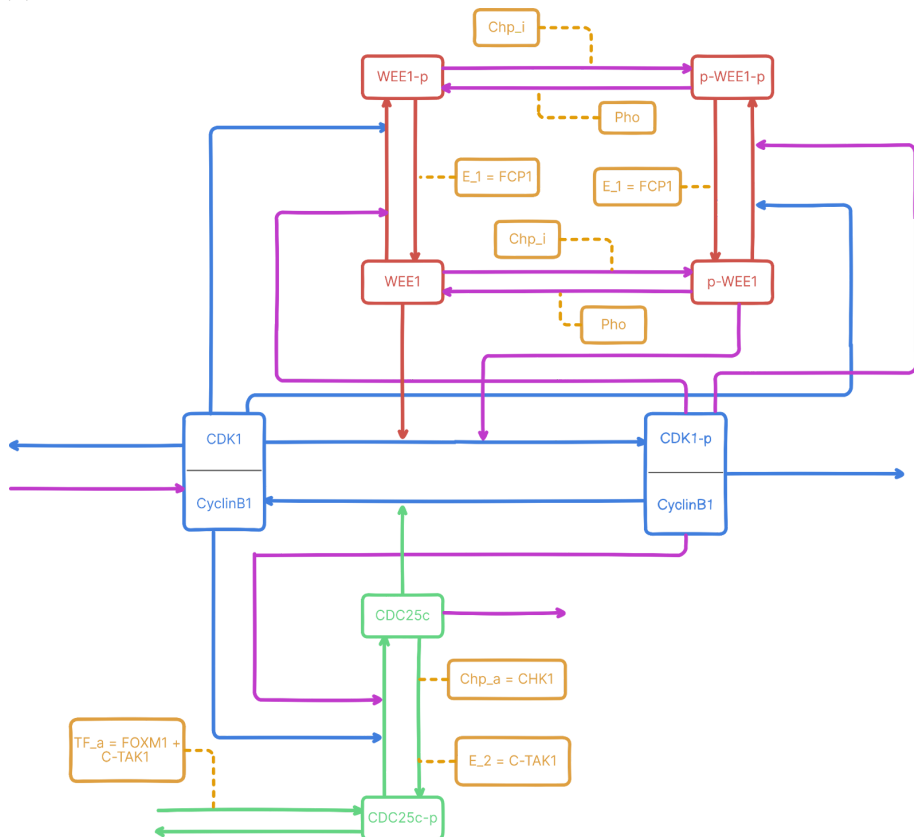


**Figure 18.Two sub-models derived by the human specific model of cell cycle G2/M transition.** Submodel (a) contains both positive feedback loops controls and checkpoints activation on both activator CDC25C and inhibitor WEE1, but the transcriptional factor only on the inhibitor ( $B_1^B$ ), whereas submodel (b) presents the same controls except for the transcriptional factor impacting only the activator ( $B_A^B$ ).

## 4.4 Integration of eQTLs data in human specific model of various tissues

We next sought the investigation of eQTLs' potential role in cell cycle transition model fluctuations. eQTLs data was integrated into the human G2/M models to elucidate the impact of these single nucleotide variants on fluctuations in average switch time and switch percentage across various tissues (Appendix Table S1).

Each eQTL tissue model was simulated 100 times, varying only one gene quantity per run before proceeding to the next gene quantity and then to a different gene. This procedure was performed to observe how genotype information alters switch time and switch percentage in the cell cycle models. Specifically, only the  $B_A^B$  and  $B_I^B$  models were simulated. The  $B_A^B$  model is characterized by feedback loops on both the activator and the inhibitor, constitutive inhibitor transcription, transcriptional regulation of the activator, and checkpoints on both the activator and inhibitor. The  $B_I^B$  model is identical to the  $B_A^B$  model, except for constitutive activator transcription and transcriptional regulation of the inhibitor.

For species regulated by multiple genes, the initial quantity for model simulation was selected in a conservative manner based on genotype-associated quantities. This involved comparing the scaled quantity values of the two genes at the same genotype status and selecting the lower of the two, reflecting a biological scenario of a limiting factor.

### $B_A^B$ model

Figure 19 presents the average switch time per species or parameter. Genotype information is encoded by symbols, and tissue information by colors. Notably, specific tissues associated with higher average switch times are observed for certain species or parameters. FOXM1 and FCP1 exhibit no significant differences in average switch time across tissues and genotypes. However, this is not the case for other species. WEE1, for instance, shows higher switch time fluctuations in several tissues, including pituitary tissue (heterozygous), skin (homozygous alternative), and brain frontal cortex (homozygous alternative). C-TAK1 similarly displays high switch time fluctuations in tissues such as the uterus (heterozygous) and thyroid (homozygous alternative). CHK1 exhibits a similar pattern in the uterus (heterozygous) and esophagus (both homozygous and heterozygous alternative). Finally, CDK1 shows high variability across several tissues, with the highest observed in the adrenal gland (heterozygous).

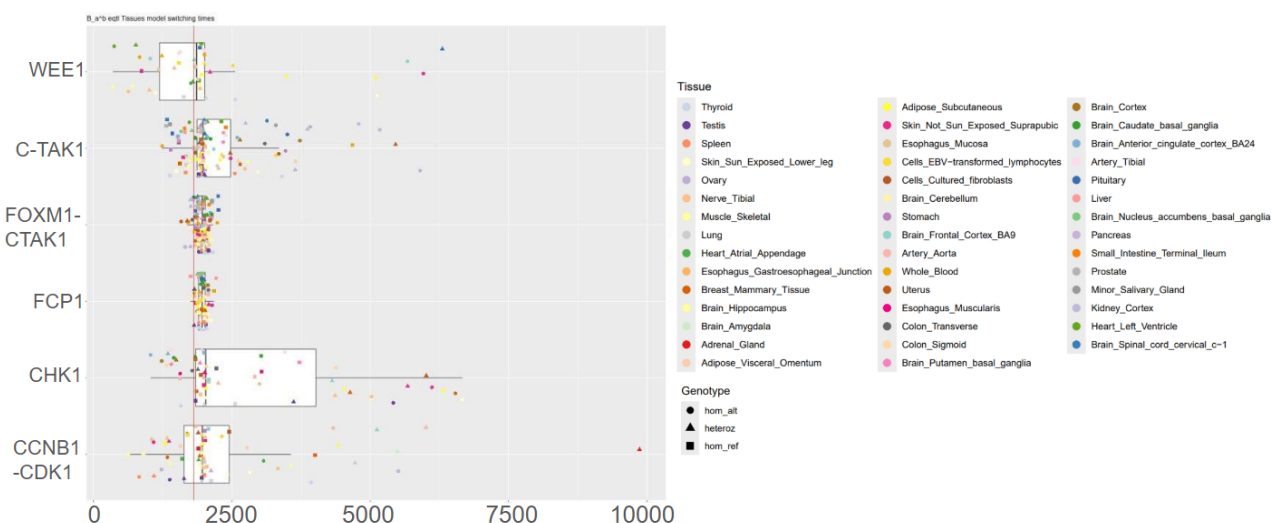
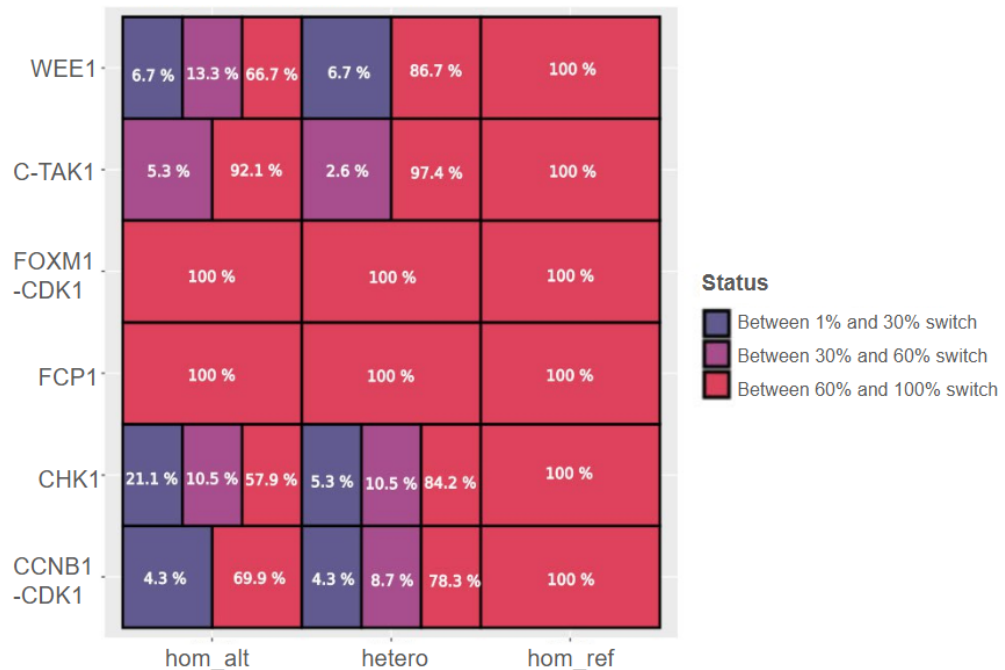


**Figure 19. Average switch time for the investigated tissues.** On the x-axis, the average switch time is depicted, on the y-axis, the several species/parameters are expressed. The symbols have been used to represent one of the three genotypes, colors are used to identify the tissues.

Figure 20 presents the switch percentage data. This plot utilizes a different approach, displaying the percentage of tissues exhibiting successful switching rather than specific tissue information. Consistent with the average switch time data, FOXM1 and FCP1 show no switch percentage fluctuations across genotypes. Similarly, all genes in the homozygous reference state exhibit 100% switching across all tissues. The majority of switch percentage fluctuations are observed in heterozygous and homozygous alternative genotypes, mirroring the trends seen in average switch time. Specifically, WEE1 shows a 6.7% tissue impairment in switch percentage under homozygous alternative conditions. CHK1, CDK1 and CCNB1 show corresponding impairments of 21.1% and 4.3%, respectively. Heterozygous cases also exhibit switch percentage impairments, though to a lesser extent, with CHK1 showing a 5.1% impairment in tissues carrying the eQTL.

Analysis reveals that the impact of eQTLs on certain genes does not consistently induce cell cycle transition switches. Specifically, WEE1, C-TAK1, CHK1, CDK1, and CCNB1 exhibit tissues where eQTLs, influencing gene expression, result in transition blockage. Notably, WEE1, C-TAK1, and CHK1 function to inhibit the transition, and eQTLs in these genes tend to cause overexpression. Conversely, eQTLs associated with CCNB1 and CDK1 generally lead to down-regulation.

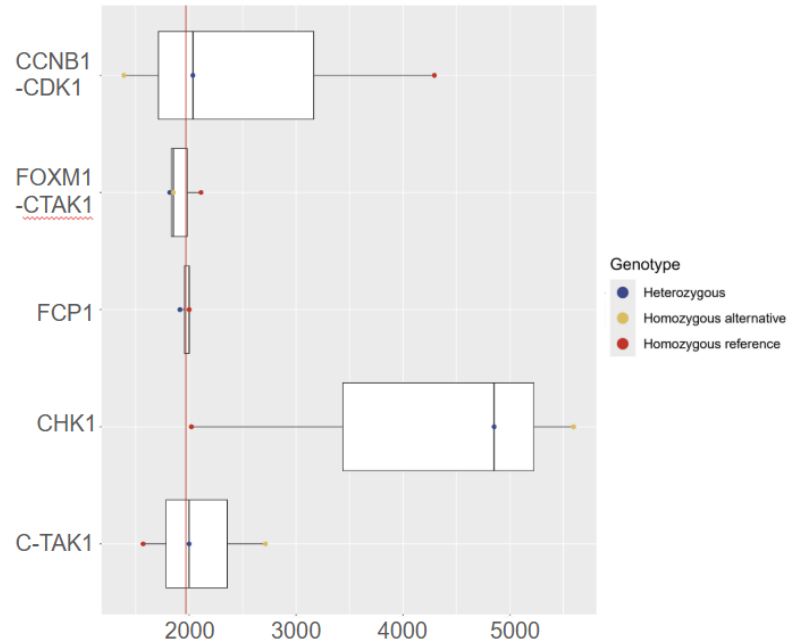
Furthermore, specific tissue-genotype interactions are observed. For instance, WEE1 eQTLs in adipose visceral omentum significantly affect the transition switch in both heterozygous and homozygous alternative genotypes. Similarly, homozygous alternative genotypes of C-TAK1 and CHK1 eQTLs impact the transition in uterine tissue. Finally, CDK1 and CCNB1 eQTLs influence the transition in stomach and esophageal gastroesophageal junction tissues, with effects observed in both or single allele instances. It is important to note that, despite these observed effects, none of these SNPs have demonstrated clinical associations within the ClinVar database<sup>254</sup>.



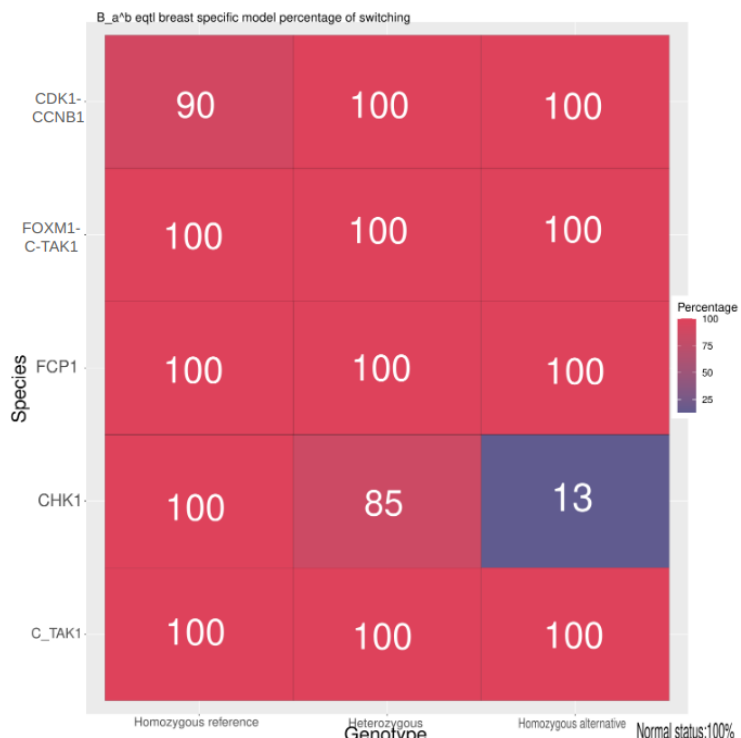
**Figure 20. Switch percentage for the investigated genotypes.** On the x-axis, the genotypes are depicted, on the y-axis, the several species/parameters are expressed. Colors represent the switch percentage while the percentages depict the percentages of tissues falling within a certain switch percentage.

Figure 21 presents the average switch time for breast tissue. This analysis was conducted to examine this tissue more closely, given its relevance to this study. As seen in the general average switch time plot, FOXM1 and FCP1 exhibit no significant switch time fluctuations. Conversely, CCNB1 and CHK1 display substantial fluctuations for the homozygous reference and homozygous alternative genotypes. Specifically, CCNB1 shows a higher switch time in the homozygous reference genotype and a lower switch time in the homozygous alternative genotype. CHK1 exhibits the opposite trend.

These observations are corroborated in Figure 22, where *CHK1* and *CCNB1* are the sole parameters for which the switch does not consistently occur, aligning with the previously noted trends. Investigation of the eQTLs associated with each gene revealed that *CCNB1* fluctuations are linked to rs28576332, an SNP causing a C>T modification in an intronic region. However, no clinical associations with this eQTL have been reported in ClinVar<sup>254</sup>. Similarly, the eQTL associated with *CHK1*, rs76118307, corresponds to an A>G modification within an intronic region.



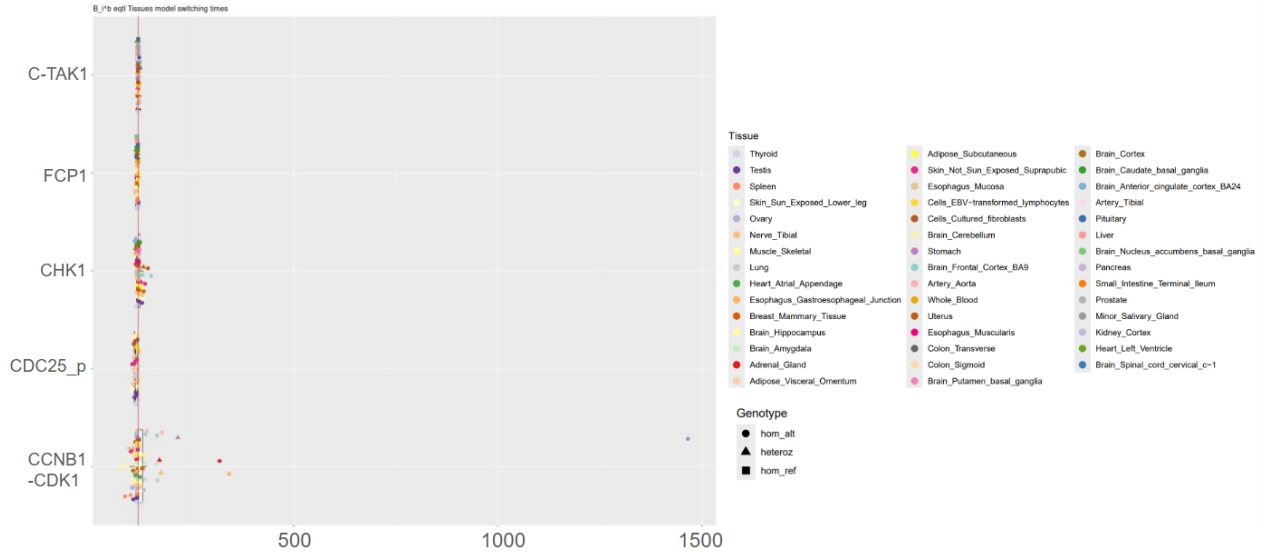
**Figure 21. Average switch time for the breast tissue.** On the x-axis, the average switch time is depicted, on the y-axis, the several species/parameters are expressed. The colors are used to identify the genotype status.



**Figure 22. Switch percentage for the breast tissue.** On the x-axis, the genotypes are depicted, on the y-axis, the several species/parameters are expressed. Colors represent the switch percentage, with the corresponding percentage value displayed in white within each cell.

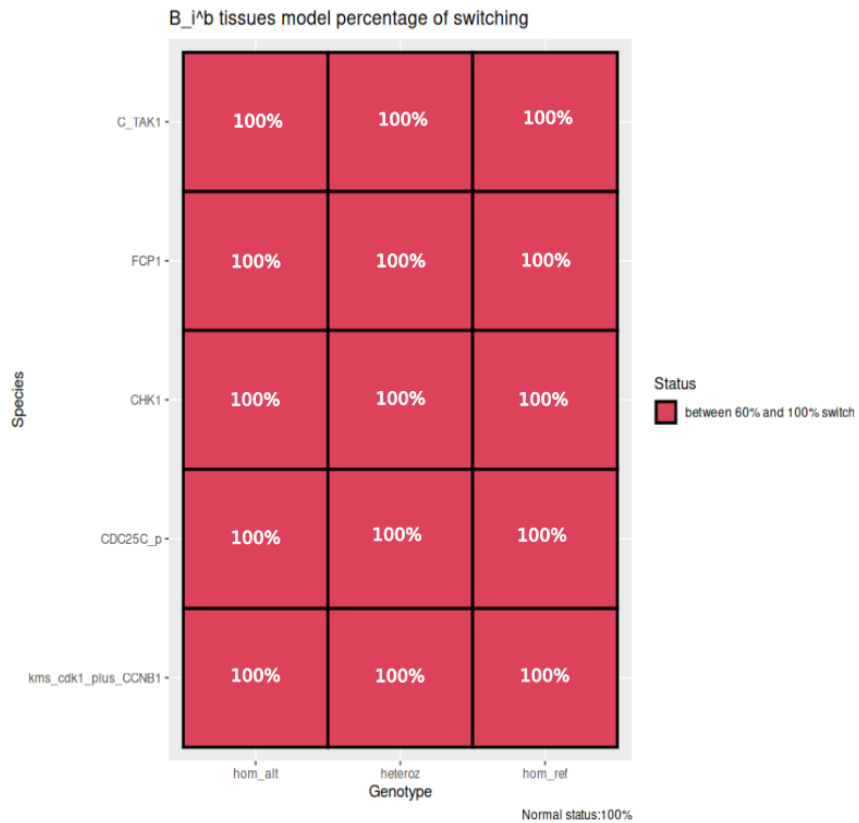
## B<sub>I</sub><sup>B</sup> model

Figure 23 illustrates the mean switch time, categorized by species or parameter. Genotype data is represented by distinct symbols, and tissue specificity is conveyed through color coding. Upon observation, significant delays in switch time are primarily evident for the CDK1 and CCNB1 species, specifically within a subset of tissues. Notably, the stomach tissue exhibits the most pronounced delay, while the esophageal gastroesophageal junction and adrenal gland tissues show moderately increased delays compared to other tissues. It is crucial to emphasize that these substantial delays are predominantly observed when the genotype in all three previously mentioned tissues is homozygous alternative.



**Figure 23. Average switch time for the investigated tissues.** On the x-axis, the average switch time is depicted, on the y-axis, the several species/parameters are expressed. The symbols have been used to represent one of the three genotypes, colors are used to identify the tissues.

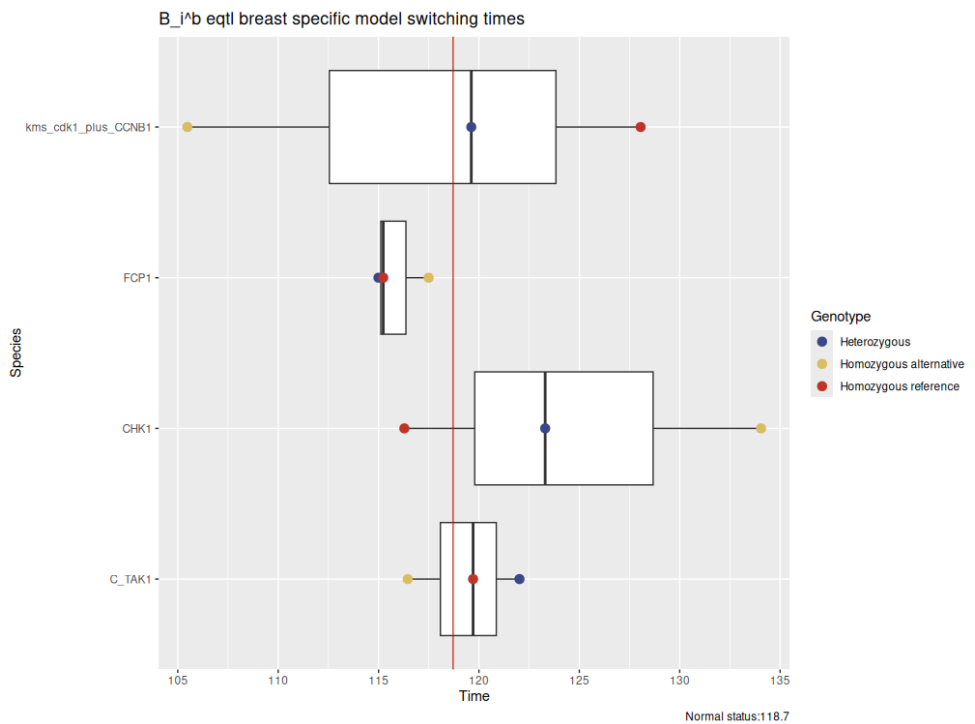
Figure 24 illustrates the switch percentage data, presenting the proportion of tissues demonstrating successful switching, rather than individual tissue details. Due to the 'GO' system characteristic of this model, and consistent with the average switch time data, all genes exhibited complete switching (100%) across all tissues, independent of genotype.



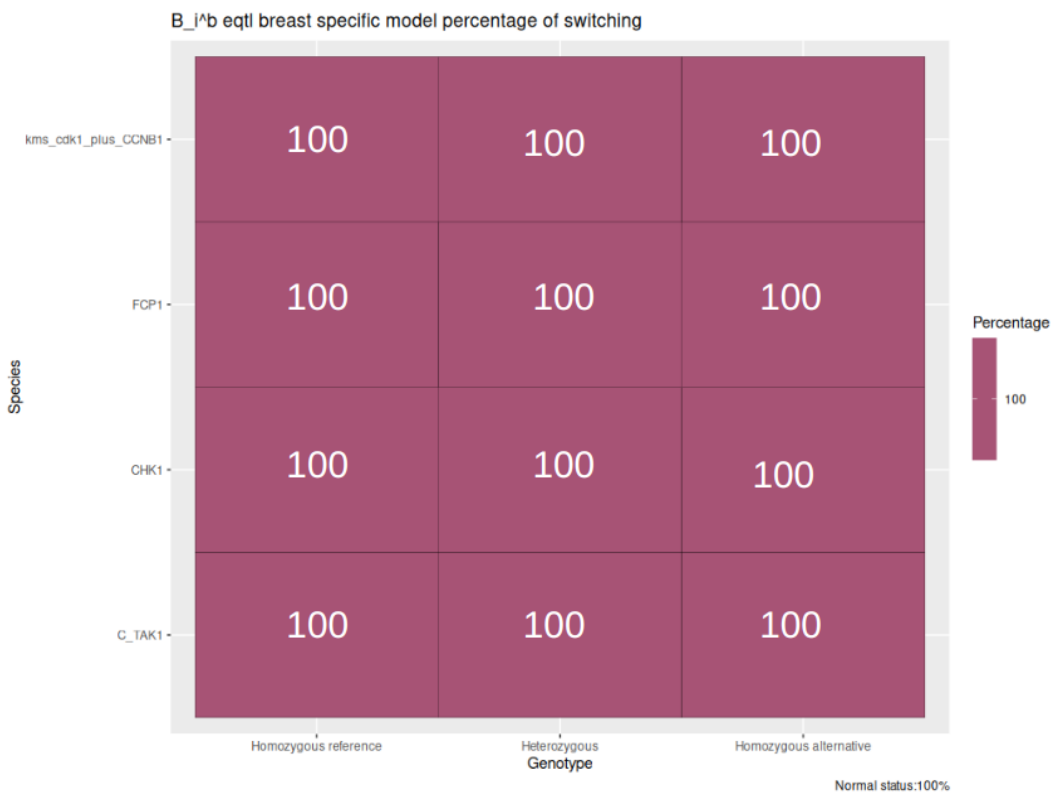
**Figure 24. Switch percentage for the investigated genotypes.** On the x-axis the genotypes are depicted, on the y-axis, the several species/parameters are expressed. Colors represent the switch percentage while the percentages depict the percentages of tissues falling within a certain switch percentage.

Figure 25 displays the average switch time for breast tissue, a tissue analyzed in detail due to its relevance to this study. While visual fluctuations are observed, particularly for CCNB1 and CHK1, the actual time differences compared to the normal average switch time are minimal. This observation aligns with the results obtained from the broader tissue comparison, and is further emphasized by the B<sub>A</sub><sup>B</sup> model, which exhibits significantly more pronounced time step variations.

These findings are corroborated by examination of Figure 26, which displays a heatmap of switch percentages in mammary breast tissue across the three genotypes. The heatmap indicates that the model consistently achieves switching, irrespective of genotype, thereby confirming the presence of the transcriptional regulator on the inhibitor, indicative of a 'GO' system.



**Figure 25. Average switch time for the breast tissue.** On the x-axis, the average switch time is depicted, on the y-axis, the several species/parameters are expressed. The colors are used to identify the genotype status.



**Figure 26. Switch percentage for the breast tissue.** On the x-axis the genotypes are depicted, on the y-axis, the several species/parameters are expressed. Colors represent the switch percentage, with the corresponding percentage value displayed in white within each cell.

This study examined the impact of eQTLs on cell cycle gene expression, specifically in heterozygous and homozygous alternative genotypes across various tissues, to determine if significant fluctuations occur. Results from the B<sub>A</sub><sup>B</sup> model indicate that, compared to the homozygous reference genotype, eQTL presence

in either heterozygous or homozygous alternative states generally correlates with transition delays in specific tissues. These delays are characterized by increased average switch times and decreased switch percentages, in some cases completely blocking the transition. This aligns with the understanding that eQTLs directly influence gene expression of target genes, often tissue-specifically, through variations in transcription factors and regulatory elements. In contrast, the  $B_1^B$  model did not demonstrate impactful gene fluctuations that would impede transition.

When the analysis was conducted specifically on breast tissue for both models, fluctuations related to CHK1 and C-TAK1 were observed, although the magnitude differed between the two models. Interestingly, CCNB1 showed an inverse relationship in both models, but again with different magnitudes. In both cases, the homozygous alternative genotype was linked to decreased switch times, indicating faster G2/M transitions. This homozygous alternative genotype was associated with higher CCNB1 expression, which correlates with faster G2/M transition, as CCNB1 encodes for CyclinB1, a component of the transition regulator complex. However, even in the  $B_1^B$  model, these fluctuations did not impede the transition.

Additionally, it would be valuable to examine whether populations carrying these eQTL exhibit specific disadvantages in breast cancer onset, given that CCNB1 is significantly overexpressed in various cancer types, including ER+ breast cancer<sup>255</sup>. Conversely, CHK1, it would be insightful to investigate whether populations carrying associated eQTLs exhibit an advantage in breast cancer onset, as lower transition rates are observed when these eQTLs impact one allele or even both. Indeed, CHK1 is observed to be overexpressed in breast cancer<sup>256,257</sup>, highlighting the importance of understanding the role of eQTLs in breast tissue.

## 4.5 Integration in human specific model of breast cancer copy number data

Somatic copy number alterations are well-established as significant contributors to cancer development<sup>258</sup>, including breast cancer<sup>259</sup>. Therefore, we aimed to investigate the impact of these variations on our cell cycle transition model. Specifically, somatic copy number alterations data from breast cancer were integrated into the human G2/M model to assess the effect of these alterations on fluctuations in average switch time and switch percentage.

To ensure the validity of integrating copy number data, we first performed a linear regression analysis. Following the extraction of G2/M cell cycle genes of interest from a dataset containing both gene expression information and somatic copy number aberrations for each cancer patient (Figure 27), this analysis aimed to determine the presence of a correlation between SCNA and gene expression levels, a relationship that has been demonstrated in numerous prior studies<sup>219</sup>.

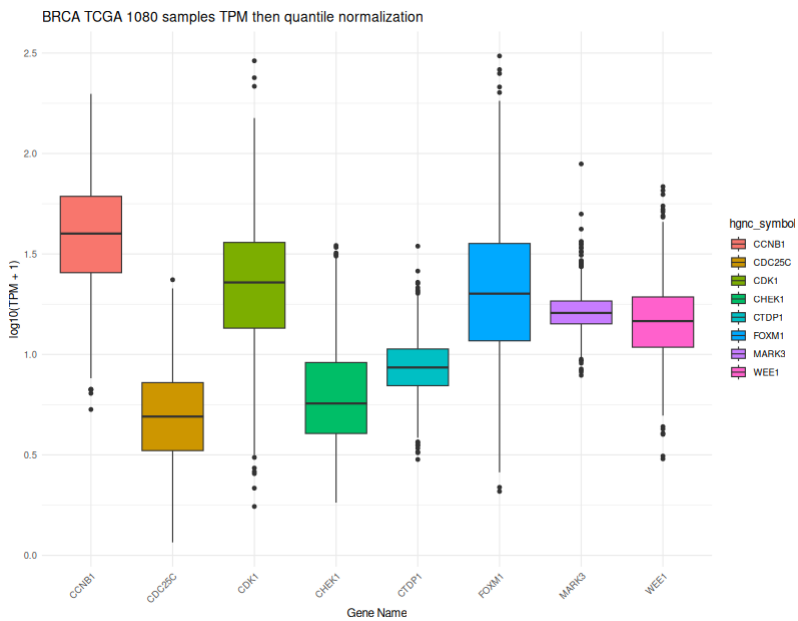


**Figure 27. Transcriptome expression across the gene of interest of G2/M cell cycle transition in human.**

The linear regression analysis revealed no observed impact for *CDC25C* and *CCNB1* (Cyclin B1 gene), as evidenced by non-significant p-values. Conversely, the remaining genes exhibited statistically significant linear correlations, with p-values consistently below  $1 \times 10^{-15}$ , although the  $R^2$  values ranged from 0.08 to 0.45. As an example, the linear regression for *MARK3*, the gene encoding C-TAK1, is presented in Figure 28.

Thus, excluding *CDC25C* and *CCNB1*, the other genes displayed a statistically significant linear correlation. The linear regression formula was subsequently utilized to adjust model parameters. In a diploid state, the quantity of each species was maintained at 500, representing the normal status. For genes where copy number information was available, values were scaled according to the respective somatic copy number alterations.

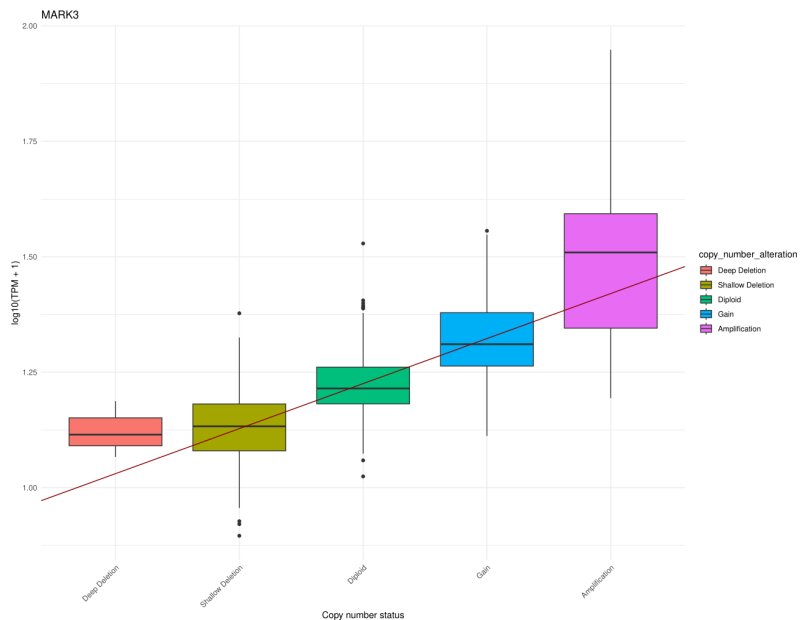


**Figure 28. Linear regression MAPK3.** Linear correlation between normalized gene expression data and somatic copy number status of MAPK3

For each of the two sub-models representing the human-specific G2/M cell cycle transition, the values of the various species were scaled to assess the impact of SCNA, related to breast cancer, on the simulated G2/M transition. It is important to note that a simplification was applied to the model featuring transcriptional control on the activator. Specifically, given that the formation of the *CDC25C*-p species is regulated by both *FOXM1*, which governs the transition, and C-TAK1, which phosphorylates *CDC25C*, the values were scaled

according to copy number status in a conservative manner. This involved comparing the scaled values of the two genes at the same copy number status and retaining the lower of the two, reflecting a biological scenario of a limiting species.

To investigate the impact of somatic copy number aberrations on cell cycle model behavior, each gene was simulated 100 times. During these simulations, only one gene quantity was varied per run before proceeding to the next gene quantity and then to a different gene. This procedure was implemented to observe how changes in gene expression, resulting from SCNAs, alter switch time and switch percentage within the cell cycle models. Specifically, simulations were performed using only the  $B_A^B$  and  $B_I^B$  models. The  $B_A^B$  model is characterized by feedback loops on both the activator and the inhibitor, constitutive inhibitor transcription, transcriptional regulation of the activator, and checkpoints on both the activator and inhibitor. The  $B_I^B$  model is identical to the  $B_A^B$  model, except for constitutive activator transcription and transcriptional regulation of the inhibitor. Consequently, fluctuations in average switch time and switch percentage were analyzed with respect to the somatic copy number alterations to observe the effects of these changes on our model's behavior (Figure 29 and 30).

In the model featuring transcriptional control linked to the activator (Figure 29), plausible results are observed, consistent with the model's design. For instance, a 'positive' modification in the copy number of genes associated with inhibition correlates with a delay in the average switch time and a decrease in the percentage of switch occurrences, potentially leading to the absence of transition in the cell cycle model. Conversely, a 'negative' modification in the copy number of genes related with the inhibitor leads to an easier transition. Furthermore, when 'positive' modifications are applied to genes that promote cell cycle progression, the inverse is observed: an increase in gene expression leads to a quicker transition compared to the normal state, whereas a decrease in expression results in a delay in the switch.

Furthermore, it is observed that presence of SCNA in *FCP1*, the gene responsible for the transition of the inhibitor to its active form, exhibit limited impact. This is likely attributable to the sub-model's configuration, wherein the inhibitor's quantity remains relatively static and is primarily inactivated by the positive feedback loop of the CDK1-CyclinB1 complex. While these results are consistent with the model's design, they are not immediately intuitive when considering the context of a cancerous environment. It is well-established that cancer often dysregulates the cell cycle by inhibiting factors that normally block progression and enhancing factors that promote transition<sup>260-262</sup>. However, based on the data retrieved and the model's output, this pattern is not evident, at least within this specific sub-model.

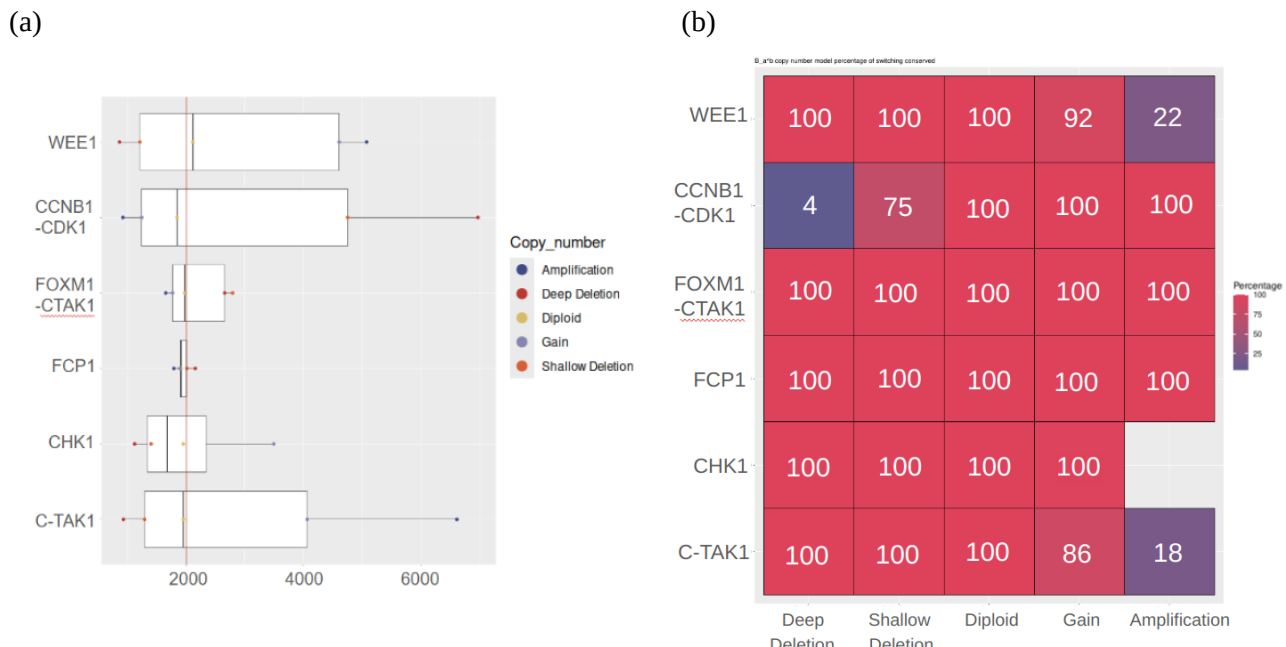


**Figure 29. SCNA analysis of the first sub-model.** This model presents both positive feedback loops controls and checkpoints activation, but the transcriptional factor impacts only the activator. (a) Average switch time and (b) switch percentage.

Conversely, in the model featuring transcriptional control only on the inhibitor (Figure 30), the results differ. Indeed, it is observed that changes in the copy number of genes related to the model do not impact the possibility of transition; a switch consistently occurs, confirming the 'GO' system as previously described. It is also noticeable that only the gene *CDK1*, which is directly related to the quantity of CDK1-cyclinB1 complex, has a slight impact on the switch time. Delays increase when expression is lower due to decreased copy numbers, while a quicker switch occurs with increased copies of this gene.

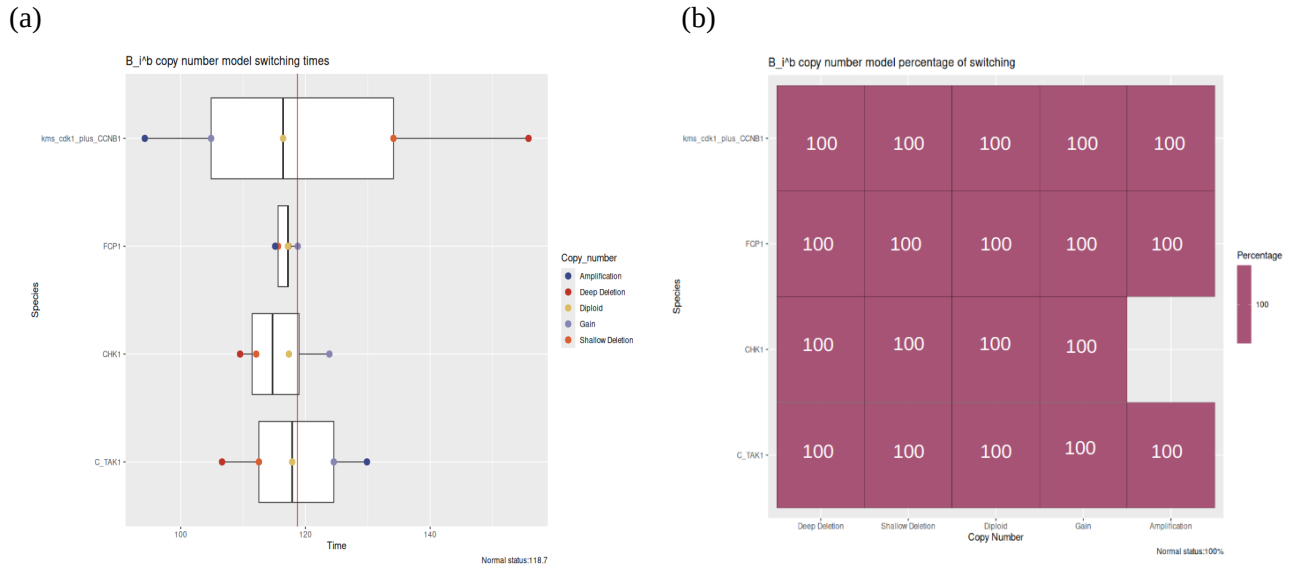


**Figure 30. SCNA analysis of the second sub-model.** This model presents both positive feedback loops controls and checkpoints activation, but the transcriptional factor impacts only the inhibitor. (a) Average switch time and (b) switch percentage.

Within the STOP model, *CDK1*, *MARK3*, and *WEE1*—encoding cyclin-dependent kinase 1, C-TAK1 kinase, and *WEE1* kinase, respectively—are identified as critical genes influencing the human G2/M cell cycle transition. Upregulation of *CDK1* is associated with a decrease in average switch time, while downregulation results in delays relative to normal average switch times. Conversely, *MARK3* and *WEE1*, which encode C-TAK1 kinase (responsible for CDC25C inhibition) and *WEE1* kinase (the inhibitor of the CDK1-CyclinB1 complex), exhibit an inverse relationship. Specifically, downregulation of *MARK3* and *WEE1* correlates with decreased switch times, whereas upregulation leads to delays in average switch time.

The upregulation of *CDK1* has been implicated in various cancers<sup>263</sup>, including breast cancer<sup>264</sup>, where it is associated with poorer patient survival outcomes<sup>264</sup>. Although a direct correlation between *MARK3* and cancer was not identified, overexpression of CDC25C, which is inhibited by C-TAK1, is associated with various cancers<sup>265</sup>, including breast cancer<sup>266</sup>. Furthermore, multiple studies have reported *WEE1* downregulation in breast cancer<sup>246</sup>.

Similar to eQTL models, output fluctuations were primarily observed in STOP systems. In contrast, GO models exhibited a more standard behavior, resembling normal conditions, with no extreme fluctuations. Notably, both eQTL and SCNA models in the STOP system showed a consistent pattern for C-TAK1 and *CDK1-CCNB1*. Specifically, higher *CDK1-CCNB1* expression (due to heterozygous or homozygous alternative eQTLs or gain/amplification SCNAs) correlated with decreased transition times and increased switch percentages.

## 4.6 Patient-specific data into human-specific model and survival analysis

Patient-specific cell cycle transition models were generated by integrating breast cancer somatic copy number data. This study aimed to determine if this integration was feasible and, specifically, to investigate whether these models could identify distinct patterns or predict differences in overall survival (OS) between patient groups. The ultimate goal was to utilize the model's dynamic behavior, particularly output fluctuations, to characterize patients.

The  $B_A^B$  model was selected for this analysis. Despite a literature review failing to establish definitive information regarding the periodic expression of either the inhibitor or activator during the cell cycle, this model was chosen due to its heightened sensitivity to variations. This selection is further justified by the G2/M checkpoint's role in regulating mitosis entry, the prevalence of aberrant mitosis in cancer<sup>267</sup>, and the assumptions outlined in *Romanel et al.*<sup>187</sup> concerning the classification of 'STOP' and 'GO' systems.

The distributions of patients' mean switch time and switch percentage were examined. Distribution plots revealed a bimodal distribution for both metrics, suggesting the presence of two distinct patient groups. In both cases, thresholds for separating these groups were determined using K-means clustering with two output clusters. Figure 31 depicts the distributions of patients' mean switch time and switch percentage, clearly illustrating the two identified groups. Specifically, for mean switch time, a threshold of 3290 was established, creating two groups: one with mean switch times less than or equal to 3290, and another with mean switch times greater than 3290. Similarly, for switch percentage, a threshold of 55 was used to create two groups.

The frequency of the somatic copy number aberrations associated with the investigated genes across the four identified groups is detailed in Appendix Tables S2. Notable differences were observed between the groups defined by average switch time and switch percentage. Specifically, frequency variations were primarily found for CDK1, mainly in shallow deletion SCNAs, and WEE1, mainly in gain SCNAs.

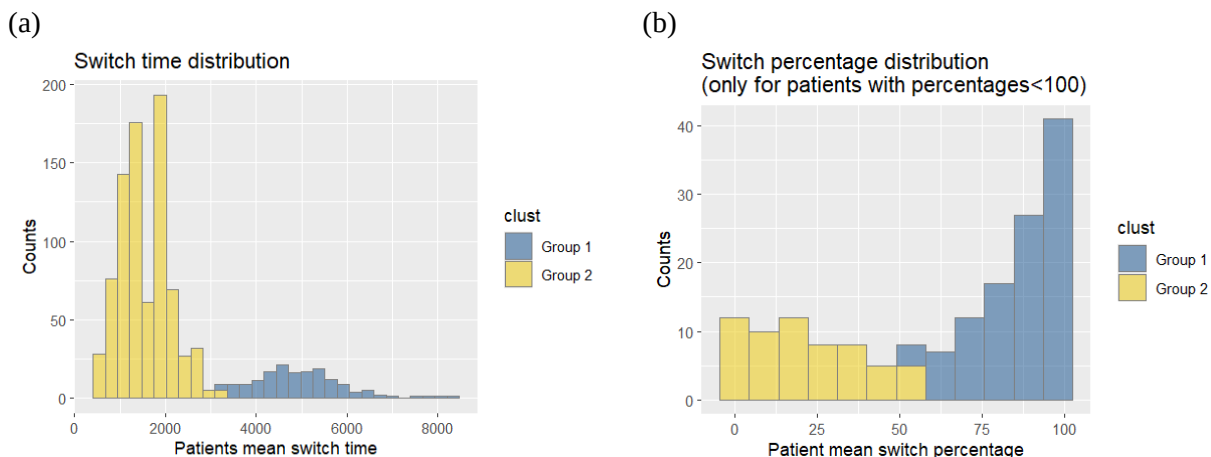


**Figure 31. Distribution plots of the patients' switch time (a) and the switch percentage (b).** A bimodal distribution for both cases can be observed, with a clear division among the two groups identified from K-clustering.

To investigate potential group-specific biological differences, we analyzed clinical data from The Cancer Genome Atlas (TCGA). Specifically, we examined Overall Survival (OS) to evaluate whether the two groups display significant differences in cancer aggressiveness and patient prognosis.

Survival analysis was performed on the identified patient groups, examining mean switch time and switch percentage while adjusting for patient age and subtype. Figure 32 displays the Kaplan-Meier plots generated from this analysis. In both cases, statistically significant differences were observed between the investigated groups. Figure 32(a) illustrates the impact of mean switch time. A statistically significant difference in survival probability was found between patients with mean switch times greater than 3290 and those with

mean switch times less than or equal to 3290, with the latter group exhibiting higher survival probability. A longer switch time indicates a delay in cell cycle transition, specifically the G2/M transition, suggesting slower cell cycle progression. Uncontrolled cell cycle progression is a hallmark of cancer. Therefore, we hypothesize that a slower cell cycle transition correlates with a better prognosis, as uncontrolled tumor growth may be slowed. Similar results were observed for patients with switch percentages lower than 55 (Figure 32(b)). The switch percentage reflects the number of times, out of 100 simulations, that the G2/M transition was observed. Since cell cycle transitions are fundamental for cell cycle progression, the same rationale applies. We hypothesize that a delay in cell cycle progression is beneficial for these patients' survival.

A recent study by *Bhattarai et al.*<sup>268</sup> demonstrated that cell cycle traverse rate can predict long-term outcomes in breast cancer patients. Cell cycle traverse rate (CCTR) measures the movement of a cell through the cell cycle, indeed, rapidly dividing cells tend to accumulate more aberrations, leading to faster tumor growth and more aggressive tumors overall. These findings are consistent, to some extent, with our analysis. Although we did not directly measure CCTR, we hypothesize that the faster G2/M transitions observed in a subset of our cohort (group 1, defined from k-clustering for mean switch time and switch percentage) correlate with poorer survival, which aligns with the observations of *Bhattarai et al.*<sup>268</sup>. This suggests that faster cell cycle transitions are indicative of more aggressive tumors. Notably, numerous studies highlight therapies targeting the G2/M transition<sup>269,270</sup>. These studies demonstrate that such therapies can inhibit cell proliferation by downregulating the G2/M transition, resulting in G2/M arrest and tumor growth suppression. This reinforces the significance of our results, as we observed a clear association between delayed cell cycle transitions and higher survival probability.

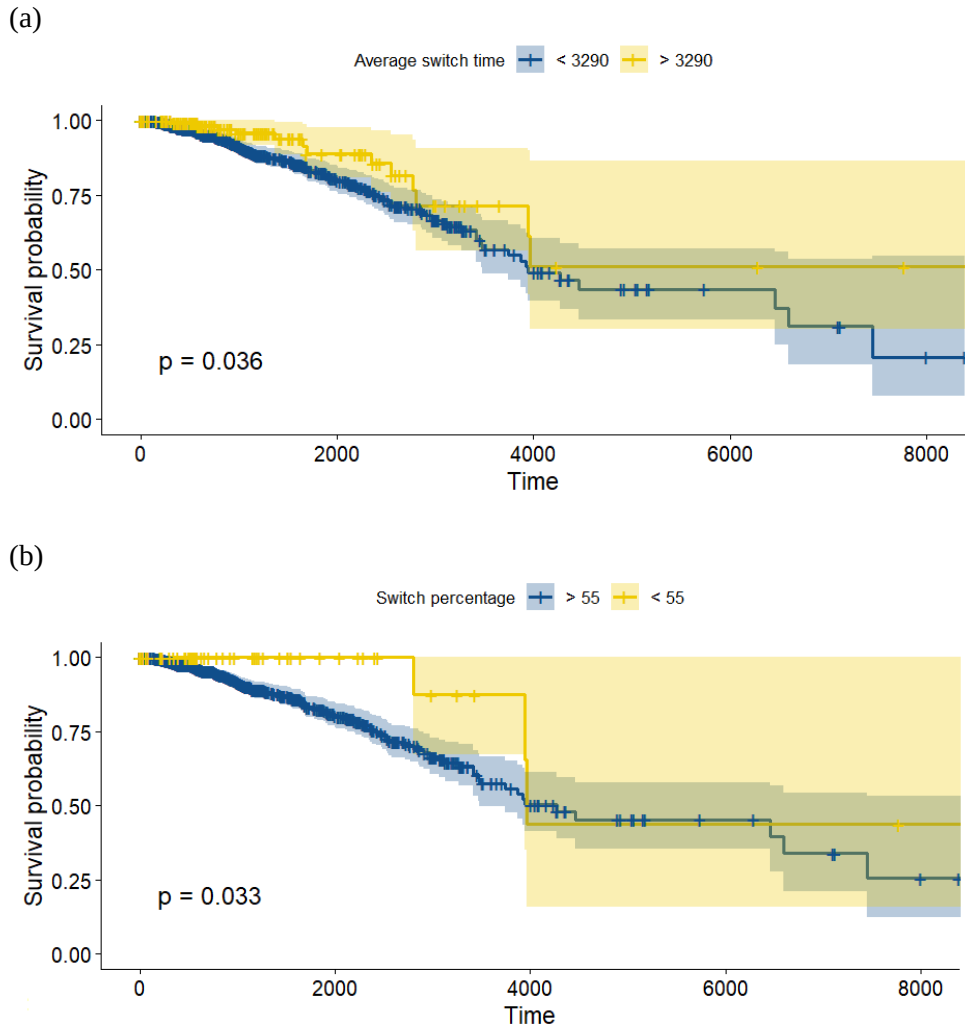
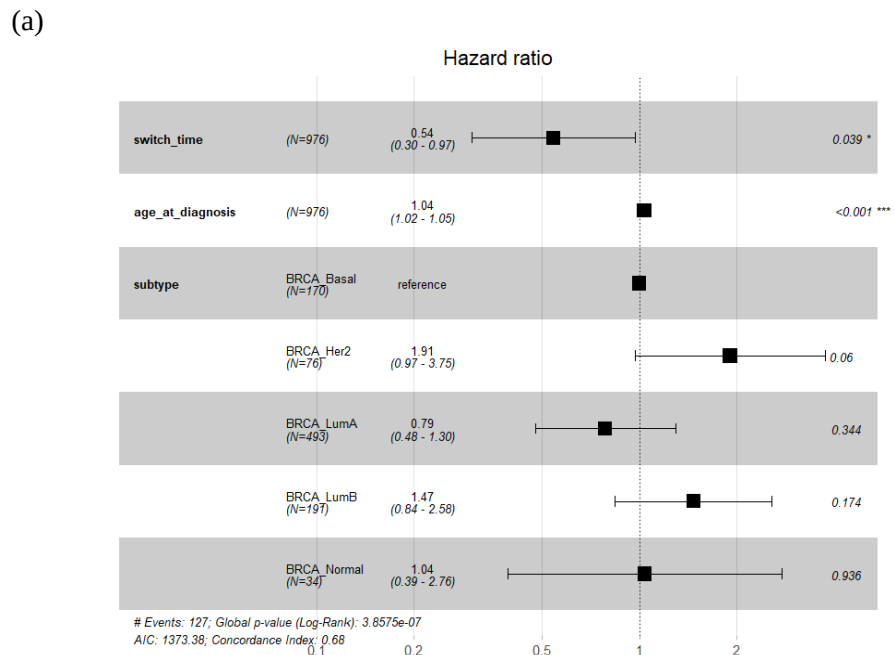


**Figure 32. Kaplan-Meier Survival Plots for Breast Cancer investigating (a) Average switch time and (b) switch percentage.** Two groups are defined for each plot, (a) the threshold is set at 3290, (b) the threshold is set at 55.

Finally, hazard ratio plots were analyzed. Figure 33 displays the hazard ratios, illustrating the risk of death for patients based on mean switch time, switch percentage, age, and breast cancer subtype. Among the investigated variables, only switch time, switch percentage, and age were found to be statistically significant in this analysis. Specifically, Figure 33(a) shows that the hazard ratio associated with mean switch time is 0.54, corresponding to a regression coefficient of -0.61. As described in the Methods section, the hazard ratio is calculated by exponentiating the regression coefficient ( $e^{\text{coeff}}$ ). The hazard ratio, and corresponding regression coefficient value, indicate that group 2 (mean switch time  $> 3290$ ) has a lower risk of death (and therefore a higher survival rate) than group 1 (mean switch time  $< 3290$ ). Specifically, belonging to group 2 reduces the hazard by 46%. This aligns with the trend observed in the corresponding Kaplan-Meier plot. Similarly, Figure 33(b) shows that the hazard ratio associated with switch percentage is 0.27, corresponding to a regression coefficient of -1.31. This result is consistent with the Kaplan-Meier curves, as group 2 (switch percentage  $< 55$ ) exhibits a lower risk of death (and therefore a higher survival rate) compared to group 1 (switch percentage  $> 55$ ). Indeed, belonging to group 2 reduces the hazard by 73%.

These results further reinforce the significance of our findings, demonstrating a clear association between delayed cell cycle transitions and improved survival probability.

Overall, although very preliminary, these results show how the integration of mathematical modeling and omics data could help in the investigation of cancer aggressiveness and patient prognosis by examining Overall Survival (OS). Further studies, increasing the patient cohort should be performed to further validate these initial findings and extract more significant patterns.



(b)

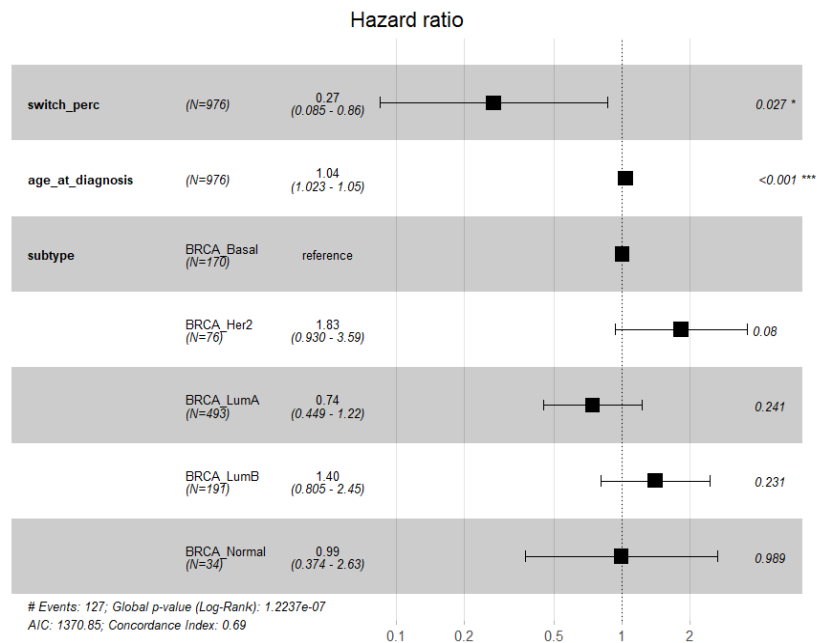


**Figure 33. Hazard ratio plots.** The x-axis represents the hazard ratio (HR). HR = 1 indicates no difference in survival between the groups, HR<1 indicates decreased hazard (death), HR>1 indicates increased hazard (death).

# 5 Conclusion

This study presents the characterization of a generic stochastic model of cell cycle transition and explores the impact that eQTL modulation and breast cancer somatic copy number deregulations have on cell cycle transition dynamics.

A sensitivity analysis of the generic cell cycle transition model was initially performed to identify species and parameters that significantly influence model output (average switch time or switch percentage). Consequently, several key factors were identified for each model. Notably, the species *E2* consistently emerged as a critical factor across all models, significantly impacting output fluctuations. *E2* regulates the transition from active to inactive activator. Consistently, high *E2* levels were observed to correlate with increased average switch times and decreased switch percentages. This is attributed to the fact that high *E2* levels reduce the availability of the activator, which is essential for activating the transition regulator and enabling the cell cycle transition.

The generic model was subsequently adapted to represent the human cell cycle G2/M transition. This was achieved through a literature review to identify key regulators of the cell cycle. Consequently, this adapted model was used to generate further models incorporating either eQTL or BRCA SCNA deregulation effects.

The analysis of average switch times across all tissues and specifically in breast tissue identified eQTL-associated tissues exhibiting significant switch time fluctuations. In breast tissue, in both the  $B_l^B$  and  $B_A^B$  models, FOXM1 and FCP1 showed no significant switch time fluctuations, whereas CCNB1 and CHK1 displayed substantial fluctuations for the heterozygous and homozygous alternative genotypes. The eQTLs associated with these two genes, rs28576332 and rs76118307, represent intronic variants with no reported clinical relevance.

The analysis of SCNAs integrated models revealed significant fluctuations. In the  $B_A^B$  models, increased copy numbers of species associated with inhibition correlated with a delay in average switch time and a decrease in switch occurrence, potentially preventing cell cycle transition. In the  $B_l^B$  models, a contrasting trend was observed; only CDK1 and CCNB1 significantly impacted switch time. Specifically, delays increased with lower expression due to decreased copy numbers, while increased copy numbers resulted in a faster switch.

A survival analysis was performed on patient-specific BRCA model  $B_A^B$  to determine whether patients exhibiting different average switch times and switch percentages also display variations in survival probability and/or hazard ratios. Specifically, we observed that patients with higher average switch times and/or lower switch percentages demonstrated an overall higher survival probability. Based on these results, we hypothesize that a delay in cell cycle progression is associated with improved patient survival. This hypothesis is supported by a recent study by Bhattarai *et al.*<sup>271</sup>, which investigated cell cycle rates in breast cancer and aligns with our findings.

The study provided valuable insight into applying a stochastic model to represent and investigate cell cycle transition, and the influence of germline and somatic mutation information. The results underscore the importance of integrating this knowledge when developing mathematical models. Moreover, the survival analysis results indicate that mathematical models can be used to describe the impact of mutations at the patient level. Creating patient-specific models could be beneficial for fields like personalized medicine, enabling the observation of potential drug impacts in individual cancer cases.

## 5.1 Future Perspectives

The preliminary results from the survival analysis demonstrate considerable potential, suggesting several avenues for future research within this project. However, to ensure the robustness of these findings, an increase in the number of patients considered would be beneficial. This would allow for a more populated pool for each subtype, permitting a subtype-specific survival analysis. Such an analysis could reveal

fluctuations in average switch time and switch percentage based on the subtype.

Furthermore, future investigations could explore the expansion of these analyses to encompass the G1/S and M/G1 checkpoints. Integrating eQTL and SCNA together could also enhance the comprehensiveness of the study. Extending this approach to other tumor types exhibiting a higher frequency of mutations in cell cycle regulatory genes is another promising direction.

Finally, the refinement or expansion of the general cell cycle transition model needs consideration. The current model, while simplified, may not adequately represent the intricate regulatory network governing cell cycle progression. Incorporating the potential impact of diverse cellular agents and accounting for multiple activators and inhibitors of transition regulators (TRs) would provide a more nuanced and accurate representation.

# Bibliography

1. Alberts B, Johnson A, Lewis J, Raff M, Roberts K, Walter P. An Overview of the Cell Cycle. In: *Molecular Biology of the Cell. 4th Edition.* Garland Science; 2002. Accessed February 22, 2025. <https://www.ncbi.nlm.nih.gov/books/NBK26869/>
2. Ong JY, Torres JZ. Dissecting the mechanisms of cell division. *J Biol Chem.* 2019;294(30):11382-11390. doi:10.1074/jbc.AW119.008149
3. Wang Z. Regulation of Cell Cycle Progression by Growth Factor-Induced Cell Signaling. *Cells.* 2021;10(12):3327. doi:10.3390/cells10123327
4. Cooper GM. The Eukaryotic Cell Cycle. In: *The Cell: A Molecular Approach. 2nd Edition.* Sinauer Associates; 2000. Accessed February 22, 2025. <https://www.ncbi.nlm.nih.gov/books/NBK9876/>
5. Shi W, Dowdy SF. Cell Cycle Controls in G1 and G0. In: Lennarz WJ, Lane MD, eds. *Encyclopedia of Biological Chemistry.* Elsevier; 2004:328-331. doi:10.1016/B0-12-443710-9/00090-9
6. Fischer M, Dang CV, DeCaprio JA. Chapter 17 - Control of Cell Division. In: Hoffman R, Benz EJ, Silberstein LE, et al., eds. *Hematology (Seventh Edition).* Elsevier; 2018:176-185. doi:10.1016/B978-0-323-35762-3.00017-2
7. Cooper GM. The Events of M Phase. In: *The Cell: A Molecular Approach. 2nd Edition.* Sinauer Associates; 2000. Accessed February 22, 2025. <https://www.ncbi.nlm.nih.gov/books/NBK9958/>
8. Alberts B, Johnson A, Lewis J, Raff M, Roberts K, Walter P. Cytokinesis. In: *Molecular Biology of the Cell. 4th Edition.* Garland Science; 2002. Accessed February 22, 2025. <https://www.ncbi.nlm.nih.gov/books/NBK26831/>
9. Kliuchnikov E, Klyshko E, Kelly MS, et al. Microtubule assembly and disassembly dynamics model: Exploring dynamic instability and identifying features of Microtubules' Growth, Catastrophe, Shortening, and Rescue. *Comput Struct Biotechnol J.* 2022;20:953-974. doi:10.1016/j.csbj.2022.01.028
10. Doxsey S, Zimmerman W, Mikule K. Centrosome control of the cell cycle. *Trends Cell Biol.* 2005;15(6):303-311. doi:10.1016/j.tcb.2005.04.008
11. Dumont S, Mitchison TJ. 4.16 Mechanical Forces in Mitosis. In: Egelman EH, ed. *Comprehensive Biophysics.* Elsevier; 2012:298-320. doi:10.1016/B978-0-12-374920-8.00419-7
12. Civelekoglu-Scholey G, Tao L, Brust-Mascher I, Wollman R, Scholey JM. Prometaphase spindle maintenance by an antagonistic motor-dependent force balance made robust by a disassembling lamin-B envelope. *J Cell Biol.* 2010;188(1):49-68. doi:10.1083/jcb.200908150
13. Kent IA, Lele TP. Microtubule-based force generation. *WIREs Nanomedicine Nanobiotechnology.* 2017;9(3):e1428. doi:10.1002/wnan.1428
14. Itoh G, Ikeda M, Iemura K, et al. Lateral attachment of kinetochores to microtubules is enriched in prometaphase rosette and facilitates chromosome alignment and bi-orientation establishment. *Sci Rep.* 2018;8(1):3888. doi:10.1038/s41598-018-22164-5
15. Tanaka TU, Desai A. Kinetochore-microtubule interactions: the means to the end. *Curr Opin Cell Biol.* 2008;20(1):53-63. doi:10.1016/j.ceb.2007.11.005
16. Torvi JR, Wong J, Serwas D, Moayed A, Drubin DG, Barnes G. Reconstitution of kinetochore motility and microtubule dynamics reveals a role for a kinesin-8 in establishing end-on attachments. DeLuca JG, Akhmanova A, Stumpff J, Westermann S, eds. *eLife.* 2022;11:e78450. doi:10.7554/eLife.78450

17. Monda JK, Cheeseman IM. The kinetochore–microtubule interface at a glance. *J Cell Sci.* 2018;131(16):jcs214577. doi:10.1242/jcs.214577
18. Godek KM, Kabeche L, Compton DA. Regulation of kinetochore–microtubule attachments through homeostatic control during mitosis. *Nat Rev Mol Cell Biol.* 2015;16(1):57-64. doi:10.1038/nrm3916
19. Walczak CE, Cai S, Khodjakov A. Mechanisms of chromosome behaviour during mitosis. *Nat Rev Mol Cell Biol.* 2010;11(2):91-102. doi:10.1038/nrm2832
20. Tanaka TU. Kinetochore–microtubule interactions: steps towards bi-orientation. *EMBO J.* 2010;29(24):4070-4082. doi:10.1038/emboj.2010.294
21. Maiato H, Gomes AM, Sousa F, Barisic M. Mechanisms of Chromosome Congression during Mitosis. *Biology.* 2017;6(1):13. doi:10.3390/biology6010013
22. Lian ATY, Chircop M. Mitosis in Animal Cells. In: Bradshaw RA, Stahl PD, eds. *Encyclopedia of Cell Biology.* Academic Press; 2016:478-493. doi:10.1016/B978-0-12-394447-4.30064-5
23. Sumara I, Vorlaufer E, Stukenberg PT, et al. The Dissociation of Cohesin from Chromosomes in Prophase Is Regulated by Polo-like Kinase. *Mol Cell.* 2002;9(3):515-525. doi:10.1016/S1097-2765(02)00473-2
24. Asbury CL. Anaphase A: Disassembling Microtubules Move Chromosomes toward Spindle Poles. *Biology.* 2017;6(1):15. doi:10.3390/biology6010015
25. Scholey JM, Civelekoglu-Scholey G, Brust-Mascher I. Anaphase B. *Biology.* 2016;5(4):51. doi:10.3390/biology5040051
26. Vukušić K, Tolić IM. Anaphase B: Long-standing models meet new concepts. *Semin Cell Dev Biol.* 2021;117:127-139. doi:10.1016/j.semcdb.2021.03.023
27. Carim SC, Kechad A, Hickson GRX. Animal Cell Cytokinesis: The Rho-Dependent Actomyosin-Aniloseptin Contractile Ring as a Membrane Microdomain Gathering, Compressing, and Sorting Machine. *Front Cell Dev Biol.* 2020;8. doi:10.3389/fcell.2020.575226
28. Miller AL. The contractile ring. *Curr Biol.* 2011;21(24):R976-R978. doi:10.1016/j.cub.2011.10.044
29. Vermeulen K, Van Bockstaele DR, Berneman ZN. The cell cycle: a review of regulation, deregulation and therapeutic targets in cancer. *Cell Prolif.* 2003;36(3):131-149. doi:10.1046/j.1365-2184.2003.00266.x
30. Malumbres M. 4 - Control of the Cell Cycle. In: Niederhuber JE, Armitage JO, Doroshow JH, Kastan MB, Tepper JE, eds. *Abeloff's Clinical Oncology (Fifth Edition).* Churchill Livingstone; 2014:52-68.e6. doi:10.1016/B978-1-4557-2865-7.00004-7
31. Pluta AJ, Studniarek C, Murphy S, Norbury CJ. Cyclin-dependent kinases: Masters of the eukaryotic universe. *WIREs RNA.* 2024;15(1):e1816. doi:10.1002/wrna.1816
32. Pellarin I, Dall'Acqua A, Favero A, et al. Cyclin-dependent protein kinases and cell cycle regulation in biology and disease. *Signal Transduct Target Ther.* 2025;10(1):1-62. doi:10.1038/s41392-024-02080-z
33. Ding L, Cao J, Lin W, et al. The Roles of Cyclin-Dependent Kinases in Cell-Cycle Progression and Therapeutic Strategies in Human Breast Cancer. *Int J Mol Sci.* 2020;21(6):1960. doi:10.3390/ijms21061960
34. Roskoski R. Cyclin-dependent protein serine/threonine kinase inhibitors as anticancer drugs. *Pharmacol Res.* 2019;139:471-488. doi:10.1016/j.phrs.2018.11.035

35. Lents NH, Baldassare JJ. Cyclins and Cyclin-Dependent Kinases. In: Bradshaw RA, Stahl PD, eds. *Encyclopedia of Cell Biology*. Academic Press; 2016:423-431. doi:10.1016/B978-0-12-394447-4.30057-8
36. Palacios-Blanco I, Martín-Castellanos C. Cyclins and CDKs in the regulation of meiosis-specific events. *Front Cell Dev Biol.* 2022;10. doi:10.3389/fcell.2022.1069064
37. Bertoli C, Skotheim JM, de Bruin RAM. Control of cell cycle transcription during G1 and S phases. *Nat Rev Mol Cell Biol.* 2013;14(8):518-528. doi:10.1038/nrm3629
38. Lau HW, Ma HT, Yeung TK, et al. Quantitative differences between cyclin-dependent kinases underlie the unique functions of CDK1 in human cells. *Cell Rep.* 2021;37(2). doi:10.1016/j.celrep.2021.109808
39. Zou T, Lin Z. The Involvement of Ubiquitination Machinery in Cell Cycle Regulation and Cancer Progression. *Int J Mol Sci.* 2021;22(11):5754. doi:10.3390/ijms22115754
40. Benanti JA. Coordination of cell growth and division by the ubiquitin–proteasome system. *Semin Cell Dev Biol.* 2012;23(5):492-498. doi:10.1016/j.semcd.2012.04.005
41. Manchado E, Eguren M, Malumbres M. The anaphase-promoting complex/cyclosome (APC/C): cell-cycle-dependent and -independent functions. *Biochem Soc Trans.* 2010;38(1):65-71. doi:10.1042/BST0380065
42. Pines J. Cubism and the cell cycle: the many faces of the APC/C. *Nat Rev Mol Cell Biol.* 2011;12(7):427-438. doi:10.1038/nrm3132
43. Bristow SL, Leman AR, Haase SB. Cell Cycle-Regulated Transcription: Effectively Using a Genomics Toolbox. In: Noguchi E, Gadaleta MC, eds. *Cell Cycle Control: Mechanisms and Protocols*. Springer; 2014:3-27. doi:10.1007/978-1-4939-0888-2\_1
44. Weidmüller P, Kholmatov M, Petsalaki E, Zaugg JB. Transcription factors: Bridge between cell signaling and gene regulation. *PROTEOMICS.* 2021;21(23-24):2000034. doi:10.1002/pmic.202000034
45. Jha RK, Kouzine F, Levens D. MYC function and regulation in physiological perspective. *Front Cell Dev Biol.* 2023;11. doi:10.3389/fcell.2023.1268275
46. Lucas M, Morris A, Townsend-Teague A, Tichit L, Habermann B, Barrat A. Inferring cell cycle phases from a partially temporal network of protein interactions. *Cell Rep Methods.* 2023;3(2):100397. doi:10.1016/j.crmeth.2023.100397
47. Golsteyn RM, Mundt KE, Fry AM, Nigg EA. Cell cycle regulation of the activity and subcellular localization of Plk1, a human protein kinase implicated in mitotic spindle function. *J Cell Biol.* 1995;129(6):1617-1628. doi:10.1083/jcb.129.6.1617
48. Itzhak DN, Tyanova S, Cox J, Borner GH. Global, quantitative and dynamic mapping of protein subcellular localization. Hegde RS, ed. *eLife.* 2016;5:e16950. doi:10.7554/eLife.16950
49. Luo L, Uerlings Y, Happel N, Asli NS, Knoetgen H, Kessel M. Regulation of Geminin Functions by Cell Cycle-Dependent Nuclear-Cytoplasmic Shuttling. *Mol Cell Biol.* 2007;27(13):4737-4744. doi:10.1128/MCB.00123-07
50. Bäumer N, Tickenbrock L, Tschanter P, et al. Inhibitor of Cyclin-dependent Kinase (CDK) Interacting with Cyclin A1 (INCA1) Regulates Proliferation and Is Repressed by Oncogenic Signaling \*. *J Biol Chem.* 2011;286(32):28210-28222. doi:10.1074/jbc.M110.203471
51. Barnum KJ, O'Connell MJ. Cell Cycle Regulation by Checkpoints. *Methods Mol Biol Clifton NJ.* 2014;1170:29-40. doi:10.1007/978-1-4939-0888-2\_2

52. Lukas J, Lukas C, Bartek J. Mammalian cell cycle checkpoints: signalling pathways and their organization in space and time. *DNA Repair*. 2004;3(8):997-1007. doi:10.1016/j.dnarep.2004.03.006
53. Enoch T, Norbury C. Cellular responses to DNA damage: cell-cycle checkpoints, apoptosis and the roles of p53 and ATM. *Trends Biochem Sci*. 1995;20(10):426-430. doi:10.1016/S0968-0004(00)89093-3
54. Pietenpol JA, Stewart ZA. Cell cycle checkpoint signaling:: Cell cycle arrest versus apoptosis. *Toxicology*. 2002;181-182:475-481. doi:10.1016/S0300-483X(02)00460-2
55. Weitzman MD, Wang JYJ. Cell Cycle: DNA Damage Checkpoints. In: Lennarz WJ, Lane MD, eds. *Encyclopedia of Biological Chemistry (Second Edition)*. Academic Press; 2013:410-416. doi:10.1016/B978-0-12-378630-2.00419-9
56. Foster DA, Yellen P, Xu L, Saqcena M. Regulation of G1 Cell Cycle Progression: Distinguishing the Restriction Point from a Nutrient-Sensing Cell Growth Checkpoint(s). *Genes Cancer*. 2010;1(11):1124-1131. doi:10.1177/1947601910392989
57. Hyun SY, Jang YJ. p53 activates G 1 checkpoint following DNA damage by doxorubicin during transient mitotic arrest. *Oncotarget*. 2014;6(7):4804-4815. doi:10.18632/oncotarget.3103
58. Hernández Borrero LJ, El-Deiry WS. Tumor suppressor p53: Biology, signaling pathways, and therapeutic targeting. *Biochim Biophys Acta - Rev Cancer*. 2021;1876(1):188556. doi:10.1016/j.bbcan.2021.188556
59. Yam CQX, Lim HH, Surana U. DNA damage checkpoint execution and the rules of its disengagement. *Front Cell Dev Biol*. 2022;10. doi:10.3389/fcell.2022.1020643
60. Wang Y, Ji P, Liu J, Broaddus RR, Xue F, Zhang W. Centrosome-associated regulators of the G2/M checkpoint as targets for cancer therapy. *Mol Cancer*. 2009;8(1):8. doi:10.1186/1476-4598-8-8
61. Poon RYC. Cell Cycle Control☆. In: *Reference Module in Biomedical Sciences*. Elsevier; 2015. doi:10.1016/B978-0-12-801238-3.98748-8
62. Stracker TH, Usui T, Petrini JHJ. Taking the time to make important decisions: The checkpoint effector kinases Chk1 and Chk2 and the DNA damage response. *DNA Repair*. 2009;8(9):1047-1054. doi:10.1016/j.dnarep.2009.04.012
63. Kalous J, Jansová D, Šušor A. Role of Cyclin-Dependent Kinase 1 in Translational Regulation in the M-Phase. *Cells*. 2020;9(7):1568. doi:10.3390/cells9071568
64. Gorbsky GJ. The spindle checkpoint and chromosome segregation in meiosis. *FEBS J*. 2015;282(13):2471-2487. doi:10.1111/febs.13166
65. Matković J, Ghosh S, Čosić M, et al. Kinetochore- and chromosome-driven transition of microtubules into bundles promotes spindle assembly. *Nat Commun*. 2022;13(1):7307. doi:10.1038/s41467-022-34957-4
66. Lara-Gonzalez P, Pines J, Desai A. Spindle assembly checkpoint activation and silencing at kinetochores. *Semin Cell Dev Biol*. 2021;117:86-98. doi:10.1016/j.semcd.2021.06.009
67. Wang Y, Jin F, Higgins R, McKnight K. The current view for the silencing of the spindle assembly checkpoint. *Cell Cycle*. 2014;13(11):1694-1701. doi:10.4161/cc.29027
68. Mazzagatti A, Engel JL, Ly P. Boveri and beyond: Chromothripsis and genomic instability from mitotic errors. *Mol Cell*. 2024;84(1):55-69. doi:10.1016/j.molcel.2023.11.002
69. Molinari M. Cell cycle checkpoints and their inactivation in human cancer. *Cell Prolif*. 2001;33(5):261-274. doi:10.1046/j.1365-2184.2000.00191.x

70. Health (US) NI of, Study BSC. Understanding Human Genetic Variation. In: *NIH Curriculum Supplement Series [Internet]*. National Institutes of Health (US); 2007. Accessed February 24, 2025. <https://www.ncbi.nlm.nih.gov/books/NBK20363/>
71. Hernandez LM, Blazer DG, Institute of Medicine (US) Committee on Assessing Interactions Among Social B. Genetics and Health. In: *Genes, Behavior, and the Social Environment: Moving Beyond the Nature/Nurture Debate*. National Academies Press (US); 2006. Accessed February 24, 2025. <https://www.ncbi.nlm.nih.gov/books/NBK19932/>
72. Lu YF, Goldstein DB, Angrist M, Cavalleri G. Personalized Medicine and Human Genetic Diversity. *Cold Spring Harb Perspect Med*. 2014;4(9):a008581. doi:10.1101/cshperspect.a008581
73. Kyrgiafini MA, Mamuris Z. Feature Papers in Population and Evolutionary Genetics and Genomics 2023: Unraveling Population Dynamics, Diversity, and Evolutionary Paths. *Genes*. 2024;15(4):446. doi:10.3390/genes15040446
74. Barton NH. Mutation and the evolution of recombination. *Philos Trans R Soc B Biol Sci*. 2010;365(1544):1281-1294. doi:10.1098/rstb.2009.0320
75. Brown TA. Mutation, Repair and Recombination. In: *Genomes. 2nd Edition*. Wiley-Liss; 2002. Accessed February 24, 2025. <https://www.ncbi.nlm.nih.gov/books/NBK21114/>
76. Chintalapati M, Moorjani P. Evolution of the mutation rate across primates. *Curr Opin Genet Dev*. 2020;62:58-64. doi:10.1016/j.gde.2020.05.028
77. Torgerson T, Ochs H. Chapter 3 - Genetics of Primary Immune Deficiencies. In: Sullivan KE, Stiehm ER, eds. *Stiehm's Immune Deficiencies*. Academic Press; 2014:73-81. doi:10.1016/B978-0-12-405546-9.00003-0
78. Milligan WR, Amster G, Sella G. The impact of genetic modifiers on variation in germline mutation rates within and among human populations. *Genetics*. 2022;221(4):iyac087. doi:10.1093/genetics/iyac087
79. Miles B, Tadi P. Genetics, Somatic Mutation. In: *StatPearls*. StatPearls Publishing; 2025. Accessed February 24, 2025. <http://www.ncbi.nlm.nih.gov/books/NBK557896/>
80. Huang AY, Lee EA. Identification of Somatic Mutations From Bulk and Single-Cell Sequencing Data. *Front Aging*. 2022;2. doi:10.3389/fragi.2021.800380
81. García-Nieto PE, Morrison AJ, Fraser HB. The somatic mutation landscape of the human body. *Genome Biol*. 2019;20(1):298. doi:10.1186/s13059-019-1919-5
82. Majérus MA. The cause of cancer: The unifying theory. *Adv Cancer Biol - Metastasis*. 2022;4:100034. doi:10.1016/j.adcanc.2022.100034
83. Agashe D, Sane M, Singhal S. Revisiting the Role of Genetic Variation in Adaptation. *Am Nat*. 2023;202(4):486-502. doi:10.1086/726012
84. Suzuki K. Nature of Mutations in Genetic Disorders. In: *Basic Neurochemistry: Molecular, Cellular and Medical Aspects. 6th Edition*. Lippincott-Raven; 1999. Accessed February 24, 2025. <https://www.ncbi.nlm.nih.gov/books/NBK27942/>
85. Sherry ST, Ward MH, Kholodov M, et al. dbSNP: the NCBI database of genetic variation. *Nucleic Acids Res*. 2001;29(1):308-311. doi:10.1093/nar/29.1.308
86. Deng N, Zhou H, Fan H, Yuan Y. Single nucleotide polymorphisms and cancer susceptibility. *Oncotarget*. 2017;8(66):110635-110649. doi:10.18632/oncotarget.22372

87. Kumar S, Clarke D, Gerstein M. Localized structural frustration for evaluating the impact of sequence variants. *Nucleic Acids Res.* 2016;44(21):gkw927. doi:10.1093/nar/gkw927
88. Fang H, Bergmann EA, Arora K, et al. Indel variant analysis of short-read sequencing data with Scalpel. *Nat Protoc.* 2016;11(12):2529-2548. doi:10.1038/nprot.2016.150
89. Arlt MF, Mulle JG, Schaibley VM, et al. Replication Stress Induces Genome-wide Copy Number Changes in Human Cells that Resemble Polymorphic and Pathogenic Variants. *Am J Hum Genet.* 2009;84(3):339-350. doi:10.1016/j.ajhg.2009.01.024
90. Harbers L, Agostini F, Nicos M, Poddighe D, Bienko M, Crosetto N. Somatic Copy Number Alterations in Human Cancers: An Analysis of Publicly Available Data From The Cancer Genome Atlas. *Front Oncol.* 2021;11. doi:10.3389/fonc.2021.700568
91. Hastings PJ, Lupski JR, Rosenberg SM, Ira G. Mechanisms of change in gene copy number. *Nat Rev Genet.* 2009;10(8):551-564. doi:10.1038/nrg2593
92. Yang L. A practical guide for structural variation detection in human genome. *Curr Protoc Hum Genet.* 2020;107(1):e103. doi:10.1002/cphg.103
93. Chiang C, Scott AJ, Davis JR, et al. The impact of structural variation on human gene expression. *Nat Genet.* 2017;49(5):692-699. doi:10.1038/ng.3834
94. Piraino SW, Furney SJ. Identification of coding and non-coding mutational hotspots in cancer genomes. *BMC Genomics.* 2017;18(1):17. doi:10.1186/s12864-016-3420-9
95. Clark DP, Pazdernik NJ, McGehee MR. Chapter 26 - Mutations and Repair. In: Clark DP, Pazdernik NJ, McGehee MR, eds. *Molecular Biology (Third Edition)*. Academic Cell; 2019:832-879. doi:10.1016/B978-0-12-813288-3.00026-4
96. Morais P, Adachi H, Yu YT. Suppression of Nonsense Mutations by New Emerging Technologies. *Int J Mol Sci.* 2020;21(12):4394. doi:10.3390/ijms21124394
97. Savino S, Desmet T, Franceus J. Insertions and deletions in protein evolution and engineering. *Biotechnol Adv.* 2022;60:108010. doi:10.1016/j.biotechadv.2022.108010
98. Gerasimavicius L, Livesey BJ, Marsh JA. Loss-of-function, gain-of-function and dominant-negative mutations have profoundly different effects on protein structure. *Nat Commun.* 2022;13(1):3895. doi:10.1038/s41467-022-31686-6
99. Scacheri CA, Scacheri PC. Mutations in the non-coding genome. *Curr Opin Pediatr.* 2015;27(6):659-664. doi:10.1097/MOP.0000000000000283
100. Zhang F, Lupski JR. Non-coding genetic variants in human disease. *Hum Mol Genet.* 2015;24(R1):R102-R110. doi:10.1093/hmg/ddv259
101. Diederichs S, Bartsch L, Berkman JC, et al. The dark matter of the cancer genome: aberrations in regulatory elements, untranslated regions, splice sites, non-coding RNA and synonymous mutations. *EMBO Mol Med.* 2016;8(5):442-457. doi:10.15252/emmm.201506055
102. Steri M, Idda ML, Whalen MB, Orrù V. Genetic Variants in mRNA Untranslated Regions. *Wiley Interdiscip Rev RNA.* 2018;9(4):e1474. doi:10.1002/wrna.1474
103. Piraino SW, Furney SJ. Beyond the exome: the role of non-coding somatic mutations in cancer. *Ann Oncol.* 2016;27(2):240-248. doi:10.1093/annonc/mdv561
104. Piraino SW, Furney SJ. Beyond the exome: the role of non-coding somatic mutations in cancer. *Ann Oncol.* 2016;27(2):240-248. doi:10.1093/annonc/mdv561

105. Johnston SE. Understanding the Genetic Basis of Variation in Meiotic Recombination: Past, Present, and Future. *Mol Biol Evol*. 2024;41(7):msae112. doi:10.1093/molbev/msae112
106. Gottlieb SF, Gulani A, Tegay DH. Genetics, Meiosis. In: *StatPearls*. StatPearls Publishing; 2025. Accessed February 24, 2025. <http://www.ncbi.nlm.nih.gov/books/NBK482462/>
107. Simon A, Coop G. The contribution of gene flow, selection, and genetic drift to five thousand years of human allele frequency change. *Proc Natl Acad Sci*. 2024;121(9):e2312377121. doi:10.1073/pnas.2312377121
108. You JS, Jones PA. Cancer Genetics and Epigenetics: Two Sides of the Same Coin? *Cancer Cell*. 2012;22(1):9-20. doi:10.1016/j.ccr.2012.06.008
109. Nedoszytko B, Arock M, Lyons JJ, et al. Clinical Impact of Inherited and Acquired Genetic Variants in Mastocytosis. *Int J Mol Sci*. 2021;22(1):411. doi:10.3390/ijms22010411
110. Xu P, Sun D, Gao Y, et al. Germline mutations in a DNA repair pathway are associated with familial colorectal cancer. *JCI Insight*. 2021;6(18). doi:10.1172/jci.insight.148931
111. Ingvarsson S. Germline mutations in DNA repair and cell cycle checkpoint genes: consequential somatic gene alterations and genome instability. *Breast Cancer Res*. 2003;5(1):37. doi:10.1186/bcr696
112. Balmain A. The critical roles of somatic mutations and environmental tumor-promoting agents in cancer risk. *Nat Genet*. 2020;52(11):1139-1143. doi:10.1038/s41588-020-00727-5
113. Lee EYHP, Muller WJ. Oncogenes and Tumor Suppressor Genes. *Cold Spring Harb Perspect Biol*. 2010;2(10):a003236. doi:10.1101/cshperspect.a003236
114. Liu J, Dang H, Wang XW. The significance of intertumor and intratumor heterogeneity in liver cancer. *Exp Mol Med*. 2018;50(1):e416-e416. doi:10.1038/emm.2017.165
115. Ock CY, Hwang JE, Keam B, et al. Genomic landscape associated with potential response to anti-CTLA-4 treatment in cancers. *Nat Commun*. 2017;8(1):1050. doi:10.1038/s41467-017-01018-0
116. Hao D, Wang L, Di L jun. Distinct mutation accumulation rates among tissues determine the variation in cancer risk. *Sci Rep*. 2016;6(1):19458. doi:10.1038/srep19458
117. Cairns J. Mutation selection and the natural history of cancer. *Nature*. 1975;255(5505):197-200. doi:10.1038/255197a0
118. Nowell PC. The Clonal Evolution of Tumor Cell Populations. *Science*. 1976;194(4260):23-28. doi:10.1126/science.959840
119. Greaves M, Maley CC. Clonal evolution in cancer. *Nature*. 2012;481(7381):306-313. doi:10.1038/nature10762
120. Kandoth C, McLellan MD, Vandin F, et al. Mutational landscape and significance across 12 major cancer types. *Nature*. 2013;502(7471):333-339. doi:10.1038/nature12634
121. Johnson BE, Mazor T, Hong C, et al. Mutational Analysis Reveals the Origin and Therapy-Driven Evolution of Recurrent Glioma. *Science*. 2014;343(6167):189-193. doi:10.1126/science.1239947
122. Murugaesu N, Wilson GA, Birkbak NJ, et al. Tracking the genomic evolution of esophageal adenocarcinoma through neoadjuvant chemotherapy. *Cancer Discov*. 2015;5(8):821-831. doi:10.1158/2159-8290.CD-15-0412
123. Notta F, Chan-Seng-Yue M, Lemire M, et al. A renewed model of pancreatic cancer evolution based on genomic rearrangement patterns. *Nature*. 2016;538(7625):378-382. doi:10.1038/nature19823

124. McPherson A, Roth A, Laks E, et al. Divergent modes of clonal spread and intraperitoneal mixing in high-grade serous ovarian cancer. *Nat Genet*. 2016;48(7):758-767. doi:10.1038/ng.3573
125. Hanahan D, Weinberg RA. The Hallmarks of Cancer. *Cell*. 2000;100(1):57-70. doi:10.1016/S0092-8674(00)81683-9
126. Hanahan D, Weinberg RA. Hallmarks of Cancer: The Next Generation. *Cell*. 2011;144(5):646-674. doi:10.1016/j.cell.2011.02.013
127. Deep G, Agarwal R. New Combination Therapies with Cell Cycle Agents. *Curr Opin Investig Drugs Lond Engl* 2000. 2008;9(6):591-604.
128. Stewart ZA, Westfall MD, Pietenpol JA. Cell-cycle dysregulation and anticancer therapy. *Trends Pharmacol Sci*. 2003;24(3):139-145. doi:10.1016/S0165-6147(03)00026-9
129. Weinstat-Saslow D, Merino MJ, Manrow RE, et al. Overexpression of cyclin D mRNA distinguishes invasive and *in situ* breast carcinomas from non-malignant lesions. *Nat Med*. 1995;1(12):1257-1260. doi:10.1038/nm1295-1257
130. Shapiro GI. Cyclin-Dependent Kinase Pathways As Targets for Cancer Treatment. *J Clin Oncol*. 2006;24(11):1770-1783. doi:10.1200/JCO.2005.03.7689
131. Schwartz GK, Shah MA. Targeting the Cell Cycle: A New Approach to Cancer Therapy. *J Clin Oncol*. 2005;23(36):9408-9421. doi:10.1200/JCO.2005.01.5594
132. Hatakeyama M, Weinberg RA. The role of RB in cell cycle control. *Prog Cell Cycle Res*. 1995;1:9-19. doi:10.1007/978-1-4615-1809-9\_2
133. Collins I, Garrett MD. Targeting the cell division cycle in cancer: CDK and cell cycle checkpoint kinase inhibitors. *Curr Opin Pharmacol*. 2005;5(4):366-373. doi:10.1016/j.coph.2005.04.009
134. Wang H, Guo M, Wei H, Chen Y. Targeting p53 pathways: mechanisms, structures and advances in therapy. *Signal Transduct Target Ther*. 2023;8(1):1-35. doi:10.1038/s41392-023-01347-1
135. Sarver MM, Breglio KF, Olsen EA. Ataxia-telangiectasia mutated (ATM) gene mutation in a patient with primary cutaneous marginal zone lymphoma. *JAAD Case Rep*. 2022;23:73-75. doi:10.1016/j.jdcr.2022.02.032
136. Bartek J, Lukas J. Chk1 and Chk2 kinases in checkpoint control and cancer. *Cancer Cell*. 2003;3(5):421-429. doi:10.1016/S1535-6108(03)00110-7
137. Kristjánsdóttir K, Rudolph J. Cdc25 Phosphatases and Cancer. *Chem Biol*. 2004;11(8):1043-1051. doi:10.1016/j.chembiol.2004.07.007
138. Cicirò Y, Ragusa D, Sala A. Expression of the checkpoint kinase BUB1 is a predictor of response to cancer therapies. *Sci Rep*. 2024;14(1):4461. doi:10.1038/s41598-024-55080-y
139. Song J, Ni C, Dong X, Sheng C, Qu Y, Zhu L. bub1 as a potential oncogene and a prognostic biomarker for neuroblastoma. *Front Oncol*. 2022;12:988415. doi:10.3389/fonc.2022.988415
140. Lee MH, Yang HY. Contributions in the domain of cancer research: Review¶Negative regulators of cyclin-dependent kinases and their roles in cancers. *Cell Mol Life Sci CMLS*. 2001;58(12):1907-1922. doi:10.1007/PL00000826
141. Cyclins and Cell Cycle Control in Cancer and Disease - Mathew C. Casimiro, Marco Crosariol, Emanuele Loro, Zhiping Li, Richard G. Pestell, 2012. Accessed March 5, 2025. <https://journals.sagepub.com/doi/full/10.1177/1947601913479022>

- 142.Cerami E, Gao J, Dogrusoz U, et al. The cBio cancer genomics portal: an open platform for exploring multidimensional cancer genomics data. *Cancer Discov.* 2012;2(5):401-404. doi:10.1158/2159-8290.CD-12-0095
- 143.Aaltonen LA, Abascal F, Abeshouse A, et al. Pan-cancer analysis of whole genomes. *Nature.* 2020;578(7793):82-93. doi:10.1038/s41586-020-1969-6
- 144.Wilkinson L, Gathani T. Understanding breast cancer as a global health concern. *Br J Radiol.* 2022;95(1130):20211033. doi:10.1259/bjr.20211033
- 145.Bray F, Ferlay J, Laversanne M, et al. Cancer Incidence in Five Continents: Inclusion criteria, highlights from Volume X and the global status of cancer registration. *Int J Cancer.* 2015;137(9):2060-2071. doi:10.1002/ijc.29670
- 146.Perou CM, Sørlie T, Eisen MB, et al. Molecular portraits of human breast tumours. *Nature.* 2000;406(6797):747-752. doi:10.1038/35021093
- 147.Harbeck N, Penault-Llorca F, Cortes J, et al. Breast cancer. *Nat Rev Dis Primer.* 2019;5(1):1-31. doi:10.1038/s41572-019-0111-2
- 148.Allinen M, Beroukhim R, Cai L, et al. Molecular characterization of the tumor microenvironment in breast cancer. *Cancer Cell.* 2004;6(1):17-32. doi:10.1016/j.ccr.2004.06.010
- 149.Petrucelli N, Daly MB, Pal T. BRCA1- and BRCA2-Associated Hereditary Breast and Ovarian Cancer. In: Adam MP, Feldman J, Mirzaa GM, Pagon RA, Wallace SE, Amemiya A, eds. *GeneReviews®.* University of Washington, Seattle; 1993. Accessed February 24, 2025. <http://www.ncbi.nlm.nih.gov/books/NBK1247/>
- 150.Godet I, Gilkes DM. BRCA1 and BRCA2 mutations and treatment strategies for breast cancer. *Integr Cancer Sci Ther.* 2017;4(1):10.15761/ICST.1000228.
- 151.Petrucelli N, Daly MB, Feldman GL. Hereditary breast and ovarian cancer due to mutations in *BRCA1* and *BRCA2*. *Genet Med.* 2010;12(5):245-259. doi:10.1097/GIM.0b013e3181d38f2f
- 152.Shiovitz S, Korde LA. Genetics of breast cancer: a topic in evolution. *Ann Oncol.* 2015;26(7):1291-1299. doi:10.1093/annonc/mdv022
- 153.Mustafa MdK, Tanoue Y, Tateishi C, Vaziri C, Tateishi S. Roles of Chk2/CHEK2 in guarding against environmentally induced DNA damage and replication-stress. *Environ Mol Mutagen.* 2020;61(7):730-735. doi:10.1002/em.22397
- 154.Nevanlinna H, Bartek J. The CHEK2 gene and inherited breast cancer susceptibility. *Oncogene.* 2006;25(43):5912-5919. doi:10.1038/sj.onc.1209877
- 155.Nik-Zainal S, Davies H, Staaf J, et al. Landscape of somatic mutations in 560 breast cancer whole-genome sequences. *Nature.* 2016;534(7605):47-54. doi:10.1038/nature17676
- 156.Heitzer E, Haque IS, Roberts CES, Speicher MR. Current and future perspectives of liquid biopsies in genomics-driven oncology. *Nat Rev Genet.* 2019;20(2):71-88. doi:10.1038/s41576-018-0071-5
- 157.Harbeck N, Penault-Llorca F, Cortes J, et al. Breast cancer. *Nat Rev Dis Primer.* 2019;5(1):1-31. doi:10.1038/s41572-019-0111-2
- 158.Turashvili G, Brogi E. Tumor Heterogeneity in Breast Cancer. *Front Med.* 2017;4. doi:10.3389/fmed.2017.00227
- 159.Paul MR, Pan T chi, Pant DK, et al. Genomic landscape of metastatic breast cancer identifies preferentially dysregulated pathways and targets. *J Clin Invest.* 2020;130(8):4252-4265.

- 160.Turner NC, Swift C, Kilburn L, et al. ESR1 Mutations and Overall Survival on Fulvestrant versus Exemestane in Advanced Hormone Receptor–Positive Breast Cancer: A Combined Analysis of the Phase III SoFEA and EFECT Trials. *Clin Cancer Res.* 2020;26(19):5172-5177. doi:10.1158/1078-0432.CCR-20-0224
- 161.Liu J, Deng H, Jia W, et al. Comparison of ER/PR and HER2 statuses in primary and paired liver metastatic sites of breast carcinoma in patients with or without treatment. *J Cancer Res Clin Oncol.* 2012;138(5):837-842. doi:10.1007/s00432-012-1150-1
- 162.Curtit E, Nerich V, Mansi L, et al. Discordances in Estrogen Receptor Status, Progesterone Receptor Status, and HER2 Status Between Primary Breast Cancer and Metastasis. *The Oncologist.* 2013;18(6):667-674. doi:10.1634/theoncologist.2012-0350
- 163.Niikura N, Liu J, Hayashi N, et al. Loss of Human Epidermal Growth Factor Receptor 2 (HER2) Expression in Metastatic Sites of HER2-Overexpressing Primary Breast Tumors. *J Clin Oncol.* 2012;30(6):593-599. doi:10.1200/JCO.2010.33.8889
- 164.Thu K, Soria-Bretones I, Mak T, Cescon D. Targeting the cell cycle in breast cancer: towards the next phase. *Cell Cycle.* 2018;17(15):1871-1885. doi:10.1080/15384101.2018.1502567
- 165.Chen J. The Cell-Cycle Arrest and Apoptotic Functions of p53 in Tumor Initiation and Progression. *Cold Spring Harb Perspect Med.* 2016;6(3):a026104. doi:10.1101/cshperspect.a026104
- 166.Chou J, Provot S, Werb Z. GATA3 in Development and Cancer Differentiation: Cells GATA Have It! *J Cell Physiol.* 2010;222(1):42-49. doi:10.1002/jcp.21943
- 167.Glaviano A, Foo ASC, Lam HY, et al. PI3K/AKT/mTOR signaling transduction pathway and targeted therapies in cancer. *Mol Cancer.* 2023;22(1):138. doi:10.1186/s12943-023-01827-6
- 168.Arnold A, Papanikolaou A. Cyclin D1 in Breast Cancer Pathogenesis. *J Clin Oncol.* 2005;23(18):4215-4224. doi:10.1200/JCO.2005.05.064
- 169.Mir MA, Khan SU, Aisha S. Cell Cycle Dysregulation in Breast Cancer. In: Mir M, ed. *Therapeutic Potential of Cell Cycle Kinases in Breast Cancer.* Springer Nature; 2023:103-131. doi:10.1007/978-981-19-8911-7\_5
- 170.Wei Z, Gan J, Feng X, et al. APOBEC3B is overexpressed in cervical cancer and promotes the proliferation of cervical cancer cells through apoptosis, cell cycle, and p53 pathway. *Front Oncol.* 2022;12. doi:10.3389/fonc.2022.864889
- 171.Stemke-Hale K, Gonzalez-Angulo AM, Lluch A, et al. An Integrative Genomic and Proteomic Analysis of PIK3CA, PTEN, and AKT Mutations in Breast Cancer. *Cancer Res.* 2008;68(15):6084-6091. doi:10.1158/0008-5472.CAN-07-6854
- 172.Hoadley KA, Yau C, Hinoue T, et al. Cell-of-Origin Patterns Dominate the Molecular Classification of 10,000 Tumors from 33 Types of Cancer. *Cell.* 2018;173(2):291-304.e6. doi:10.1016/j.cell.2018.03.022
- 173.Li Q, Stram A, Chen C, et al. Expression QTL-based analyses reveal candidate causal genes and loci across five tumor types. *Hum Mol Genet.* 2014;23(19):5294-5302. doi:10.1093/hmg/ddu228
- 174.Albert FW, Kruglyak L. The role of regulatory variation in complex traits and disease. *Nat Rev Genet.* 2015;16(4):197-212. doi:10.1038/nrg3891
- 175.Ko BS, Lee SB, Kim TK. A brief guide to analyzing expression quantitative trait loci. *Mol Cells.* 2024;47(11):100139. doi:10.1016/j.molcell.2024.100139

- 176.Nica AC, Dermitzakis ET. Expression quantitative trait loci: present and future. *Philos Trans R Soc B Biol Sci.* 2013;368(1620):20120362. doi:10.1098/rstb.2012.0362
- 177.Wittkopp PJ, Haerum BK, Clark AG. Evolutionary changes in cis and trans gene regulation. *Nature.* 2004;430(6995):85-88. doi:10.1038/nature02698
- 178.Pickrell JK, Marioni JC, Pai AA, et al. Understanding mechanisms underlying human gene expression variation with RNA sequencing. *Nature.* 2010;464(7289):768-772. doi:10.1038/nature08872
- 179.Doss S, Schadt EE, Drake TA, Lusis AJ. Cis-acting expression quantitative trait loci in mice. *Genome Res.* 2005;15(5):681-691. doi:10.1101/gr.3216905
- 180.Rockman MV, Kruglyak L. Genetics of global gene expression. *Nat Rev Genet.* 2006;7(11):862-872. doi:10.1038/nrg1964
- 181.Banerjee S, Simonetti FL, Detrois KE, et al. Tejaas: reverse regression increases power for detecting trans-eQTLs. *Genome Biol.* 2021;22:142. doi:10.1186/s13059-021-02361-8
- 182.Battle A, Mostafavi S, Zhu X, et al. Characterizing the genetic basis of transcriptome diversity through RNA-sequencing of 922 individuals. *Genome Res.* 2014;24(1):14-24. doi:10.1101/gr.155192.113
- 183.Albert FW, Bloom JS, Siegel J, Day L, Kruglyak L. Genetics of trans-regulatory variation in gene expression. Wittkopp PJ, ed. *eLife.* 2018;7:e35471. doi:10.7554/eLife.35471
- 184.Musunuru K, Strong A, Frank-Kamenetsky M, et al. From noncoding variant to phenotype via SORT1 at the 1p13 cholesterol locus. *Nature.* 2010;466(7307):714-719. doi:10.1038/nature09266
- 185.Cardelli L, Hernansaiz-Ballesteros RD, Dalchau N, Csikász-Nagy A. Efficient Switches in Biology and Computer Science. *PLOS Comput Biol.* 2017;13(1):e1005100. doi:10.1371/journal.pcbi.1005100
- 186.Distributed information processing in biological and computational systems | Communications of the ACM. Accessed February 24, 2025. <https://dl.acm.org/doi/10.1145/2678280>
- 187.Romanel A, Jensen LJ, Cardelli L, Csikász-Nagy A. Transcriptional Regulation Is a Major Controller of Cell Cycle Transition Dynamics. *PLOS ONE.* 2012;7(1):e29716. doi:10.1371/journal.pone.0029716
- 188.Goodwin BC. Oscillatory behavior in enzymatic control processes. *Adv Enzyme Regul.* 1965;3:425-437. doi:10.1016/0065-2571(65)90067-1
- 189.Griffith JS. Mathematics of cellular control processes I. Negative feedback to one gene. *J Theor Biol.* 1968;20(2):202-208. doi:10.1016/0022-5193(68)90189-6
- 190.Angeli D, Ferrell JE, Sontag ED. Detection of multistability, bifurcations, and hysteresis in a large class of biological positive-feedback systems. *Proc Natl Acad Sci.* 2004;101(7):1822-1827. doi:10.1073/pnas.0308265100
- 191.Csikász-Nagy A, Battogtokh D, Chen KC, Novák B, Tyson JJ. Analysis of a Generic Model of Eukaryotic Cell-Cycle Regulation. *Biophys J.* 2006;90(12):4361-4379. doi:10.1529/biophysj.106.081240
- 192.Morgan DO. Principles of CDK regulation. *Nature.* 1995;374(6518):131-134. doi:10.1038/374131a0
- 193.O'Farrell PH. Triggering the all-or-nothing switch into mitosis. *Trends Cell Biol.* 2001;11(12):512-519. doi:10.1016/S0962-8924(01)02142-0
- 194.Trunnell NB, Poon AC, Kim SY, Ferrell JE. Ultrasensitivity in the Regulation of Cdc25C by Cdk1. *Mol Cell.* 2011;41(3):263-274. doi:10.1016/j.molcel.2011.01.012

- 195.Kim SY, Ferrell JE. Substrate Competition as a Source of Ultrasensitivity in the Inactivation of Wee1. *Cell*. 2007;128(6):1133-1145. doi:10.1016/j.cell.2007.01.039
- 196.Ferrell JE, Ha SH. Ultrasensitivity part III: cascades, bistable switches, and oscillators. *Trends Biochem Sci*. 2014;39(12):612-618. doi:10.1016/j.tibs.2014.10.002
- 197.Zámborszky J. Cell Cycle Transitions, G2/M. In: Dubitzky W, Wolkenhauer O, Cho KH, Yokota H, eds. *Encyclopedia of Systems Biology*. Springer; 2013:329-333. doi:10.1007/978-1-4419-9863-7\_38
- 198.Novak B, Tyson JJ, Gyorffy B, Csikasz-Nagy A. Irreversible cell-cycle transitions are due to systems-level feedback. *Nat Cell Biol*. 2007;9(7):724-728. doi:10.1038/ncb0707-724
- 199.Reed SI. Ratchets and clocks: the cell cycle, ubiquitylation and protein turnover. *Nat Rev Mol Cell Biol*. 2003;4(11):855-864. doi:10.1038/nrm1246
- 200.Hershko A. Roles of ubiquitin-mediated proteolysis in cell cycle control. *Curr Opin Cell Biol*. 1997;9(6):788-799. doi:10.1016/S0955-0674(97)80079-8
- 201.King RW, Deshaies RJ, Peters JM, Kirschner MW. How Proteolysis Drives the Cell Cycle. *Science*. 1996;274(5293):1652-1659. doi:10.1126/science.274.5293.1652
- 202.Vodermaier HC. APC/C and SCF: Controlling Each Other and the Cell Cycle. *Curr Biol*. 2004;14(18):R787-R796. doi:10.1016/j.cub.2004.09.020
- 203.Nurse P. Universal control mechanism regulating onset of M-phase. *Nature*. 1990;344(6266):503-508. doi:10.1038/344503a0
- 204.Csikász-Nagy A. Computational systems biology of the cell cycle. *Brief Bioinform*. 2009;10(4):424-434. doi:10.1093/bib/bbp005
- 205.Ferrell JE, Tsai TYC, Yang Q. Modeling the Cell Cycle: Why Do Certain Circuits Oscillate? *Cell*. 2011;144(6):874-885. doi:10.1016/j.cell.2011.03.006
- 206.Csikász-Nagy A, Mura I. Role of Computational Modeling in Understanding Cell Cycle Oscillators. In: Coutts AS, Weston L, eds. *Cell Cycle Oscillators: Methods and Protocols*. Springer; 2016:59-70. doi:10.1007/978-1-4939-2957-3\_3
- 207.Modeling of Gene Expression. In: *Systems Biology in Practice*. John Wiley & Sons, Ltd; 2005:257-288. doi:10.1002/3527603603.ch8
- 208.Adler SO, Spiesser TW, Uschner F, et al. A yeast cell cycle model integrating stress, signaling, and physiology. *FEMS Yeast Res*. 2022;22(1):foac026. doi:10.1093/femsyr/foac026
- 209.Mura I, Csikász-Nagy A. Stochastic Petri Net extension of a yeast cell cycle model. *J Theor Biol*. 2008;254(4):850-860. doi:10.1016/j.jtbi.2008.07.019
- 210.Lecca P. Stochastic chemical kinetics. *Biophys Rev*. 2013;5(4):323-345. doi:10.1007/s12551-013-0122-2
- 211.Gillespie DT. Exact stochastic simulation of coupled chemical reactions. ACS Publications. doi:10.1021/j100540a008
- 212.Barik D, Ball DA, Peccoud J, Tyson JJ. A Stochastic Model of the Yeast Cell Cycle Reveals Roles for Feedback Regulation in Limiting Cellular Variability. *PLOS Comput Biol*. 2016;12(12):e1005230. doi:10.1371/journal.pcbi.1005230
- 213.Dematté L, Larcher R, Palmisano A, Priami C, Romanel A. Programming Biology in BlenX. In: Choi S, ed. *Systems Biology for Signaling Networks*. Springer; 2010:777-820. doi:10.1007/978-1-4419-5797-9\_31

- 214.Dematté L, Priami C, Romanel A. The Beta Workbench: a computational tool to study the dynamics of biological systems. *Brief Bioinform.* 2008;9(5):437-449. doi:10.1093/bib/bbn023
- 215.Sysoev A. Sensitivity Analysis of Mathematical Models. *Computation.* 2023;11(8):159. doi:10.3390/computation11080159
- 216.Iooss B, Saltelli A. Introduction to Sensitivity Analysis. In: Ghanem R, Higdon D, Owhadi H, eds. *Handbook of Uncertainty Quantification.* Springer International Publishing; 2017:1103-1122. doi:10.1007/978-3-319-12385-1\_31
- 217.recount3. Bioconductor. Accessed March 9, 2025. <http://bioconductor.org/packages/recount3/>
- 218.Bolstad BM, Irizarry RA, Åstrand M, Speed TP. A comparison of normalization methods for high density oligonucleotide array data based on variance and bias. *Bioinformatics.* 2003;19(2):185-193. doi:10.1093/bioinformatics/19.2.185
- 219.Shao X, Lv N, Liao J, et al. Copy number variation is highly correlated with differential gene expression: a pan-cancer study. *BMC Med Genet.* 2019;20(1):175. doi:10.1186/s12881-019-0909-5
- 220.Wickham H. dplyr: A Grammar of Data Manipulation. Published online 2023. <https://github.com/tidyverse/dplyr>
- 221.Zhao Y, Li MC, Konaté MM, et al. TPM, FPKM, or Normalized Counts? A Comparative Study of Quantification Measures for the Analysis of RNA-seq Data from the NCI Patient-Derived Models Repository. *J Transl Med.* 2021;19(1):269. doi:10.1186/s12967-021-02936-w
- 222.Li B, Dewey CN. RSEM: accurate transcript quantification from RNA-Seq data with or without a reference genome. *BMC Bioinformatics.* 2011;12(1):323. doi:10.1186/1471-2105-12-323
- 223.Mohammadi P, Castel SE, Brown AA, Lappalainen T. Quantifying the regulatory effect size of cis-acting genetic variation using allelic fold change. *Genome Res.* 2017;27(11):1872-1884. doi:10.1101/gr.216747.116
- 224.Lonsdale J, Thomas J, Salvatore M, et al. The Genotype-Tissue Expression (GTEx) project. *Nat Genet.* 2013;45(6):580-585. doi:10.1038/ng.2653
- 225.Mansur YA, Rojano E, Ranea JAG, Perkins JR. Chapter 7 - Analyzing the Effects of Genetic Variation in Noncoding Genomic Regions. In: Deigner HP, Kohl M, eds. *Precision Medicine.* Academic Press; 2018:119-144. doi:10.1016/B978-0-12-805364-5.00007-X
- 226.Oscanoa J, Sivapalan L, Gadaleta E, Dayem Ullah AZ, Lemoine NR, Chelala C. SNPnexus: a web server for functional annotation of human genome sequence variation (2020 update). *Nucleic Acids Res.* 2020;48(W1):W185-W192. doi:10.1093/nar/gkaa420
- 227.Therneau TM, Grambsch PM. *Modeling Survival Data: Extending the Cox Model.* Springer; 2000. doi:10.1007/978-1-4757-3294-8
- 228.Kassambara A, Kosinski M, Biecek P, Fabian S. survminer: Drawing Survival Curves using “ggplot2.” Published online October 30, 2024. Accessed March 8, 2025. <https://cran.r-project.org/web/packages/survminer/index.html>
- 229.Bolar K. STAT: Interactive Document for Working with Basic Statistical Analysis. Published online April 1, 2019. Accessed March 8, 2025. <https://cran.r-project.org/web/packages/STAT/index.html>
- 230.Kapuy O, He E, López-Avilés S, Uhlmann F, Tyson JJ, Novák B. System-level feedbacks control cell cycle progression. *FEBS Lett.* 2009;583(24):3992-3998. doi:10.1016/j.febslet.2009.08.023
- 231.Lindqvist A, Rodríguez-Bravo V, Medema RH. The decision to enter mitosis: feedback and redundancy

- in the mitotic entry network. *J Cell Biol.* 2009;185(2):193-202. doi:10.1083/jcb.200812045
- 232.Perry JA, Kornbluth S. Cdc25 and Wee1: analogous opposites? *Cell Div.* 2007;2(1):12. doi:10.1186/1747-1028-2-12
- 233.Keaton MA. Morgan DO: The Cell Cycle: Principles of Control (Primers in Biology). *Cell Div.* 2007;2(1):27. doi:10.1186/1747-1028-2-27
- 234.Lukas J, Lukas C, Bartek J. Mammalian cell cycle checkpoints: signalling pathways and their organization in space and time. *DNA Repair.* 2004;3(8):997-1007. doi:10.1016/j.dnarep.2004.03.006
- 235.Ciliberto A, Capuani F, Tyson JJ. Modeling Networks of Coupled Enzymatic Reactions Using the Total Quasi-Steady State Approximation. *PLOS Comput Biol.* 2007;3(3):e45. doi:10.1371/journal.pcbi.0030045
- 236.Deibler RW, Kirschner MW. Quantitative Reconstitution of Mitotic CDK1 Activation in Somatic Cell Extracts. *Mol Cell.* 2010;37(6):753-767. doi:10.1016/j.molcel.2010.02.023
- 237.Ciliberto A, Novak B, Tyson JJ. Mathematical model of the morphogenesis checkpoint in budding yeast. *J Cell Biol.* 2003;163(6):1243-1254. doi:10.1083/jcb.200306139
- 238.Ng SS, Anderson M, White S, McInerny CJ. mik1 + G1-S transcription regulates mitotic entry in fission yeast. *FEBS Lett.* 2001;503(2-3):131-134. doi:10.1016/S0014-5793(01)02720-X
- 239.Rupeš I. Checking cell size in yeast. *Trends Genet.* 2002;18(9):479-485. doi:10.1016/S0168-9525(02)02745-2
- 240.Sunada S, Saito H, Zhang D, Xu Z, Miki Y. CDK1 inhibitor controls G2/M phase transition and reverses DNA damage sensitivity. *Biochem Biophys Res Commun.* 2021;550:56-61. doi:10.1016/j.bbrc.2021.02.117
- 241.Massacci G, Perfetto L, Sacco F. The Cyclin-dependent kinase 1: more than a cell cycle regulator. *Br J Cancer.* 2023;129(11):1707-1716. doi:10.1038/s41416-023-02468-8
- 242.Liu K, Zheng M, Lu R, et al. The role of CDC25C in cell cycle regulation and clinical cancer therapy: a systematic review. *Cancer Cell Int.* 2020;20(1):213. doi:10.1186/s12935-020-01304-w
- 243.Busch C, Barton O, Morgenstern E, et al. The G2/M checkpoint phosphatase cdc25C is located within centrosomes. *Int J Biochem Cell Biol.* 2007;39(9):1707-1713. doi:10.1016/j.biocel.2007.04.022
- 244.Enders GH. Gauchos and ochos: a Wee1-Cdk tango regulating mitotic entry. *Cell Div.* 2010;5(1):12. doi:10.1186/1747-1028-5-12
- 245.Donzelli M, Draetta GF. Regulating mammalian checkpoints through Cdc25 inactivation. *EMBO Rep.* 2003;4(7):671-677. doi:10.1038/sj.emboj.emboj887
- 246.Ghelli Luserna di Rorà A, Cerchione C, Martinelli G, Simonetti G. A WEE1 family business: regulation of mitosis, cancer progression, and therapeutic target. *J Hematol Oncol Hematol Oncol.* 2020;13(1):126. doi:10.1186/s13045-020-00959-2
- 247.Watanabe N, Arai H, Iwasaki JI, et al. Cyclin-dependent kinase (CDK) phosphorylation destabilizes somatic Wee1 via multiple pathways. *Proc Natl Acad Sci U S A.* 2005;102(33):11663-11668. doi:10.1073/pnas.0500410102
- 248.Bucher N, Britten CD. G2 checkpoint abrogation and checkpoint kinase-1 targeting in the treatment of cancer. *Br J Cancer.* 2008;98(3):523-528. doi:10.1038/sj.bjc.6604208
- 249.Sanchez Y, Wong C, Thoma RS, et al. Conservation of the Chk1 Checkpoint Pathway in Mammals:

Linkage of DNA Damage to Cdk Regulation Through Cdc25. *Science*. 1997;277(5331):1497-1501. doi:10.1126/science.277.5331.1497

250. Donzelli M, Draetta GF. Regulating mammalian checkpoints through Cdc25 inactivation. *EMBO Rep.* 2003;4(7):671-677. doi:10.1038/sj.embo.embor887
251. Hsu CC, Yao X, Chen SY, Tsuo TC, Wang IC. The conformation of FOXM1 homodimers in vivo is crucial for regulating transcriptional activities. *Nucleic Acids Res.* 2024;52(22):13625-13643. doi:10.1093/nar/gkae988
252. Bouhaddou M, Barrette AM, Stern AD, et al. A mechanistic pan-cancer pathway model informed by multi-omics data interprets stochastic cell fate responses to drugs and mitogens. *PLOS Comput Biol.* 2018;14(3):e1005985. doi:10.1371/journal.pcbi.1005985
253. Gérard C, Goldbeter A. Temporal self-organization of the cyclin/Cdk network driving the mammalian cell cycle. *Proc Natl Acad Sci.* 2009;106(51):21643-21648. doi:10.1073/pnas.0903827106
254. Landrum MJ, Lee JM, Benson M, et al. ClinVar: improving access to variant interpretations and supporting evidence. *Nucleic Acids Res.* 2018;46(D1):D1062-D1067. doi:10.1093/nar/gkx1153
255. CCNB1 is a novel prognostic biomarker and promotes proliferation, migration and invasion in Wilms tumor | BMC Medical Genomics | Full Text. Accessed March 10, 2025. <https://bmcmedgenomics.biomedcentral.com/articles/10.1186/s12920-023-01627-3>
256. Kim HJ, Seo BG, Seo EC, Lee KM, Hwangbo C. Checkpoint Kinase 1 (CHK1) Functions as Both a Diagnostic Marker and a Regulator of Epithelial-to-Mesenchymal Transition (EMT) in Triple-Negative Breast Cancer. *Curr Issues Mol Biol.* 2022;44(12):5848-5865. doi:10.3390/cimb44120398
257. Huang HL, Chiang CH, Hung WC, Hou MF. Targeting of TGF- $\beta$ -activated protein kinase 1 inhibits chemokine (C-C motif) receptor 7 expression, tumor growth and metastasis in breast cancer. *Oncotarget.* 2014;6(2):995-1007.
258. Harbers L, Agostini F, Nicos M, Poddighe D, Bienko M, Crosetto N. Somatic Copy Number Alterations in Human Cancers: An Analysis of Publicly Available Data From The Cancer Genome Atlas. *Front Oncol.* 2021;11. doi:10.3389/fonc.2021.700568
259. Loo LWM, Wang Y, Flynn EM, et al. Genome-wide copy number alterations in subtypes of invasive breast cancers in young white and African American women. *Breast Cancer Res Treat.* 2011;127(1):297-308. doi:10.1007/s10549-010-1297-x
260. Liu J, Campen A, Huang S, et al. Identification of a gene signature in cell cycle pathway for breast cancer prognosis using gene expression profiling data. *BMC Med Genomics.* 2008;1(1):39. doi:10.1186/1755-8794-1-39
261. Montalto FI, De Amicis F. Cyclin D1 in Cancer: A Molecular Connection for Cell Cycle Control, Adhesion and Invasion in Tumor and Stroma. *Cells.* 2020;9(12):2648. doi:10.3390/cells9122648
262. Almalki SG. The pathophysiology of the cell cycle in cancer and treatment strategies using various cell cycle checkpoint inhibitors. *Pathol - Res Pract.* 2023;251:154854. doi:10.1016/j.prp.2023.154854
263. Wang Q, Bode AM, Zhang T. Targeting CDK1 in cancer: mechanisms and implications. *Npj Precis Oncol.* 2023;7(1):1-14. doi:10.1038/s41698-023-00407-7
264. Sofi S, Mehraj U, Qayoom H, et al. Targeting cyclin-dependent kinase 1 (CDK1) in cancer: molecular docking and dynamic simulations of potential CDK1 inhibitors. *Med Oncol.* 2022;39(9):133. doi:10.1007/s12032-022-01748-2
265. Zhang W, Shang X, Yang F, et al. CDC25C as a Predictive Biomarker for Immune Checkpoint Inhibitors

in Patients With Lung Adenocarcinoma. *Front Oncol.* 2022;12. doi:10.3389/fonc.2022.867788

- 266.Liu K, Zheng M, Zhao Q, et al. Different p53 genotypes regulating different phosphorylation sites and subcellular location of CDC25C associated with the formation of polyploid giant cancer cells. *J Exp Clin Cancer Res.* 2020;39(1):83. doi:10.1186/s13046-020-01588-w
- 267.Loddo M, Andryszkiewicz J, Rodriguez-Acebes S, et al. Pregnancy-associated plasma protein A regulates mitosis and is epigenetically silenced in breast cancer. *J Pathol.* 2014;233(4):344-356. doi:10.1002/path.4393
- 268.Bhattarai S, Rupji M, Chao H ping, et al. Cell cycle traverse rate predicts long-term outcomes in a multi-institutional cohort of patients with triple-negative breast cancer. *BJC Rep.* 2024;2(1):1-10. doi:10.1038/s44276-024-00097-z
- 269.Liu S, Xie SM, Liu W, et al. Targeting CXCR4 abrogates resistance to trastuzumab by blocking cell cycle progression and synergizes with docetaxel in breast cancer treatment. *Breast Cancer Res.* 2023;25(1):62. doi:10.1186/s13058-023-01665-w
- 270.Sofianidi A, Dumbrava EE, Syrigos KN, Nasrazadani A. Triple-Negative Breast Cancer and Emerging Therapeutic Strategies: ATR and CHK1/2 as Promising Targets. *Cancers.* 2024;16(6):1139. doi:10.3390/cancers16061139
- 271.Bhattarai S, Rupji M, Chao H ping, et al. Cell cycle traverse rate predicts long-term outcomes in a multi-institutional cohort of patients with triple-negative breast cancer. *BJC Rep.* 2024;2(1):1-10. doi:10.1038/s44276-024-00097-z

# Appendix

**Table S1.** Table that contains for each tissue the eQTLs of the genes of interest, inside the cell are present rsID for each SNP.

	WEE1	MARK3	FOXM1	CTDP1	CHEK1	CDK1	CDC25C	CCNB1
Adipose Subcutaneous	rs1835790	rs28444993		rs9958397	rs7935039			rs164386
Adipose Visceral Omentum	rs7951669	rs11627052					rs10036665	rs148511921
Adrenal Gland								rs148511921
Artery Aorta		rs12147741		rs75928802	rs498667	rs68045193		
Artery Tibial	rs11042430	rs11627567			rs11220164			
Brain Amygdala								rs59387311
Brain Anterior cingulate cortex BA24		rs28496120			rs7939100			
Brain Caudate basal ganglia		rs1951391		rs12458462	rs7110899			
Brain Cerebellum		rs2246490		rs113376412			rs41294564	
Brain Cortex		rs2296486		rs11660714	rs12807809			
Brain Frontal Cortex BA9	rs7483960	rs45441198			rs117110188	rs2448357		
Brain Hippocampus		rs35862113						rs185755201
Brain Nucleus accumbens basal ganglia		rs74085289		rs2035085				
Brain Putamen basal ganglia		rs45441198			rs1941367			
Brain Spinal cord cervical c-1		rs2246490						

Breast Mammary Tissue		rs286260 81		rs124584 62	rs761183 07			rs28576332
Cells Cultured fibroblasts		rs145085 091	rs118233 0562			rs244833 8	rs1393191 82	
Cells EBV-transformed lymphocytes	rs228907 4	rs116275 67		rs620996 05		rs10711	rs6596430	
Colon Sigmoid					rs559671 26			
Colon Transverse		rs227370 3		rs593378	rs284922 3			
Esophagus Gastroesophageal Junction						rs707067 9		rs6862253
Esophagus Mucosa	rs712387 3	rs714360 9	rs128224 87		rs783940 87	rs190441 2	rs1155023 34	
Esophagus Muscularis				rs571152				
Heart Atrial Appendage	rs115535 79							rs3087334
Heart Left Ventricle	rs138618 203	rs201688 592						
Kidney Cortex		rs101325 14						
Liver		rs224649 0		rs530806				
Lung		rs224649 0					rs6238124 4	rs18121262 7
Minor Salivary Gland		rs114148 60						
Muscle Skeletal	rs138618 203	rs101413 88		rs359288 63				rs350099
Nerve Tibial	rs138618 203	rs229648 6		rs200748 3	rs138871 024	rs321307 7	rs1717137 0	rs2932771
Ovary		rs116243 67						rs9291949
Pancreas		rs116238 69	rs192793 347					

Pituitary	rs118272 77	rs286260 81		rs359288 63				
Prostate		rs286260 81						
Skin Not Sun Exposed Suprapubic	rs793954 1	rs101516 02		rs730036 76	rs795886 68	rs674937 31	rs1393191 82	
Skin Sun Exposed Lower leg	rs793954 1	rs101516 02	rs290760 8	rs808286 2	rs118204 87	rs244834 3	rs1143739 63	rs12513817
Small Intestine Terminal Ileum		rs375957 9						
Spleen		rs714360 9		rs116621 06				rs13826406 8
Stomach		rs116289 69				rs109942 82		
Testis		rs714056 4		rs545038	rs140479 100		rs1143739 63	rs78504575
Thyroid	rs138893 388	rs138893 388	rs110623 73	rs110623 73	rs554552	rs105969 38	rs6238094 0	rs2932771
Uterus		rs555236 305			rs112507 929			
Whole Blood	rs107700 66	rs801632 6		rs496281				

**Table S2.** Tables representing the frequency of copy number aberration identified in the genes of interest in the several groups analyzed.

Group 1: average switch time > 3290

	C-TAK1	CDK1	CHK1	FCP1	FOXM1	WEE1
Amplification	0.73	/	/	0.1	0.2	0.5
Diploid	6.6	7.8	6.9	7.2	8.4	7.4
Gain	6.9	0.72	4.3	2.7	4.7	7.5
S. Deletion	2.4	8.1	8.1	6.1	3.3	1.25

D. Deletion	/	/	0.1	0.5	/	/
-------------	---	---	-----	-----	---	---

Group 2: average switch time < 3290

	C-TAK1	CDK1	CHK1	FCP1	FOXM1	WEE1
Amplification	0.04	0.3	/	0.08	0.3	/
Diploid	0.06	11.5	7.0	9.1	10.6	10.2
Gain	1.4	2.4	0.8	2.3	3.7	1.1
S. Deletion	5.2	2.3	2.4	5.1	2.0	5.3
D. Deletion	/	0.02	0.2	0.2	/	0.06

Group 1: switch percentage < 55

	C-TAK1	CDK1	CHK1	FCP1	FOXM1	WEE1
Amplification	0.4	/	/	/	0.1	0.2
Diploid	2.5	1.7	1.35	2.1	2.6	1.6
Gain	2.5	0.5	2.7	1.2	1.9	4.2
S. Deletion	0.8	3.9	2.2	2.8	1.7	0.3
D. Deletion	/	/	/	0.3	/	/

Group 2: switch percentage > 55

	C-TAK1	CDK1	CHK1	FCP1	FOXM1	WEE1
Amplification	0.09	0.3	/	0.3	0.3	0.05
Diploid	9.5	11.3	7.3	10.4	10.6	10.1
Gain	2.1	2.2	0.9	2.3	3.8	1.6
S. Deletion	4.9	2.8	8.2	5.1	2.1	4.8
D. Deletion	0.05	0.02	0.2	/	/	0.05

**Figure S1.**  $B_A^A$  model switch with TF on activator with quantity 500 (a) and 50 (b)

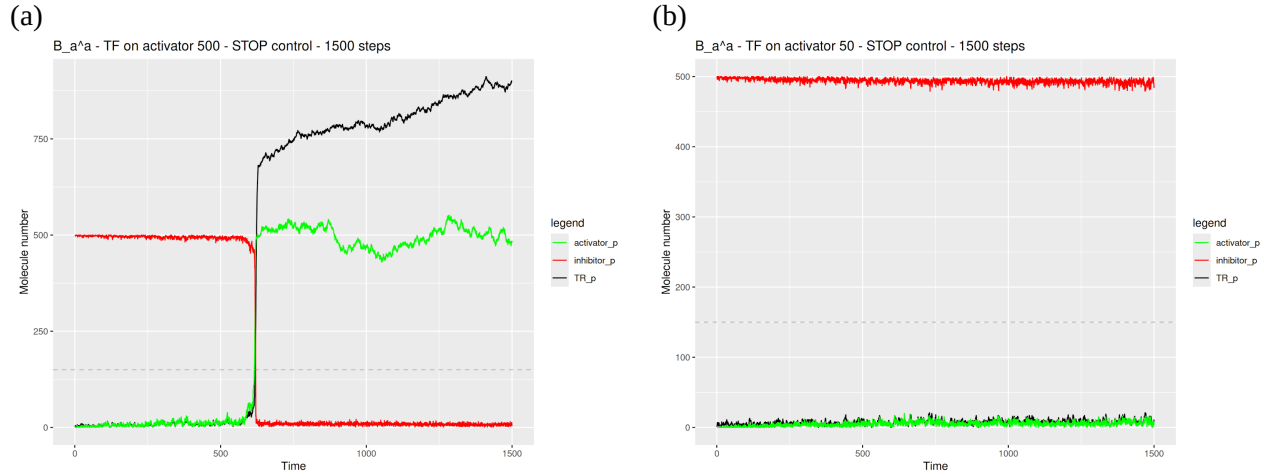


**Figure S2.**  $B_A^B$  model switch with TF on activator with quantity 500 (a) and 50 (b)

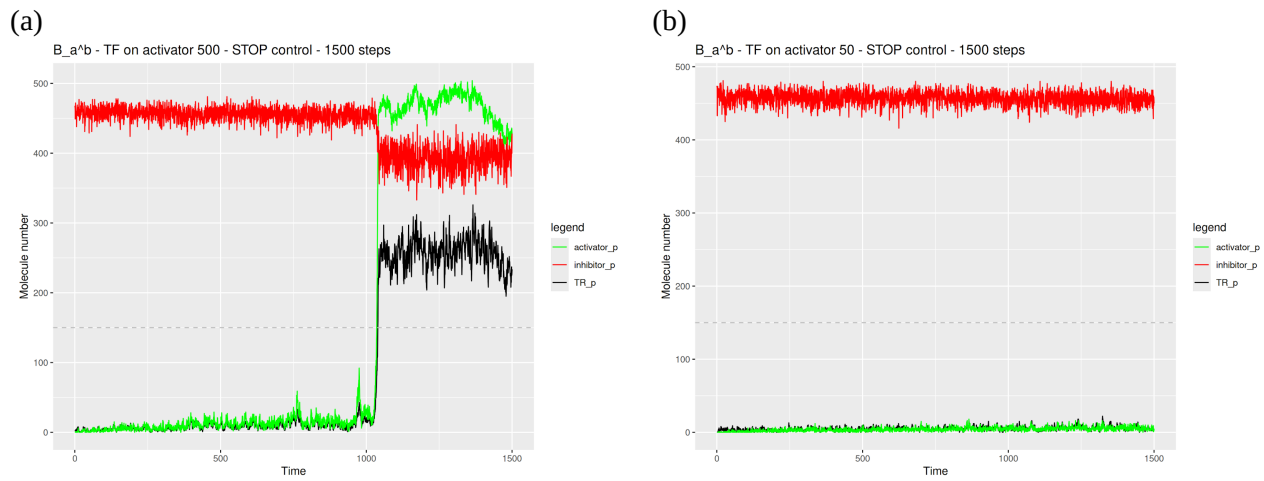


**Figure S3.**  $B_A^I$  model switch with TF on activator with quantity 500 (a) and 50 (b)

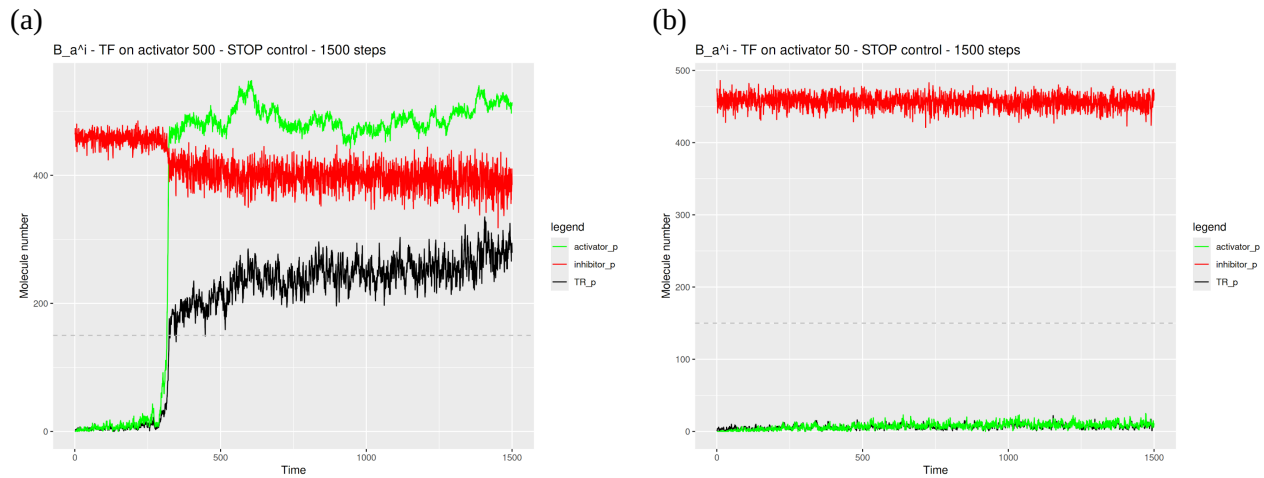


**Figure S4.**  $B_I^A$  model switch with TF on inhibitor with quantity 500 (a) and 50 (b)

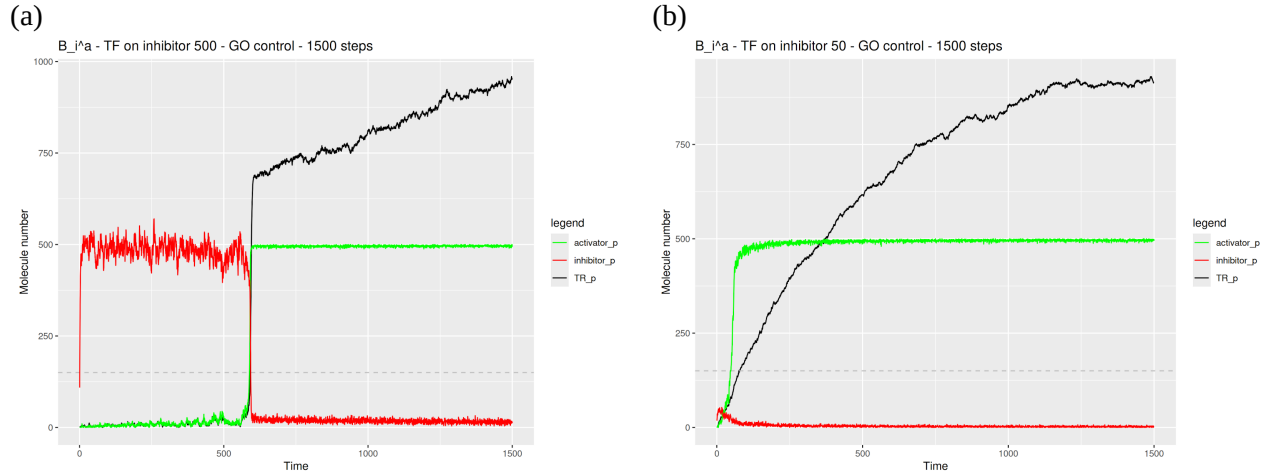


**Figure S5.**  $B_I^B$  model switch with TF on inhibitor with quantity 500 (a) and 50 (b)

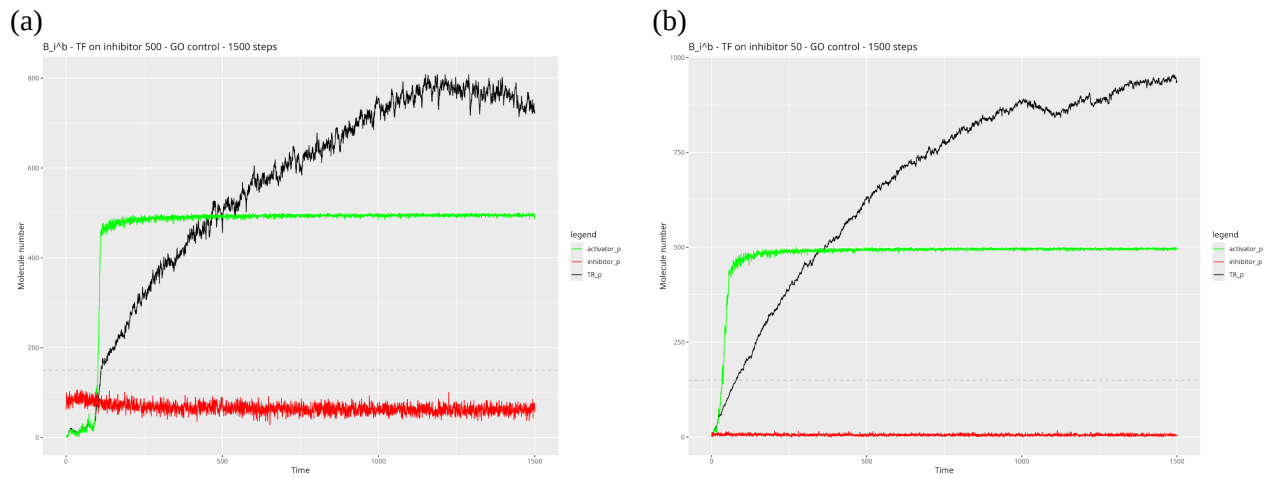


**Figure S6.**  $B_I^I$  model switch with TF on inhibitor with quantity 500 (a) and 50 (b)

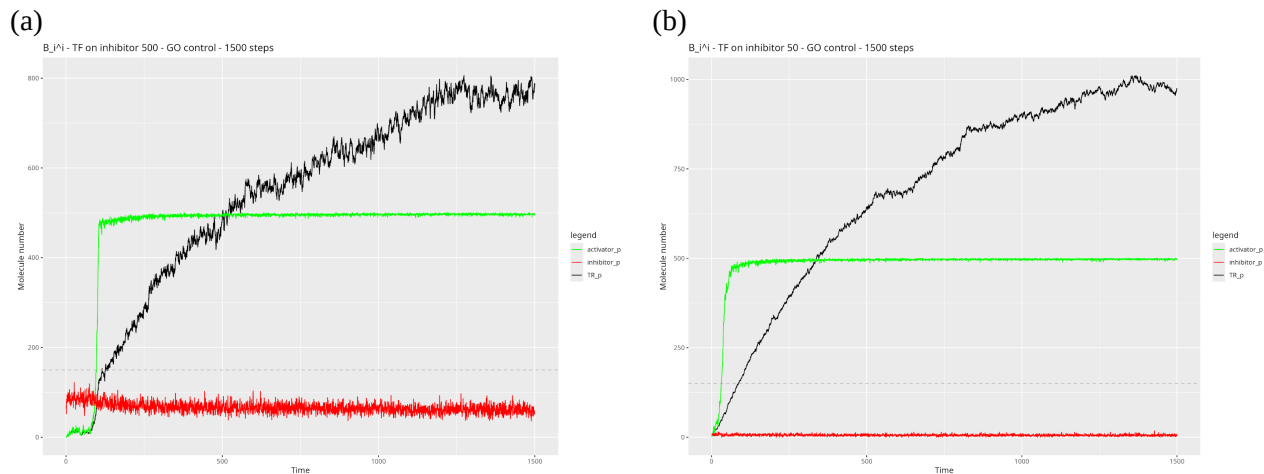


**Figure S7.**  $A_A$  model switch with TF on activator with quantity 500 (a) and 50 (b)

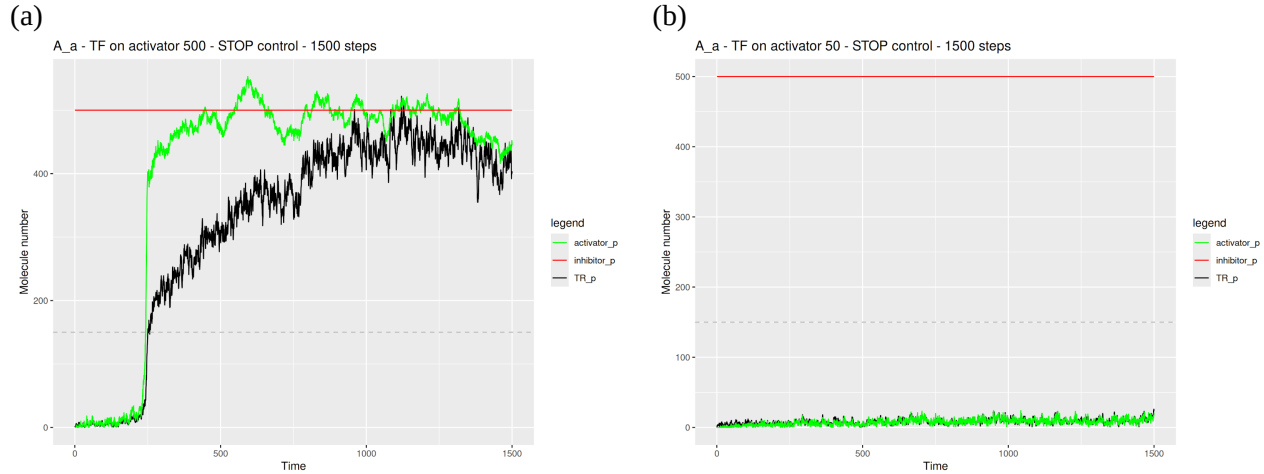


**Figure S8.**  $A_A^A$  model switch with TF on activator with quantity 500 (a) and 50 (b)

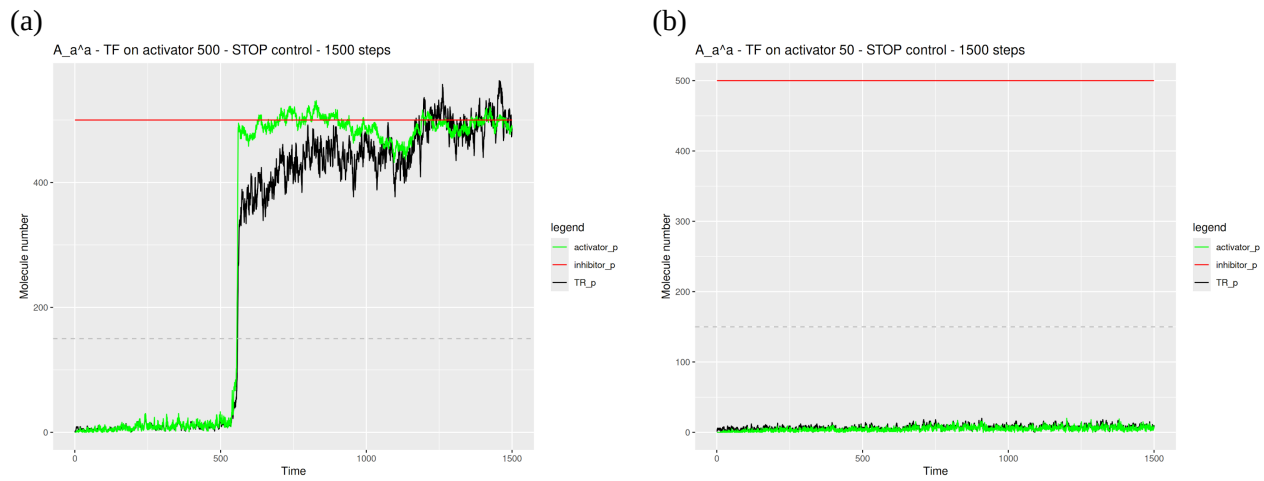


**Figure S9.**  $A_A^B$  model switch with TF on activator with quantity 500 (a) and 50 (b)

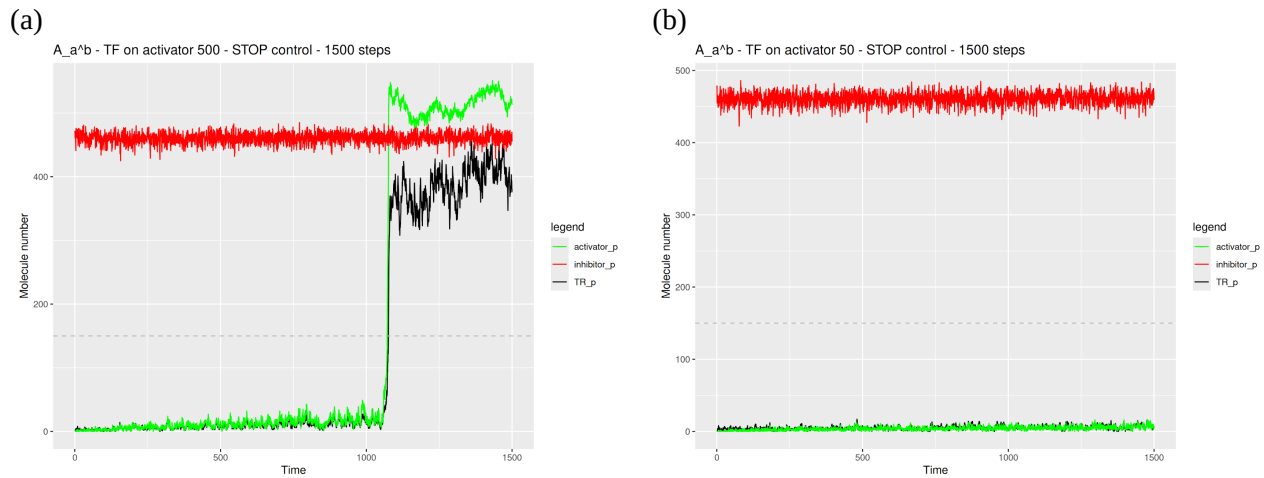


**Figure S10.**  $A_A^A$  model switch with TF on activator with quantity 500 (a) and 50 (b)

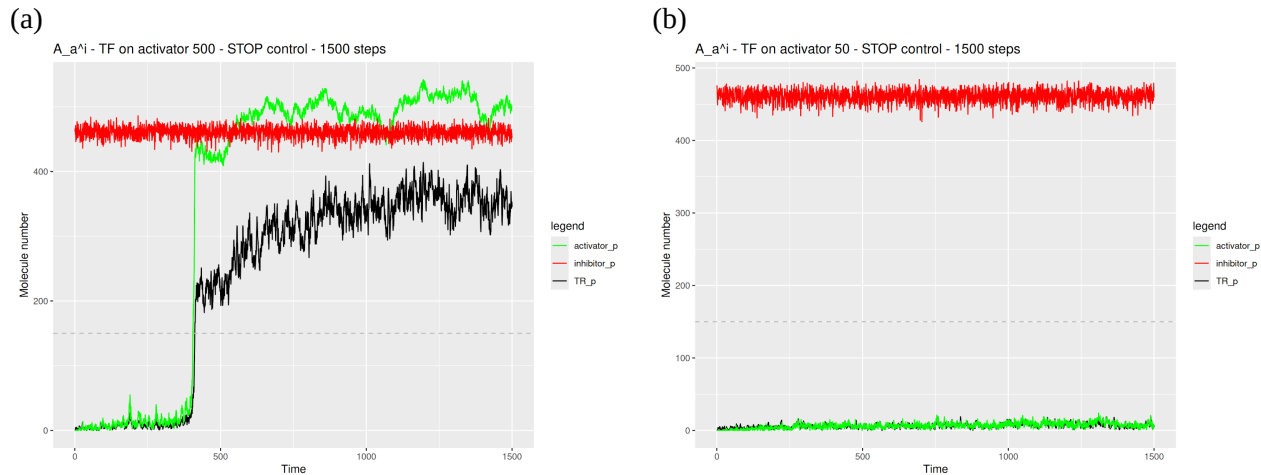


**Figure S11.**  $A_i$  model switch with TF on inhibitor with quantity 500 (a) and 50 (b)

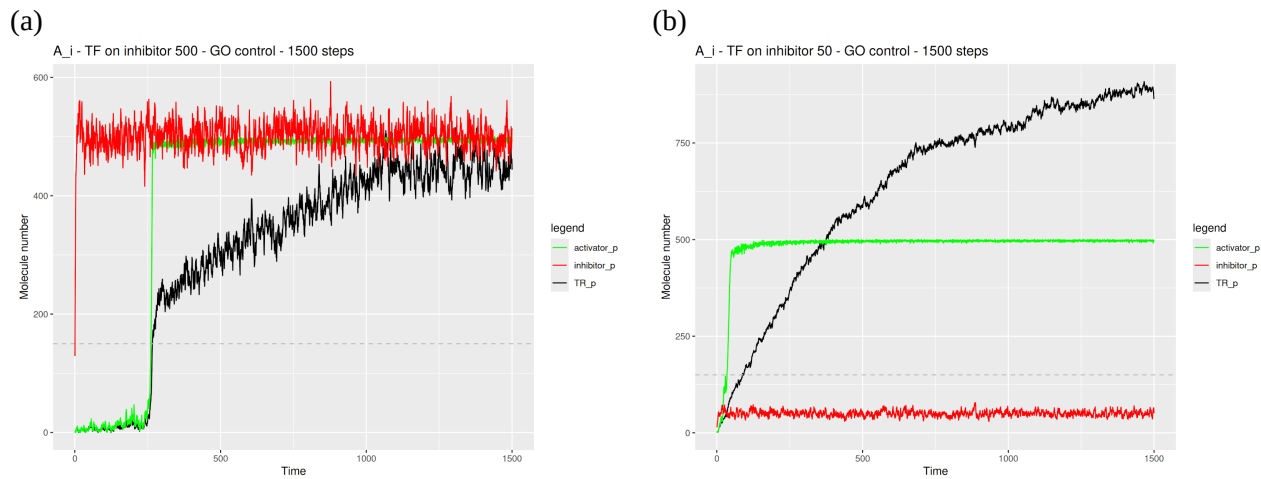


**Figure S12.**  $A_i^A$  model switch with TF on inhibitor with quantity 500 (a) and 50 (b)

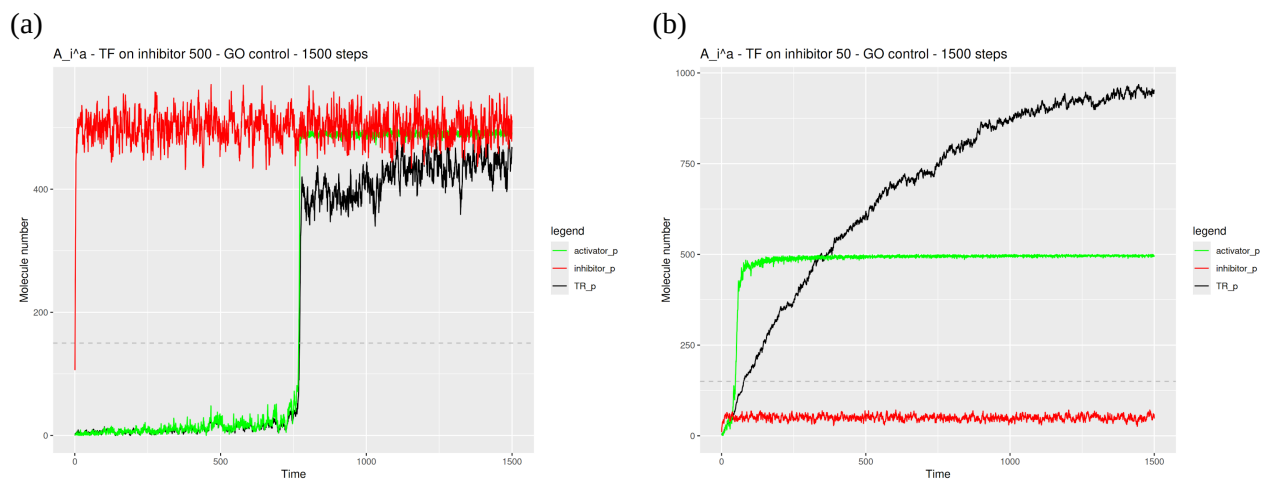


**Figure S13.**  $A_i^B$  model switch with TF on inhibitor with quantity 500 (a) and 50 (b)

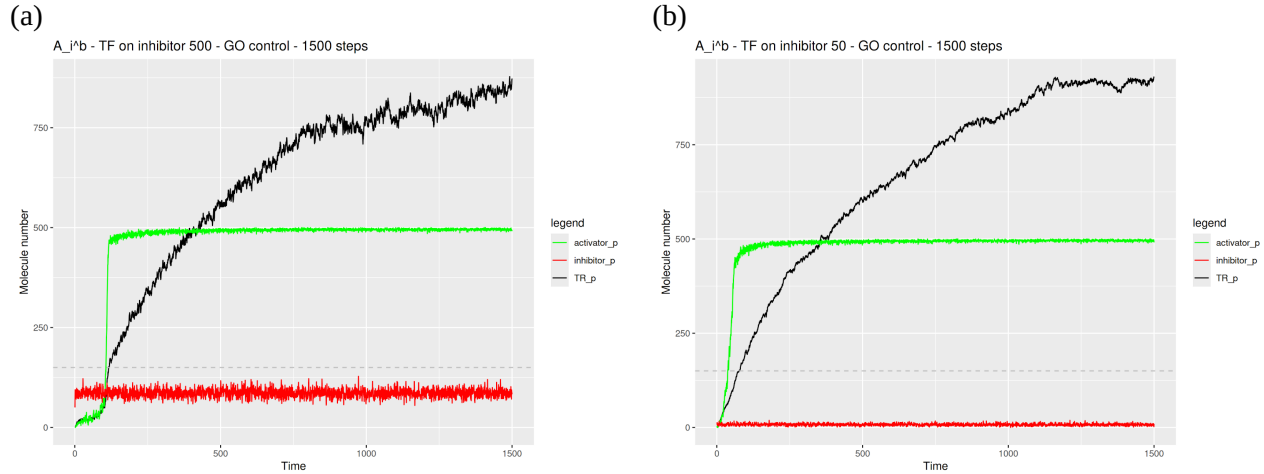


**Figure S14.**  $A_i^I$  model switch with TF on inhibitor with quantity 500 (a) and 50 (b)

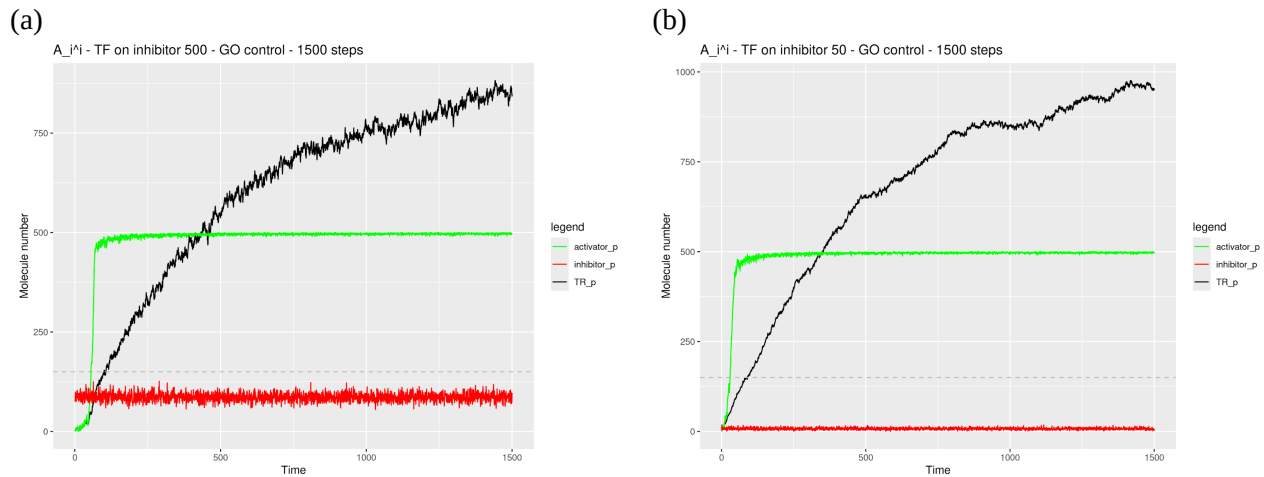


**Figure S15.**  $I_A$  model switch with TF on activator with quantity 500 (a) and 50 (b)

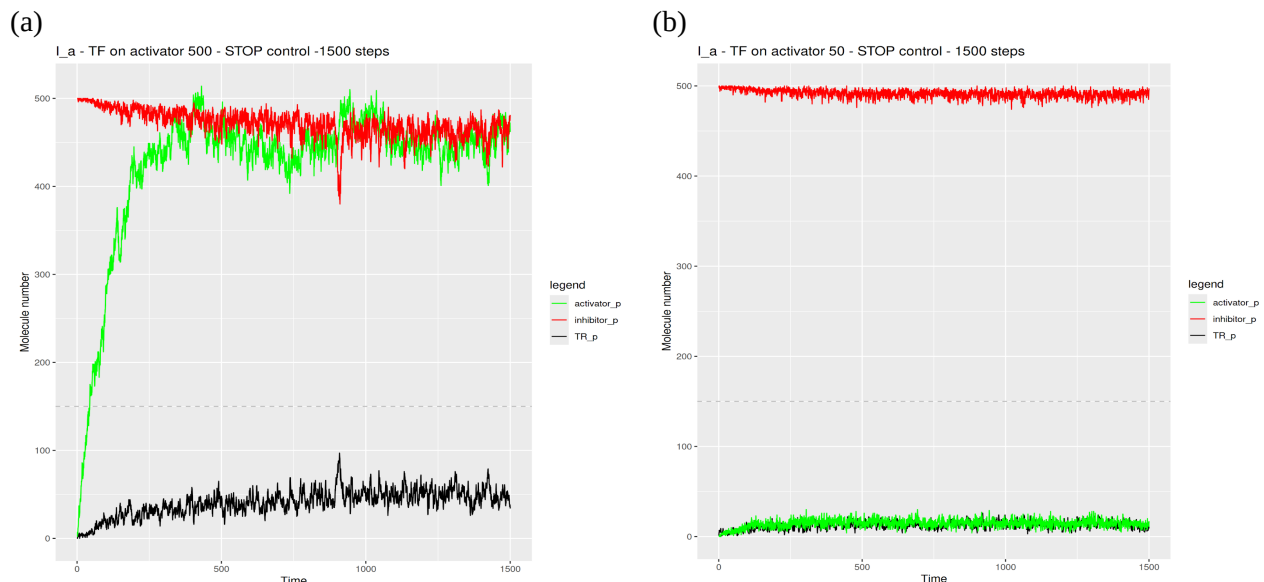


**Figure S16.**  $I_A^A$  model switch with TF on activator with quantity 500 (a) and 50 (b)

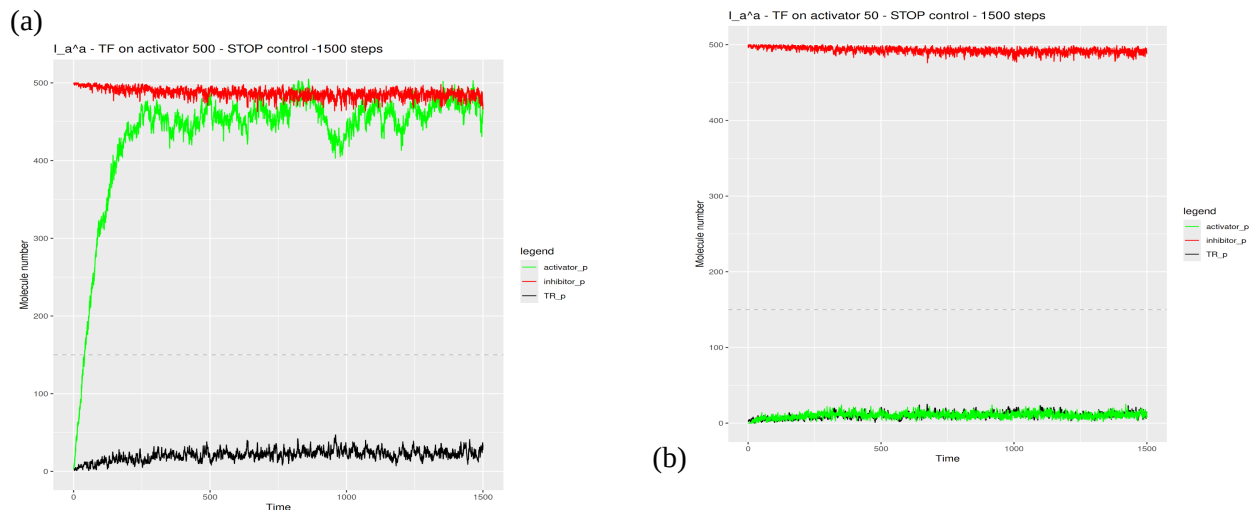


**Figure S17.**  $I_A^B$  model switch with TF on activator with quantity 500 (a) and 50 (b)

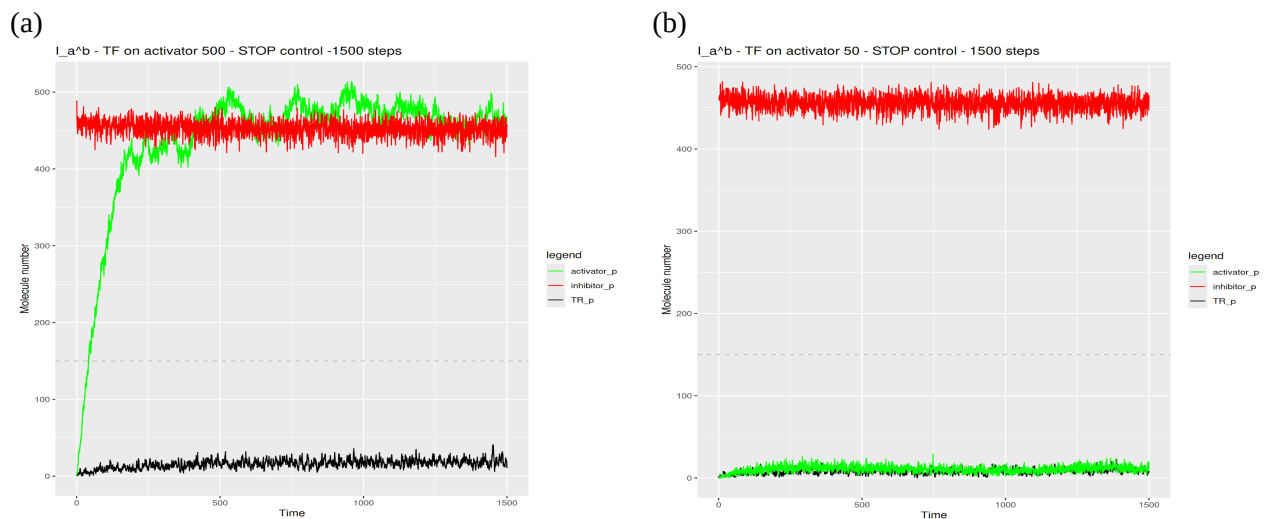


**Figure S18.**  $I_A^I$  model switch with TF on activator with quantity 500 (a) and 50 (b)

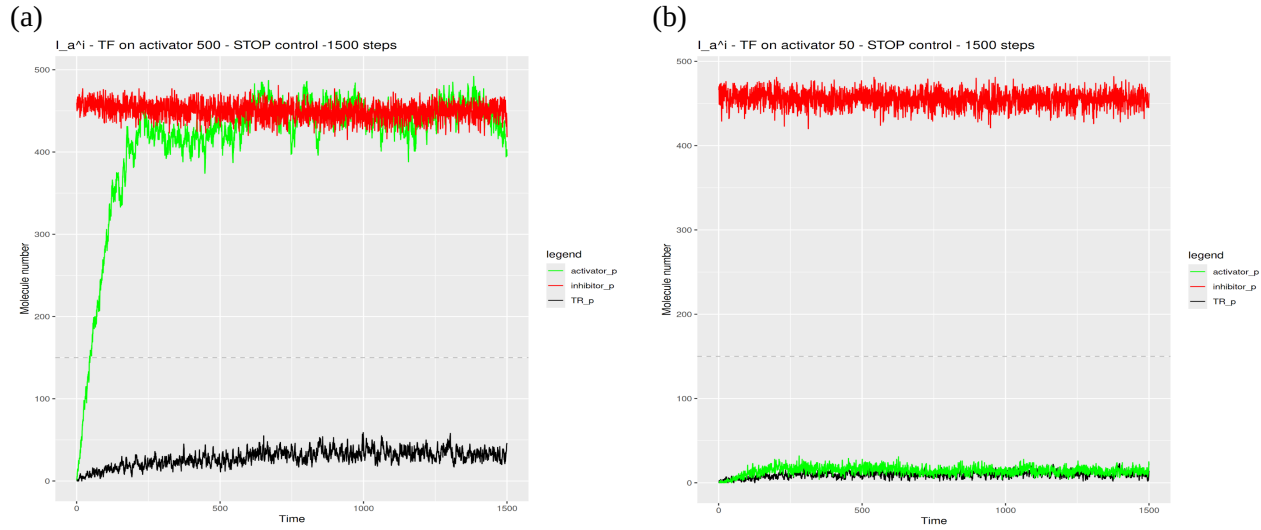


**Figure S19.**  $I_I$  model switch with TF on inhibitor with quantity 500 (a) and 50 (b)

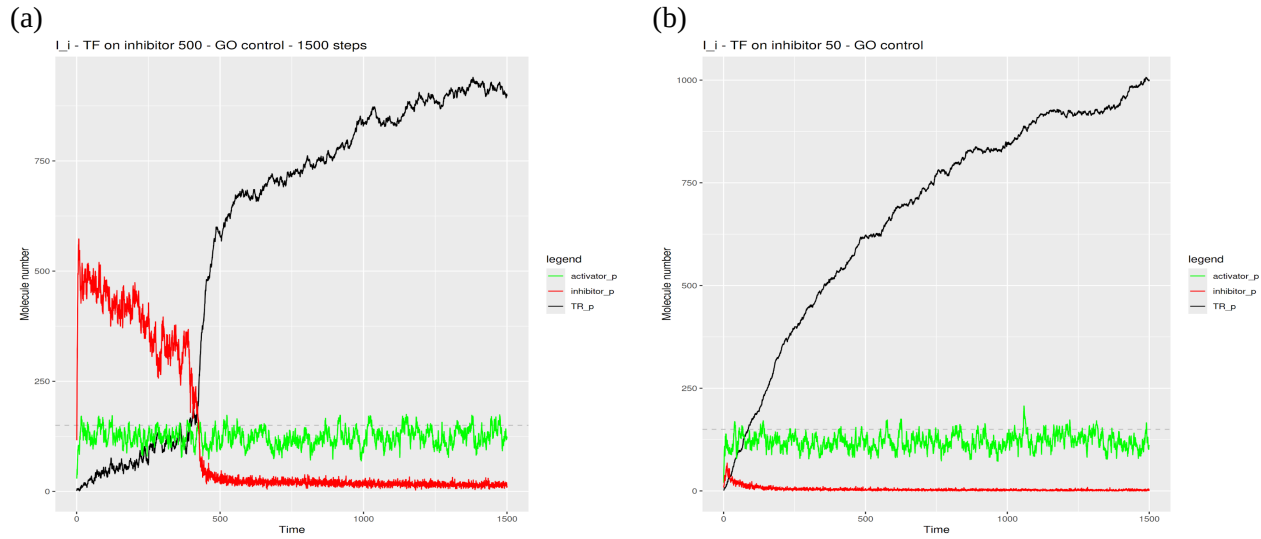


**Figure S20.**  $I_I^A$  model switch with TF on inhibitor with quantity 500 (a) and 50 (b)

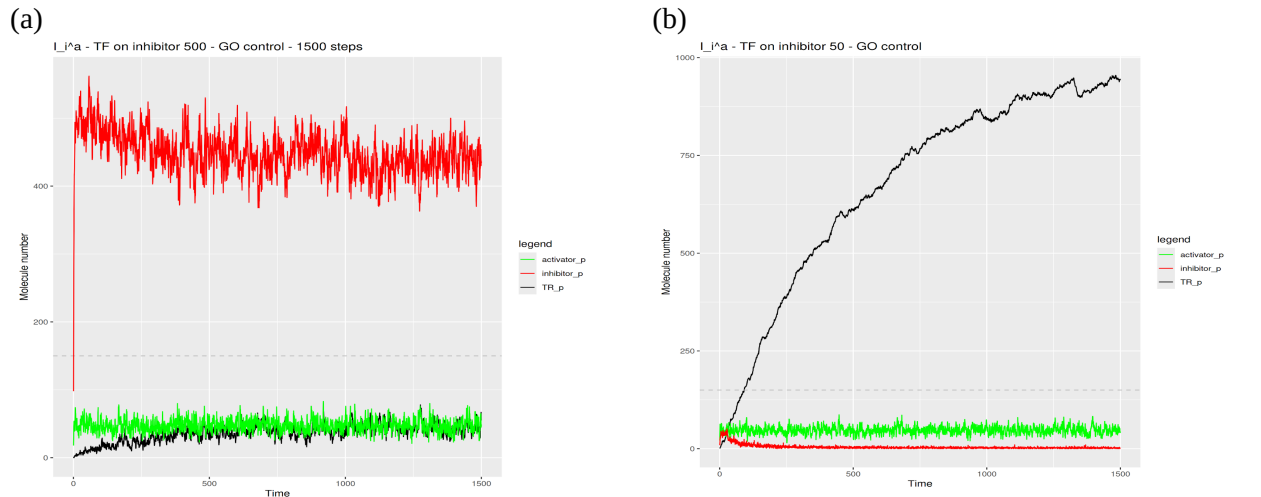


**Figure S21.**  $I_I^B$  model switch with TF on inhibitor with quantity 500 (a) and 50 (b)

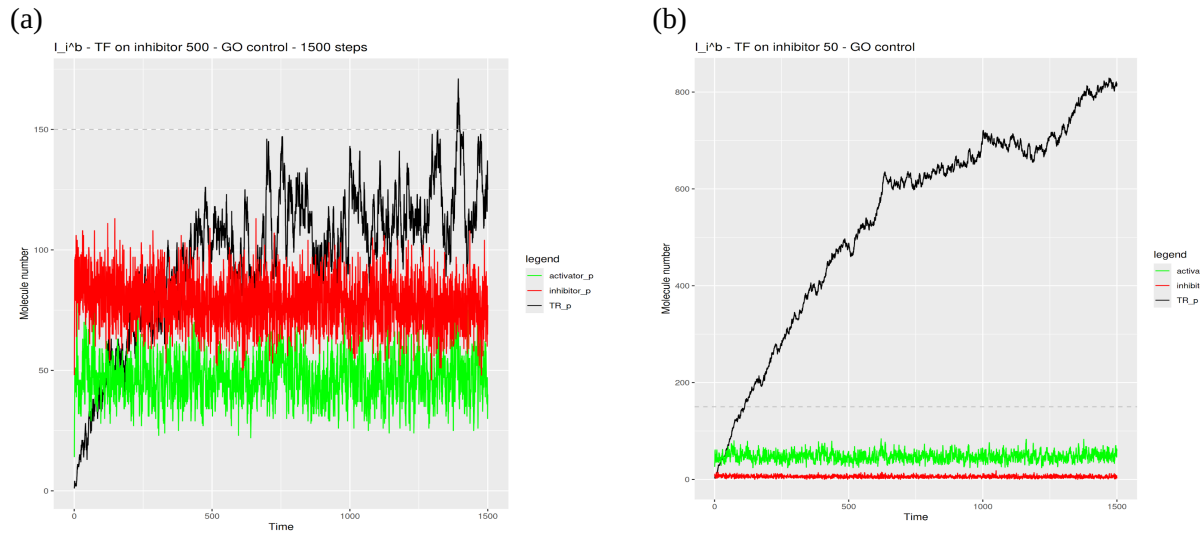


**Figure S22.**  $I_I^I$  model switch with TF on inhibitor with quantity 500 (a) and 50 (b)

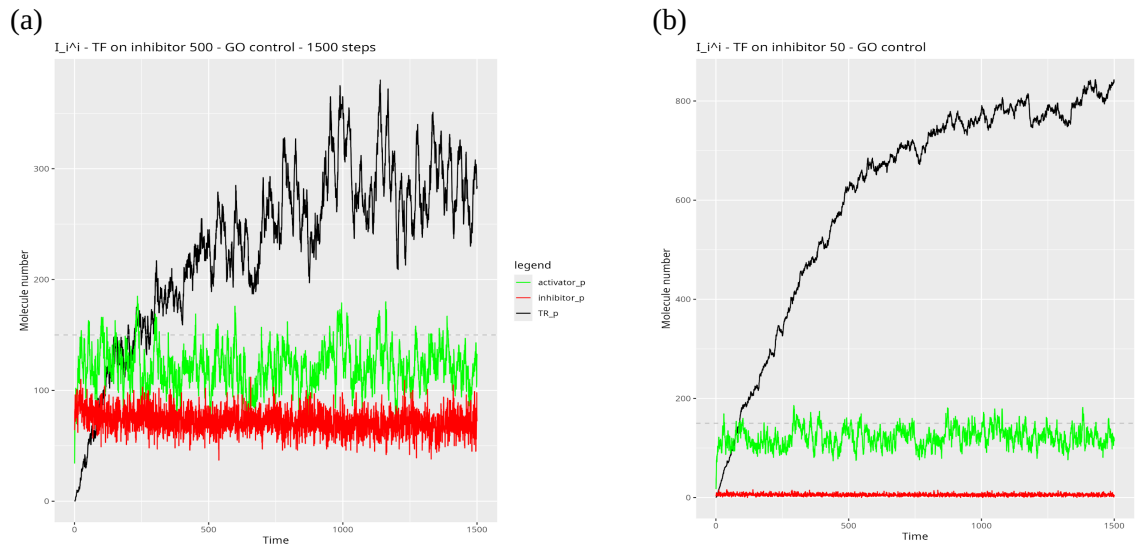
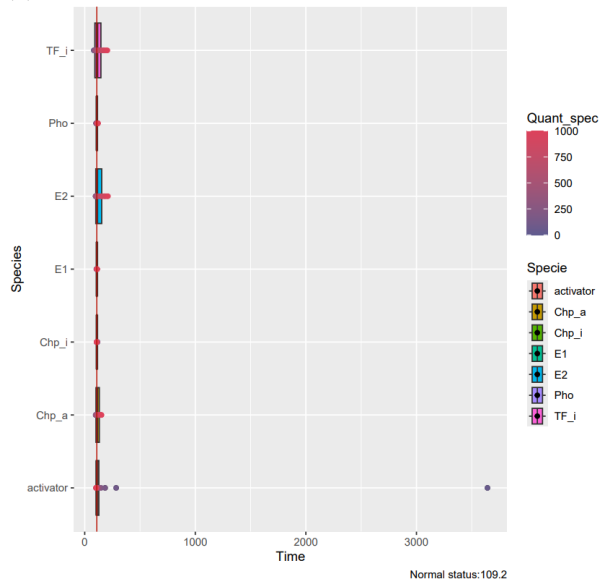


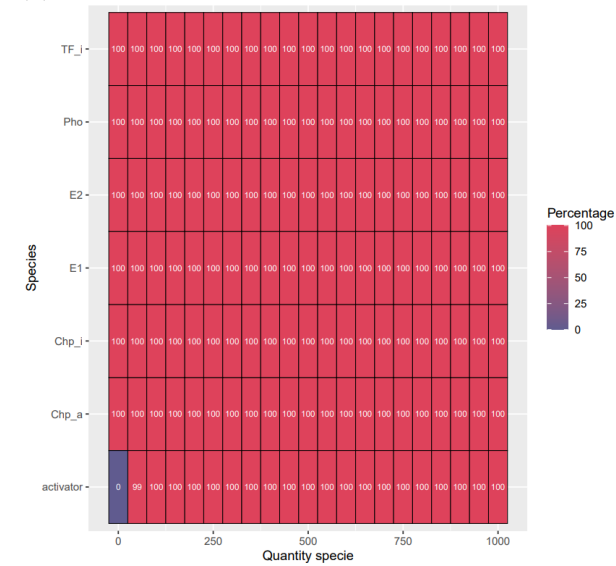
**Figure S23. Sensitivity analysis plots for the models with the positive feedback loop on the activator only.** Panel (a) and (b) represent the sensitivity plot for the species while panels (c) and (d) represent the parameters' behaviour.

$A_I^B$  species.

(a)

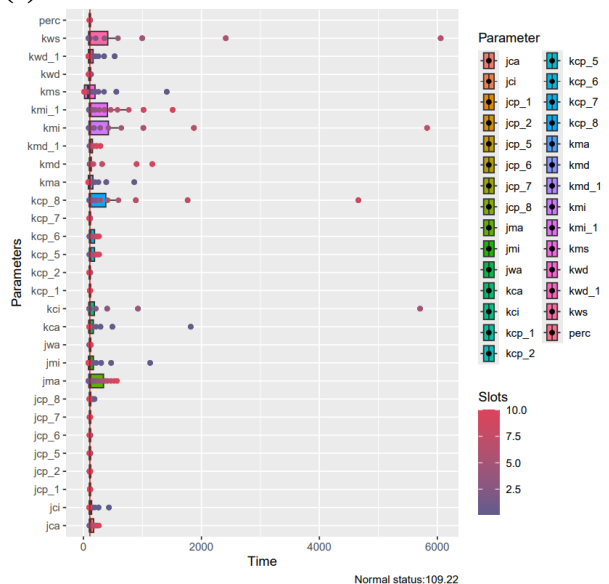


(b)

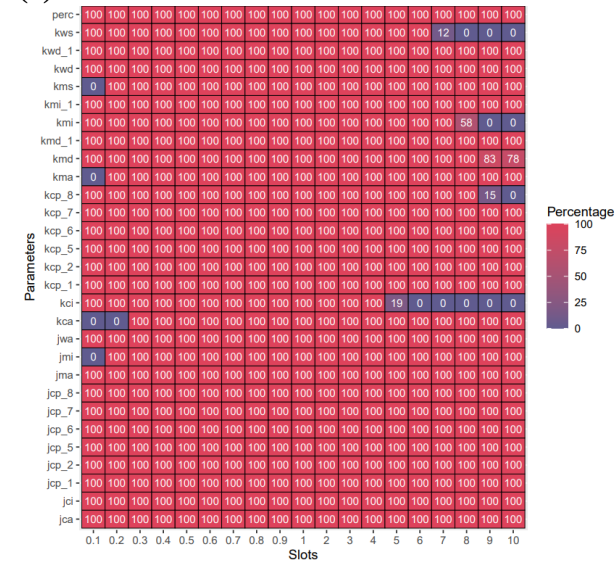


$A_I^B$  parameters

(c)

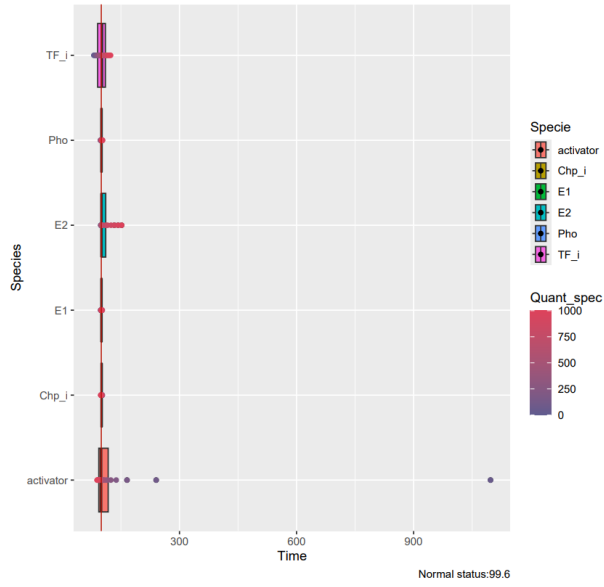


(d)

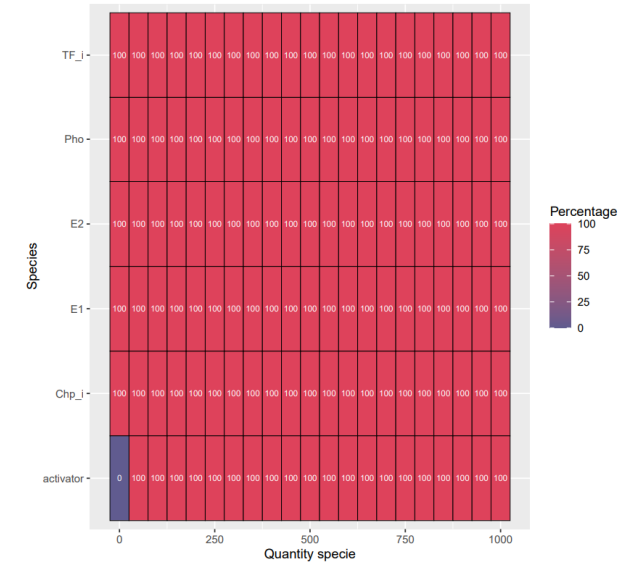


### $A_I^I$ species

(a)

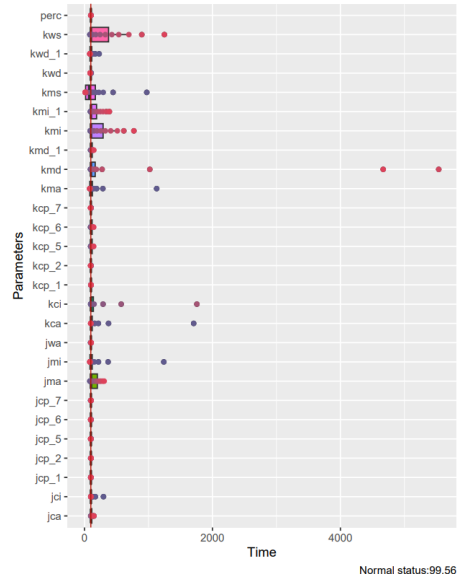


(b)

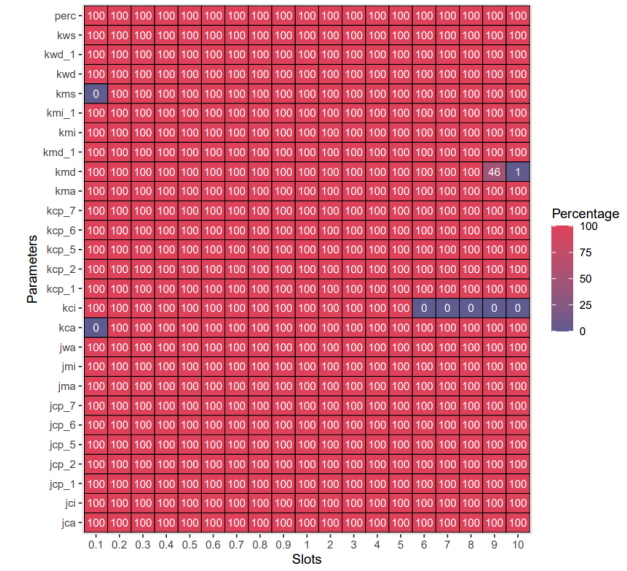


### $A_I^I$ parameters

(c)

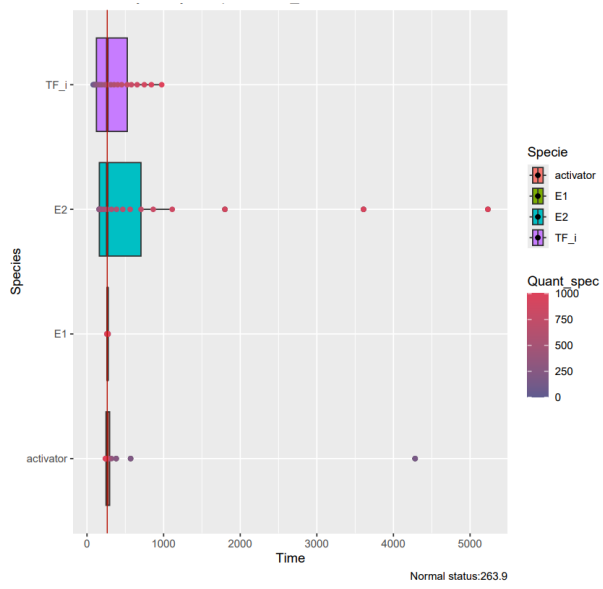


(d)

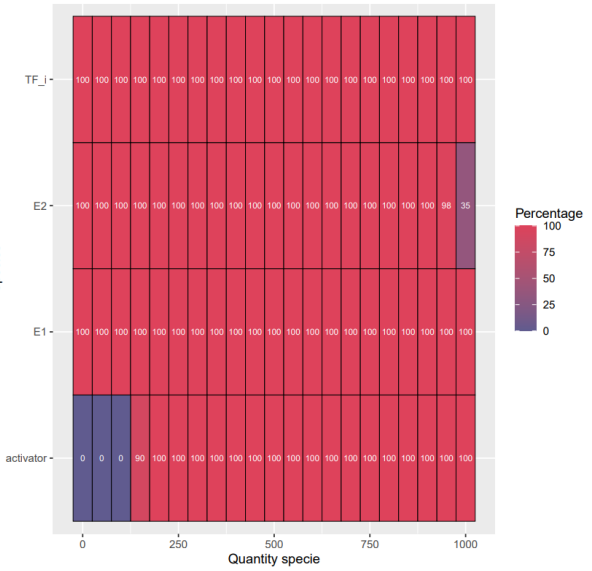


### $A_I$ species

(a)

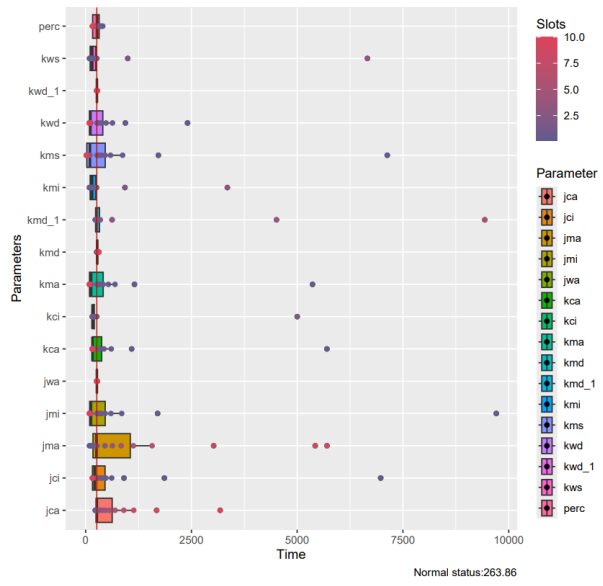


(b)

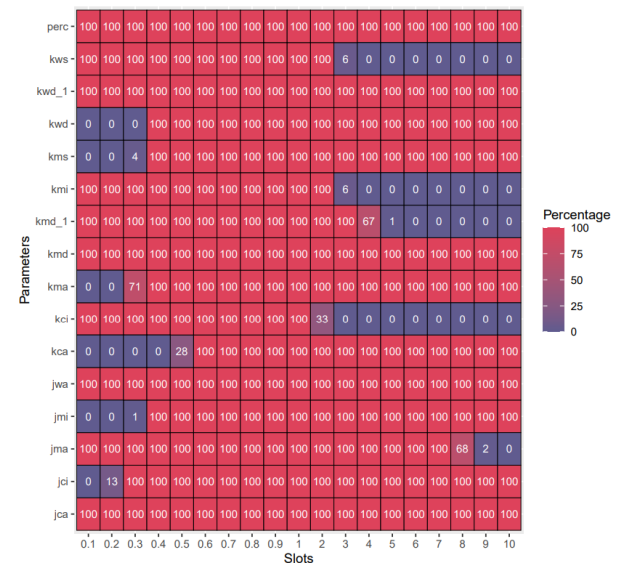


### $A_I$ parameters

(c)

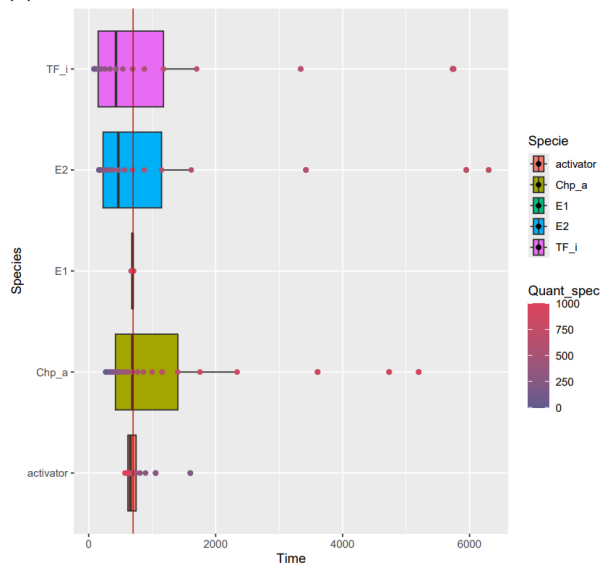


(d)

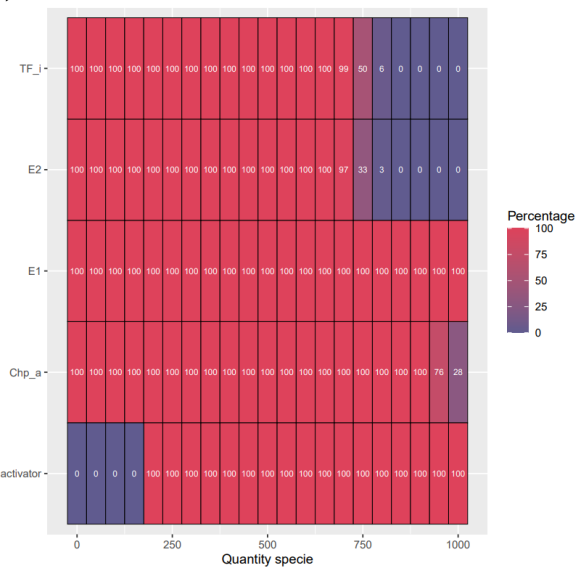


## A<sub>I</sub><sup>A</sup> paramters

(a)

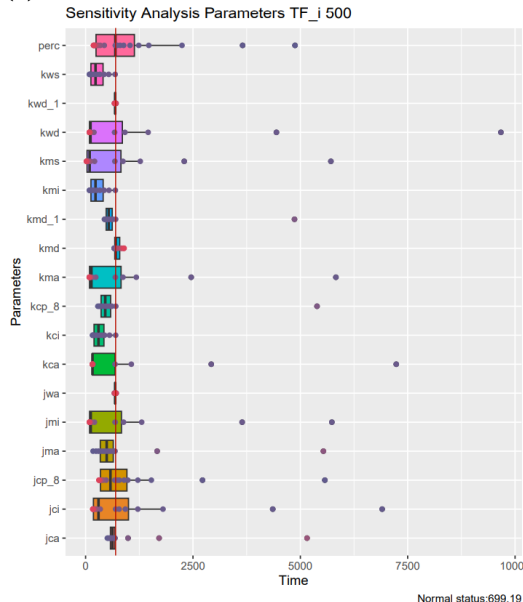


(b)

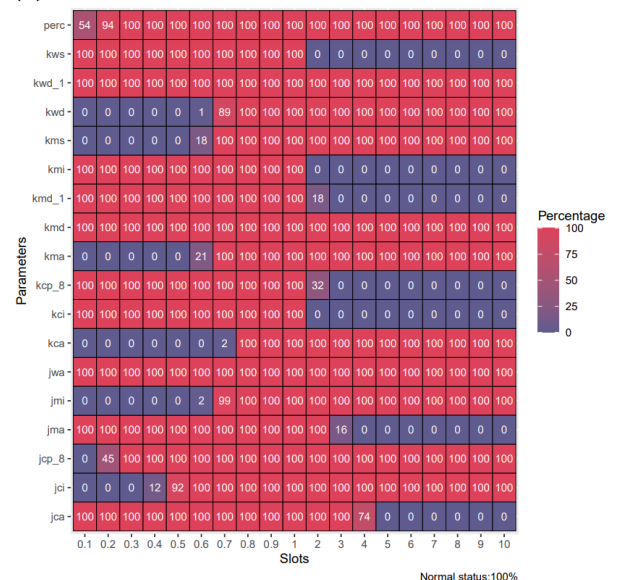


## A<sub>I</sub><sup>A</sup> paramters

(c)

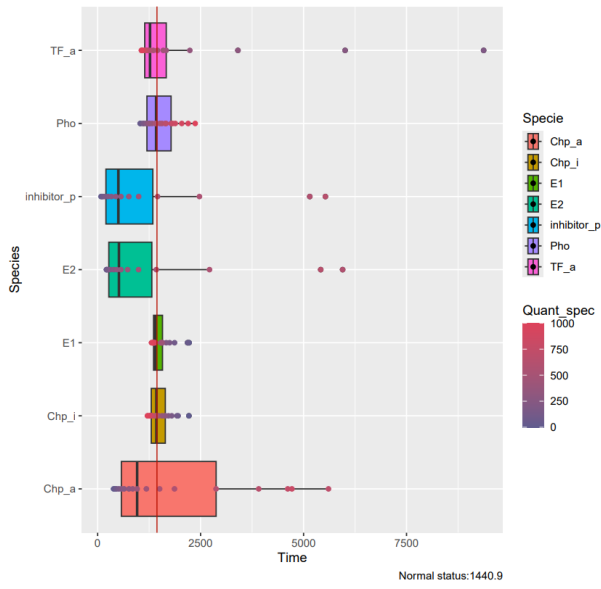


(d)

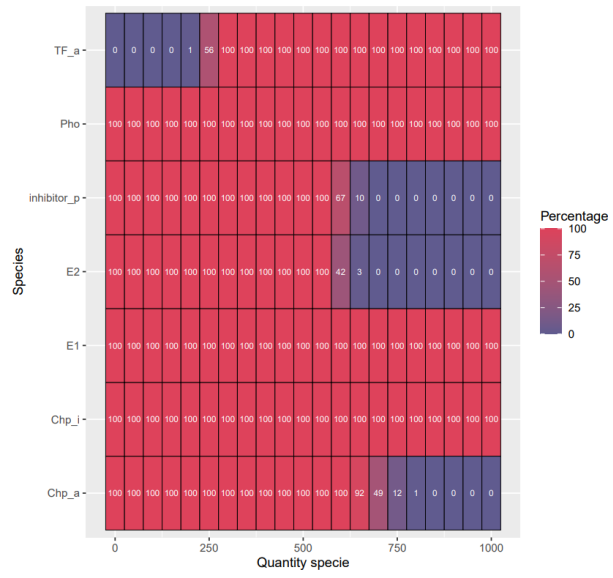


## $A_A^B$ species

(a)

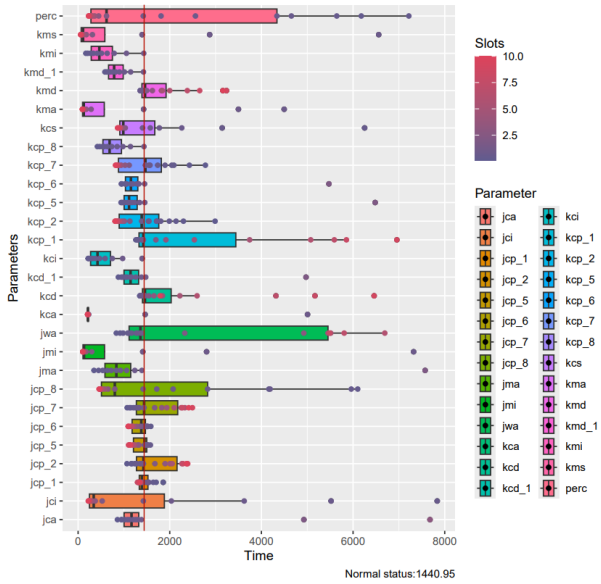


(b)

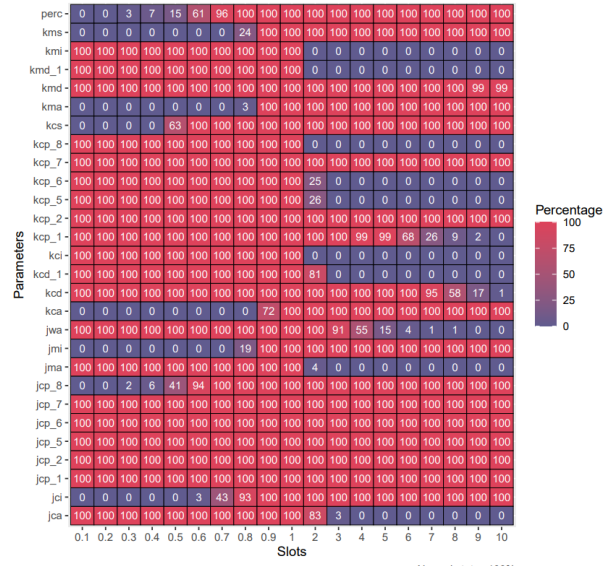


## $A_A^B$ parameters

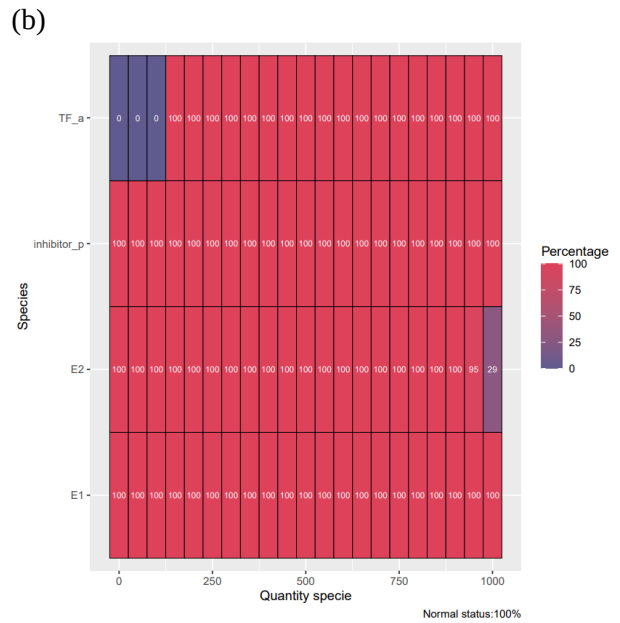
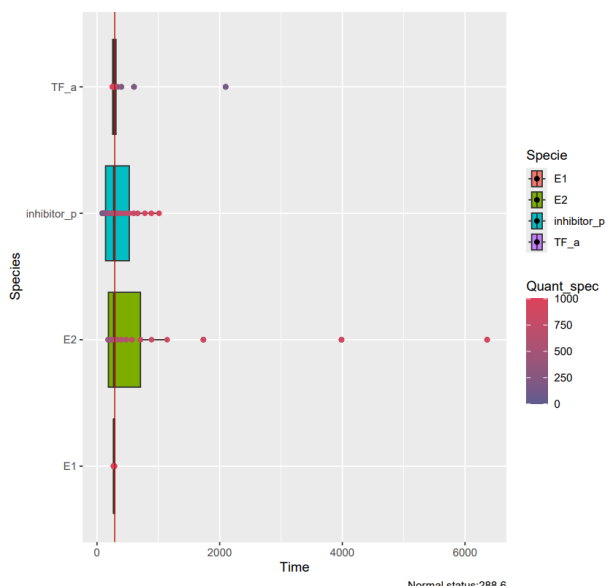
(c)



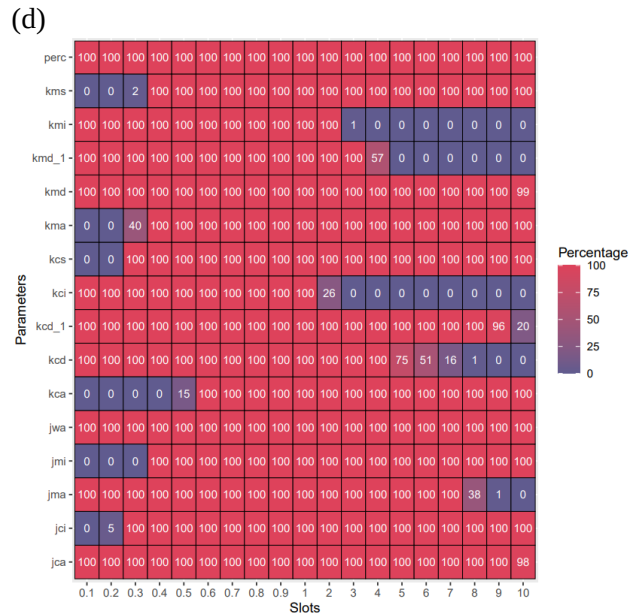
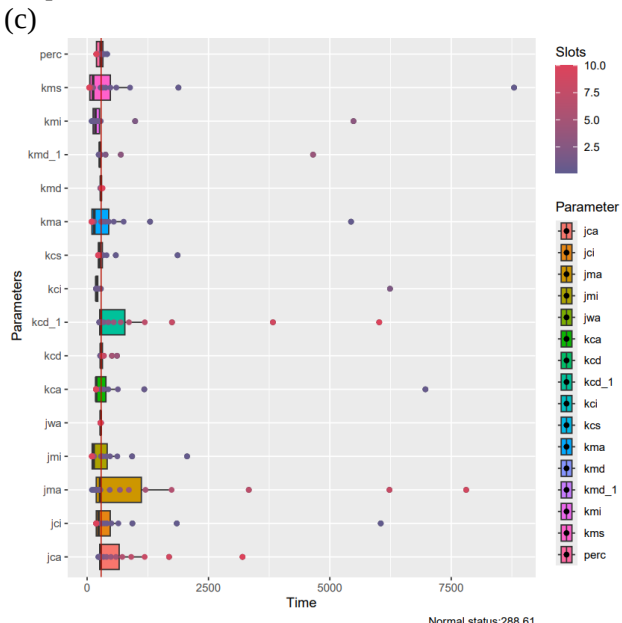
(d)



$A_A$  species  
(a)

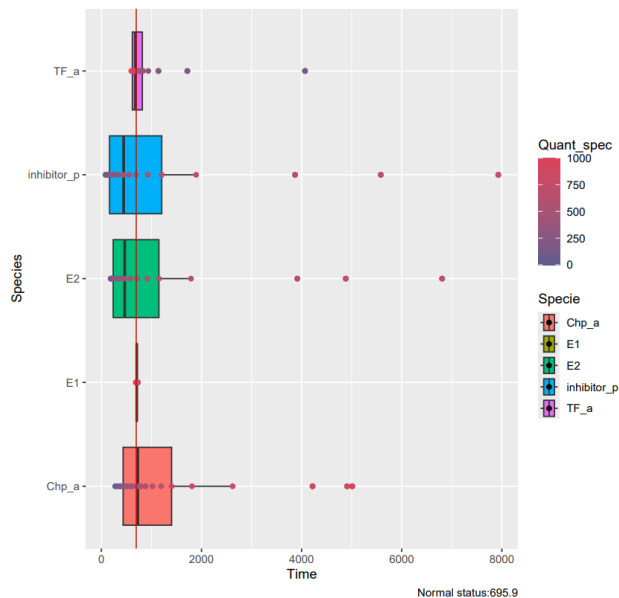


### $A_A$ parameters

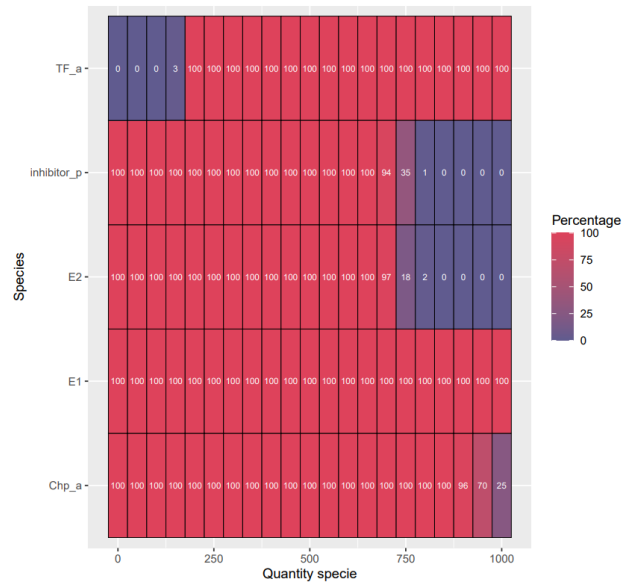


## $A_A^A$ species

(a)

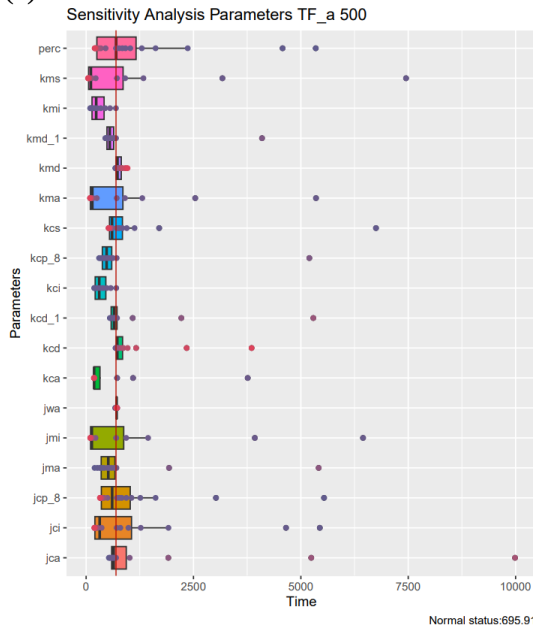


(b)

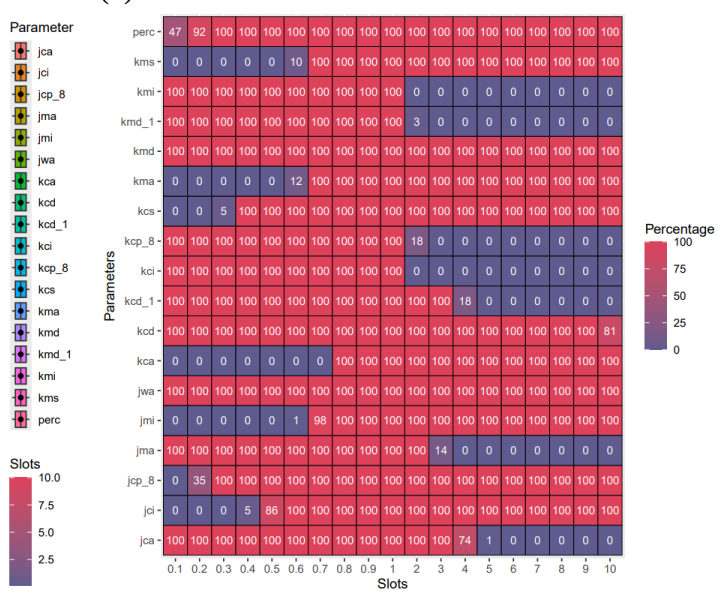


## $A_A^A$ parameters

(c)

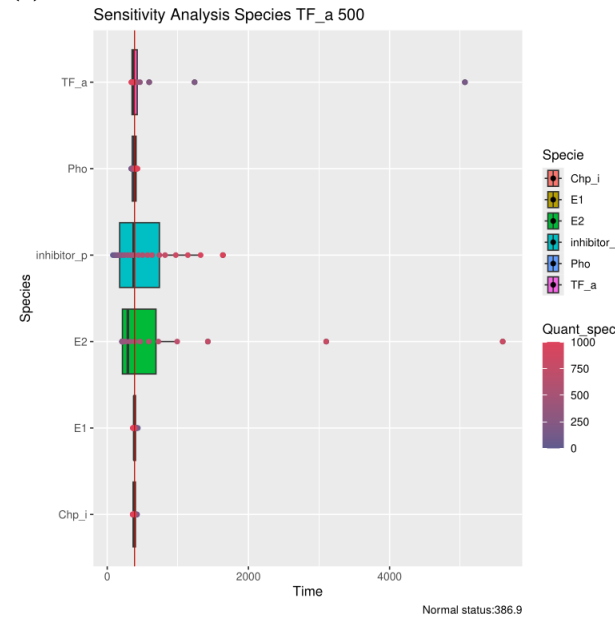


(d)

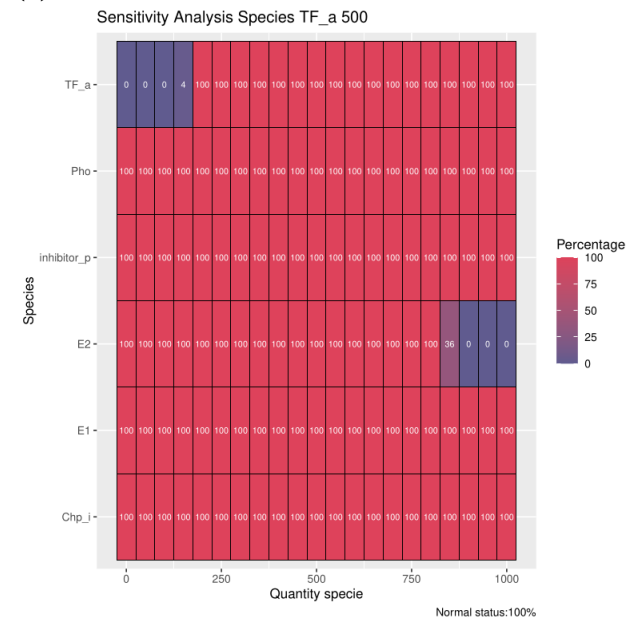


## $A_A^I$ species

(a)

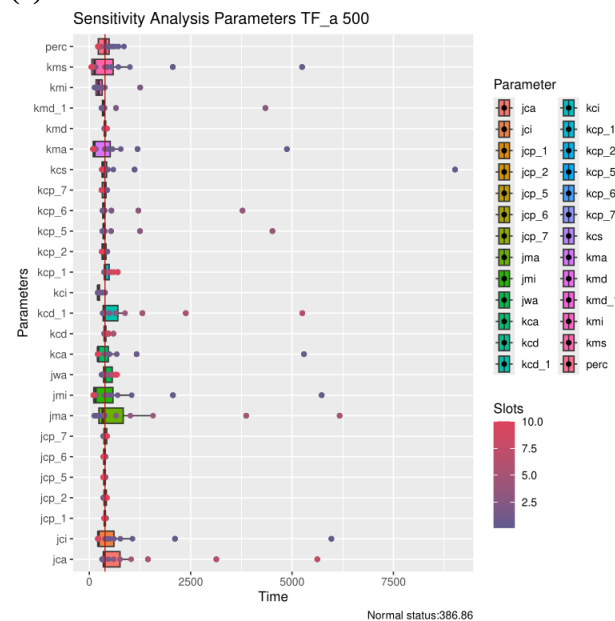


(b)



## $A_A^I$ parameters

(c)



(d)

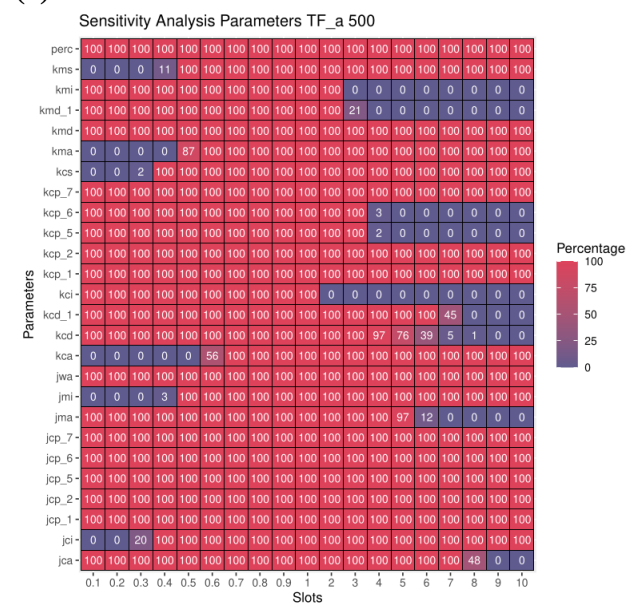
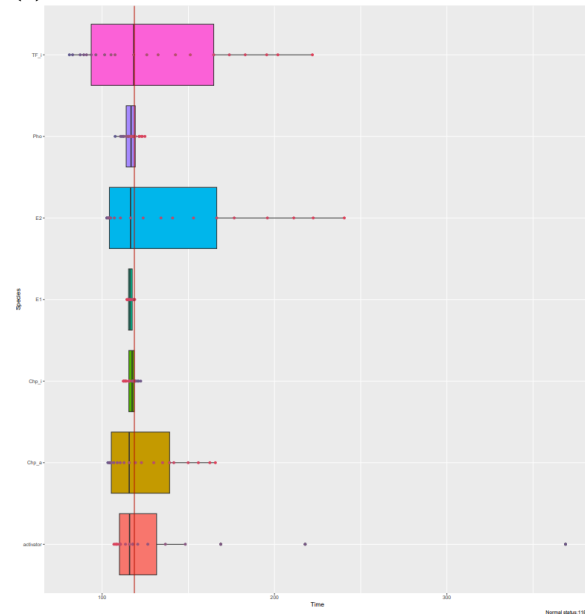


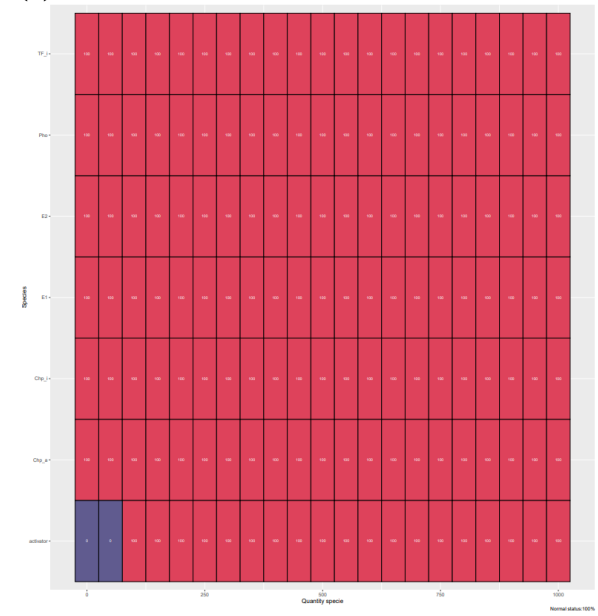
**Figure S24. Sensitivity analysis plots for the models with the positive feedback loop on both the activator and the inhibitor.** Panel (a) and (b) represent the sensitivity plot for the species while panels (c) and (d) represent the parameters' behaviour.

$B_I^B$  species

(a)

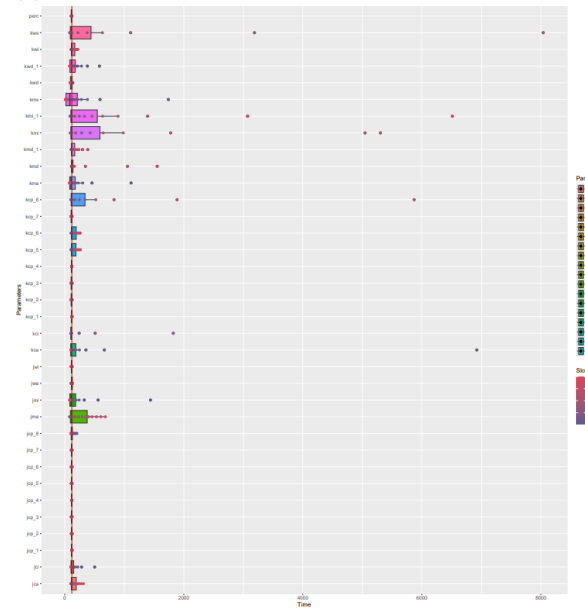


(b)



$B_I^B$  parameters

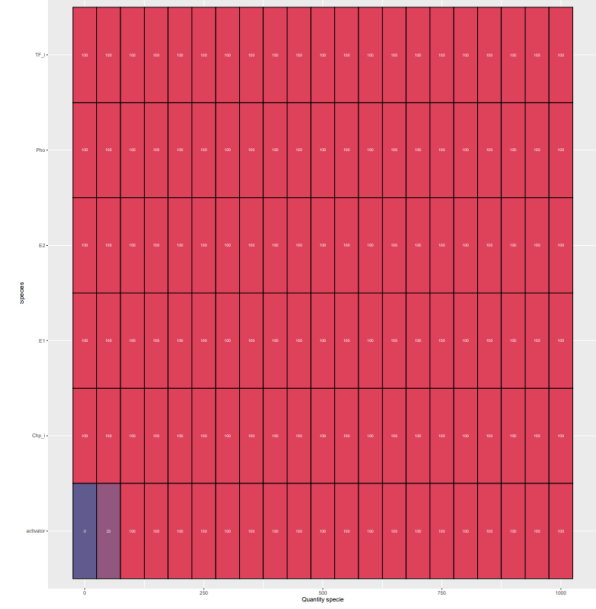
(c)



## $B_I$ species

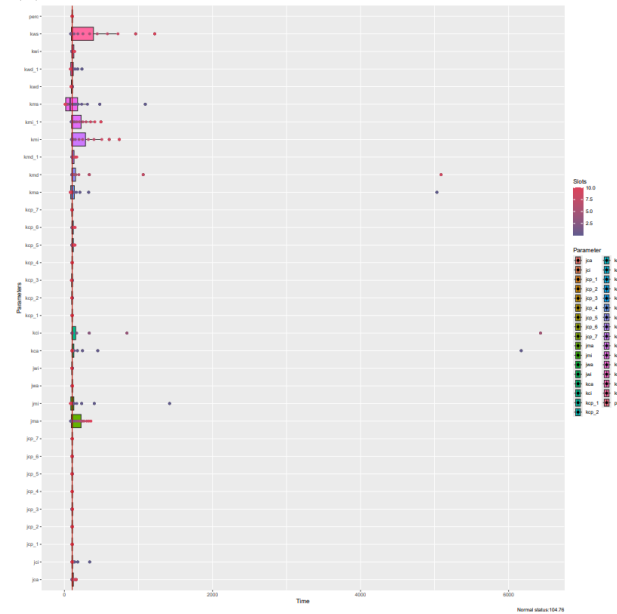
(a)

(b)

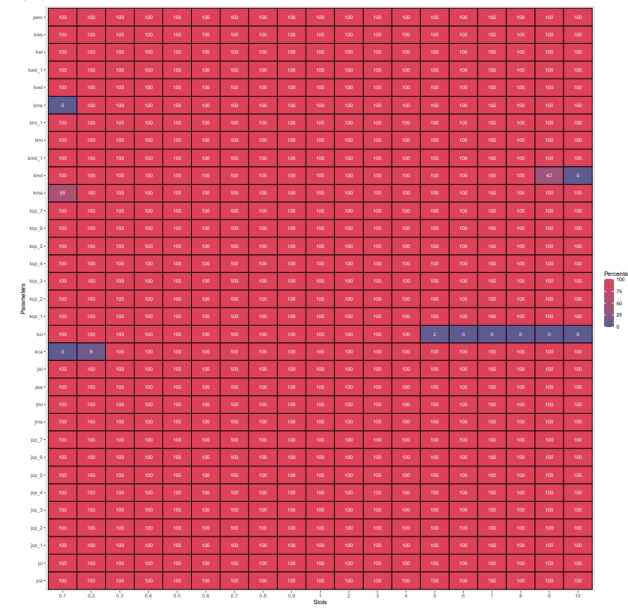


### B<sub>I</sub> parameters

(c)

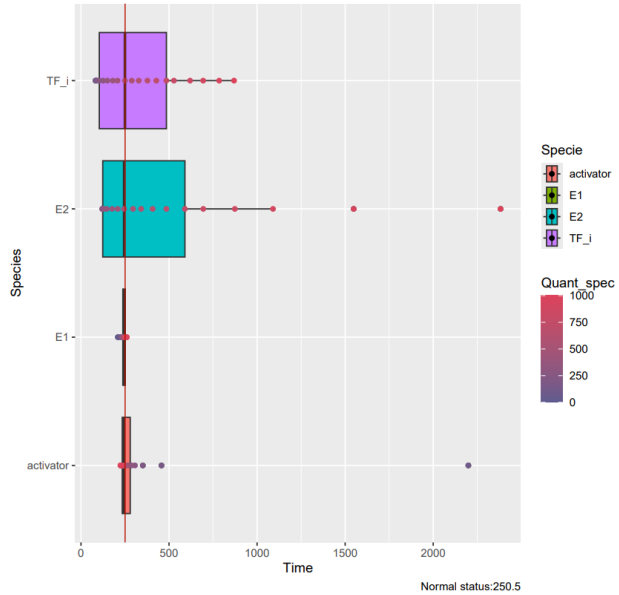


(d)

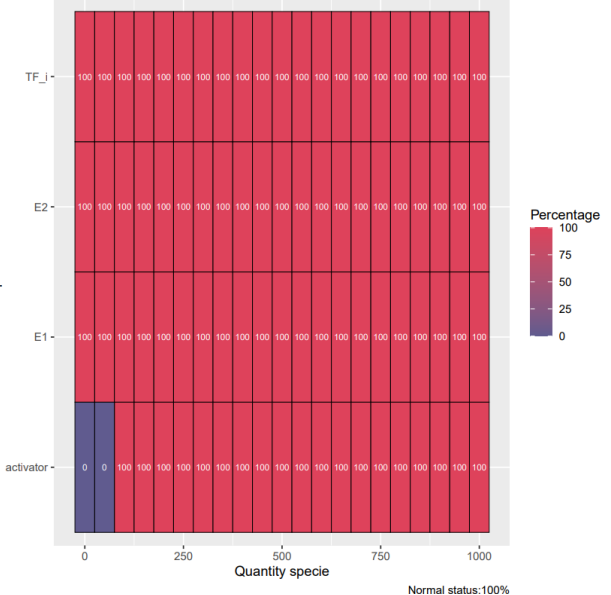


## B<sub>I</sub> Species

(a)

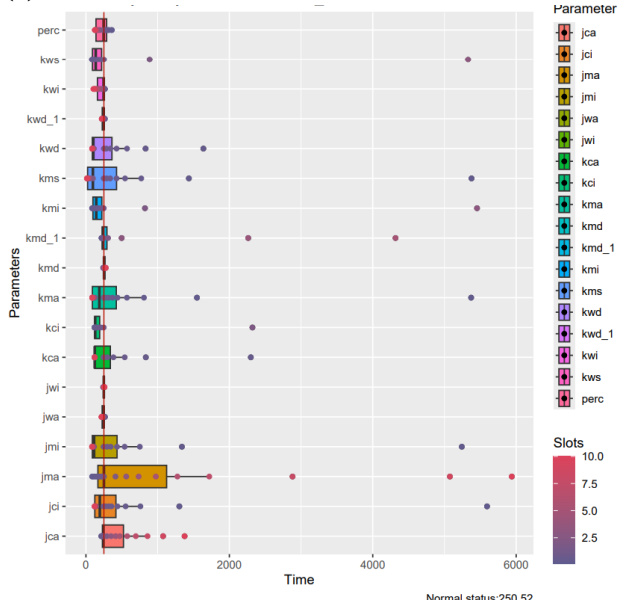


(b)

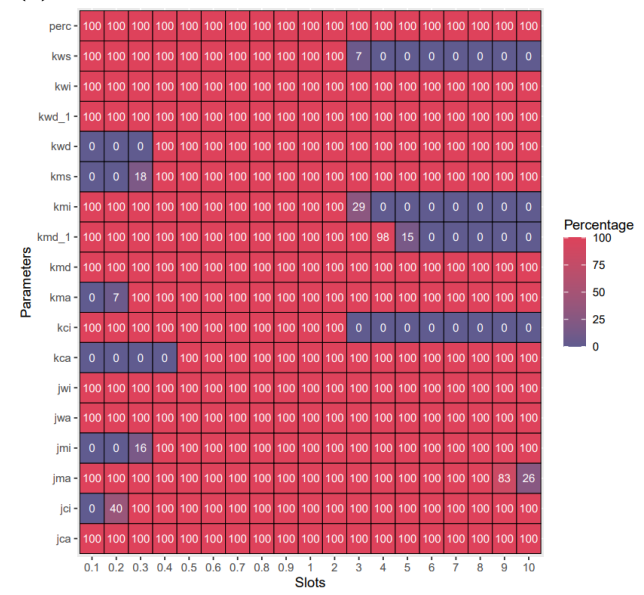


## B<sub>I</sub> Parameters

(c)

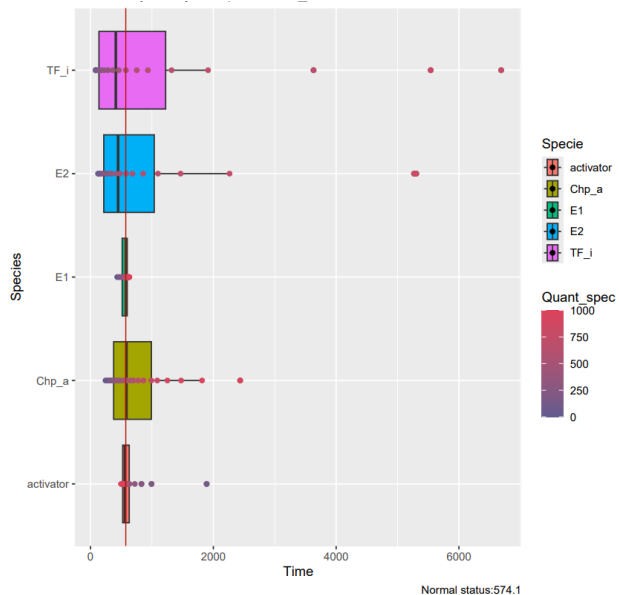


(d)

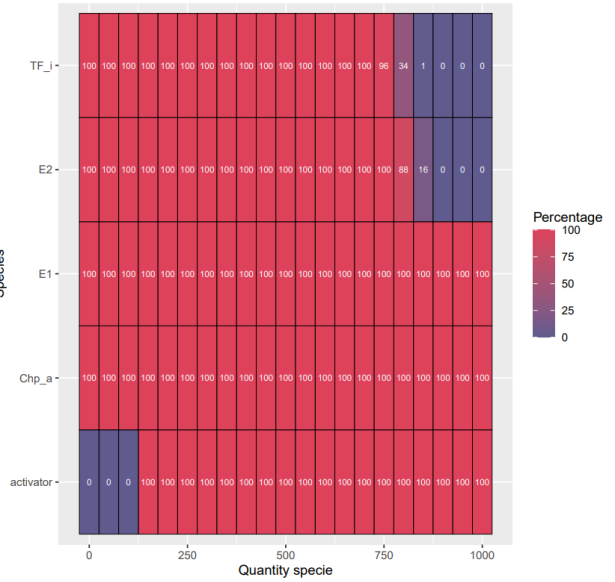


## B<sub>i</sub><sup>A</sup> Species

(a)

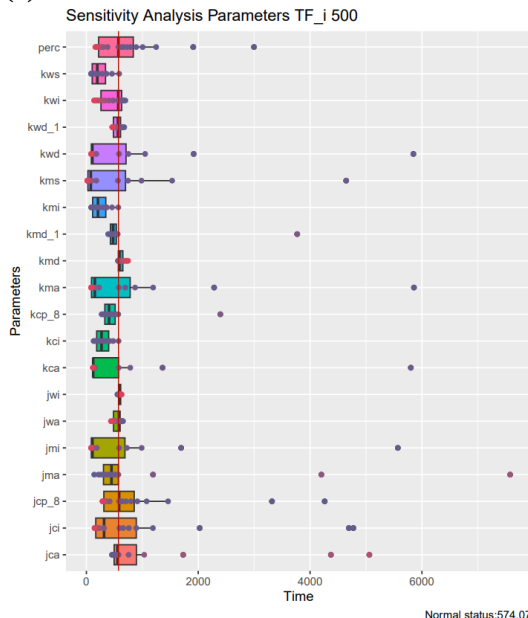


(b)

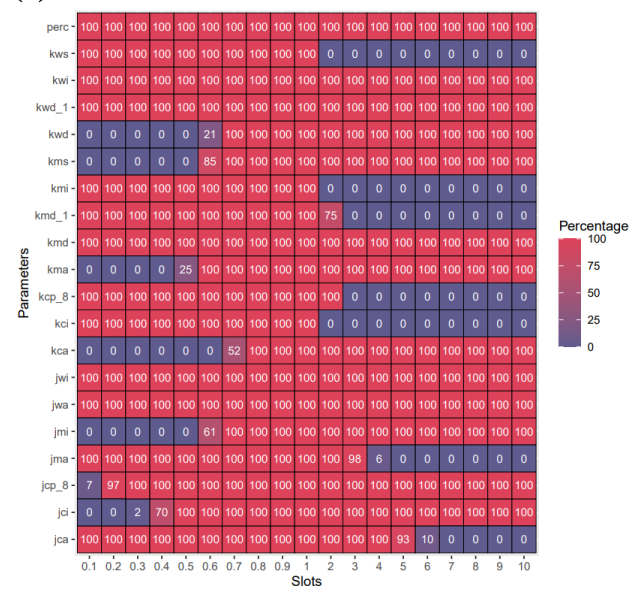


## B<sub>i</sub><sup>A</sup> Parameters

(c)

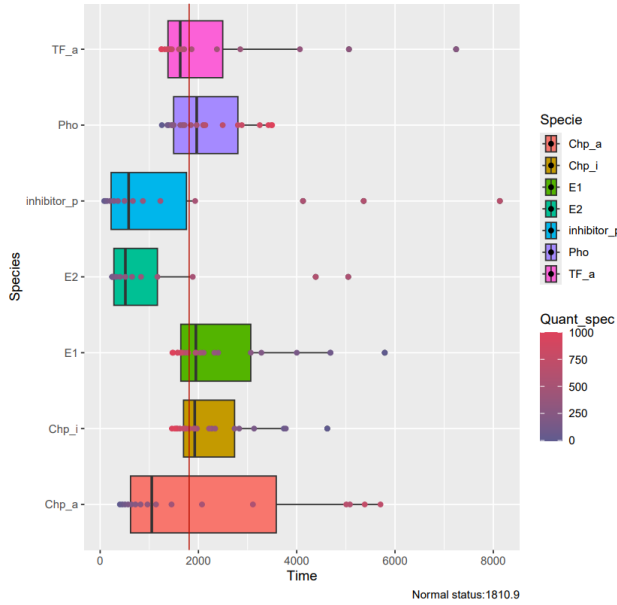


(d)

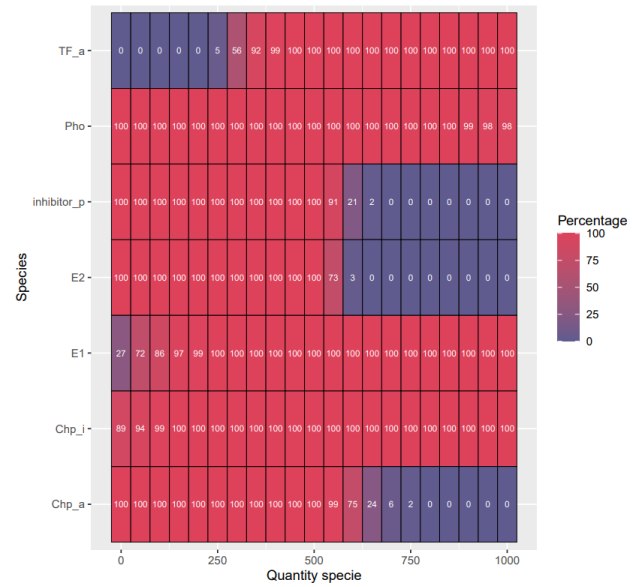


## $B_A^B$ Species

(a)

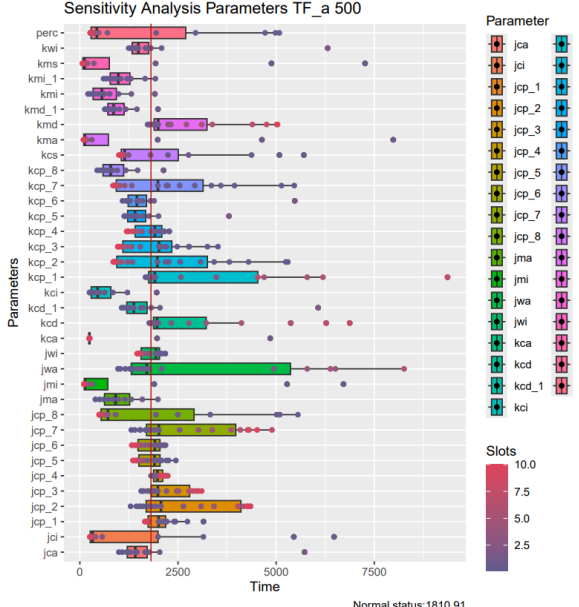


(b)

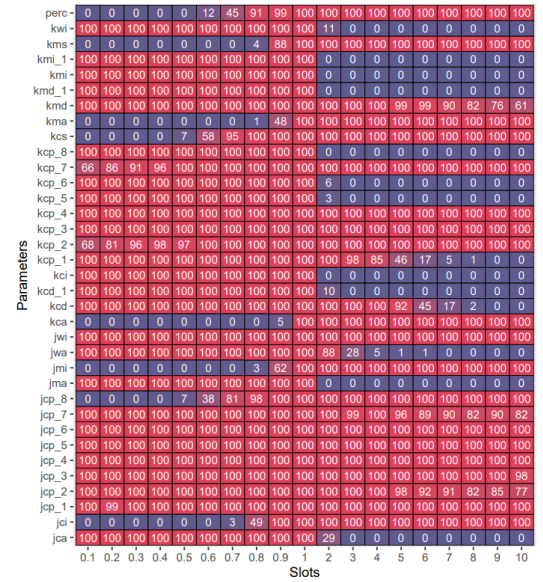


## B<sub>A</sub><sup>B</sup> Parameters

(c)

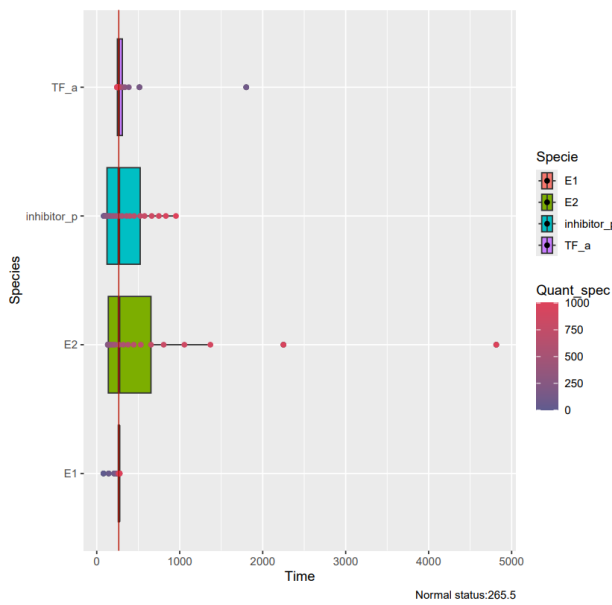


(d)

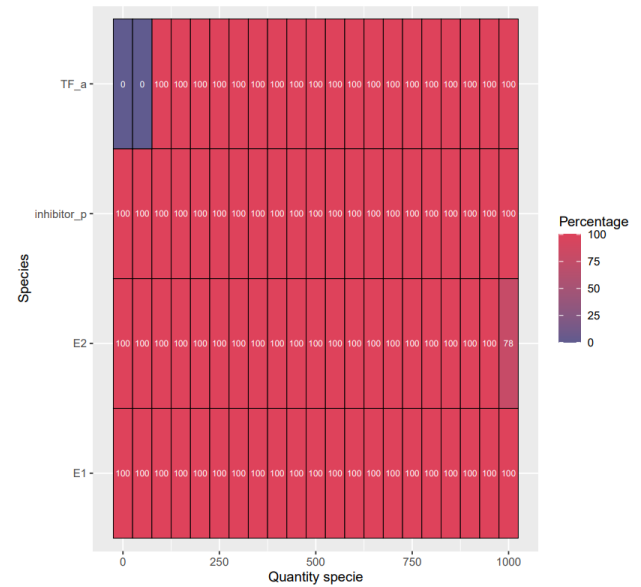


## B<sub>A</sub> Species

(a)

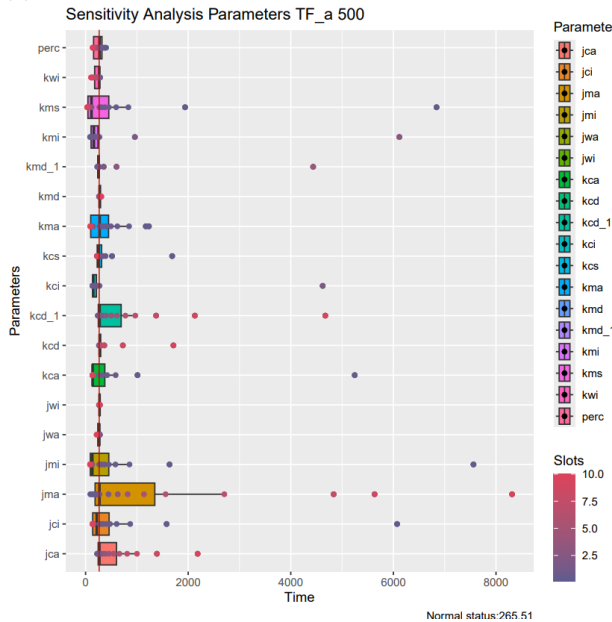


(b)

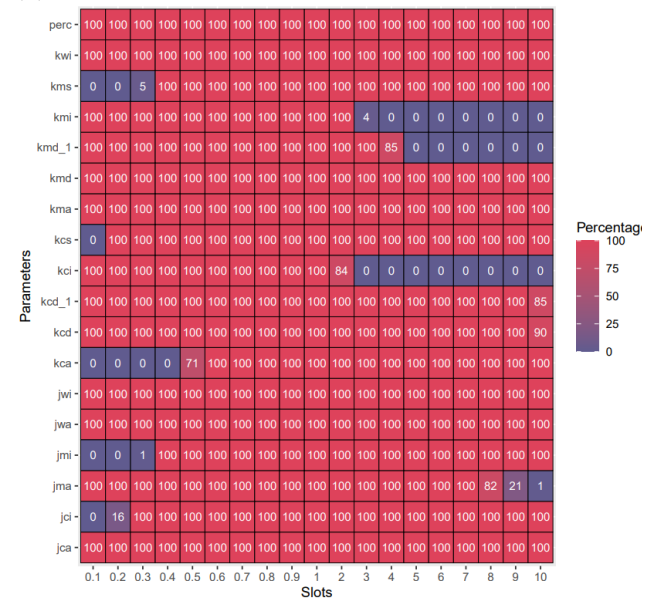


## B<sub>A</sub> Parameters

(c)

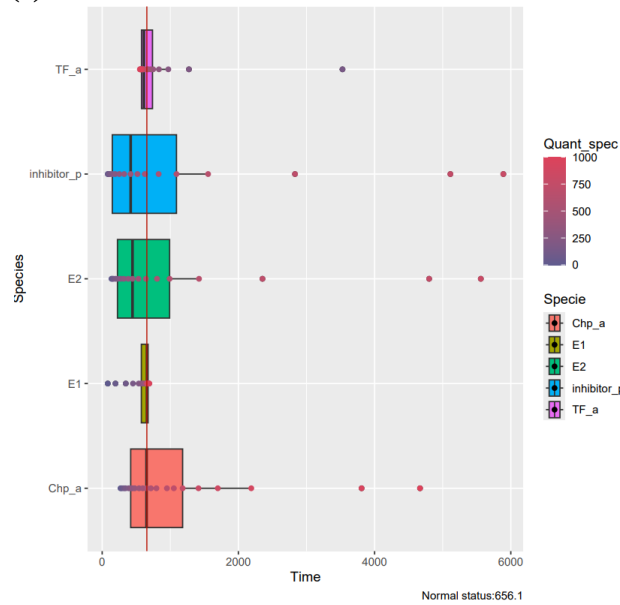


(d)

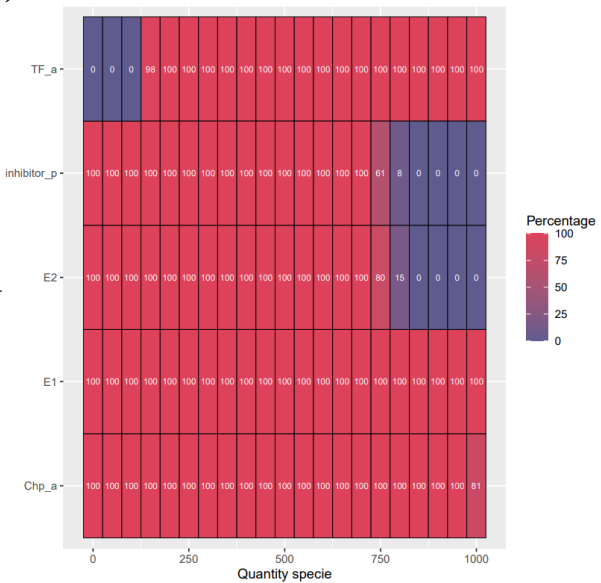


## B<sup>A</sup><sub>A</sub> Species

(a)

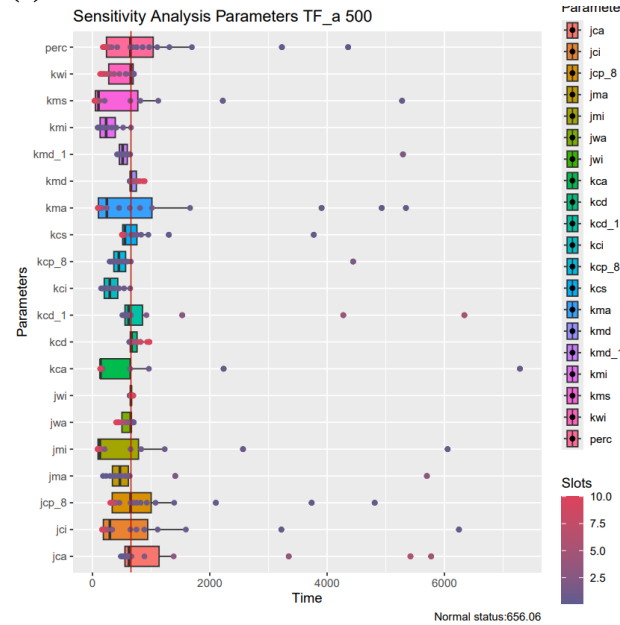


(b)

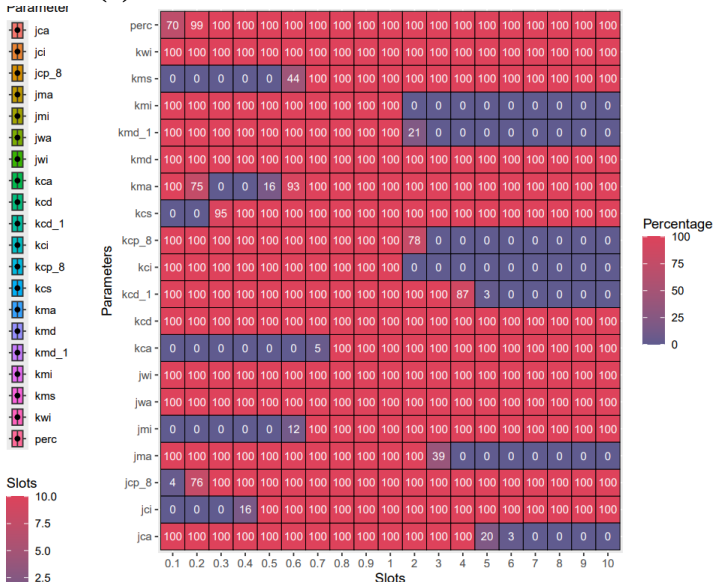


## B<sup>A</sup><sub>A</sub> Parameters

(c)

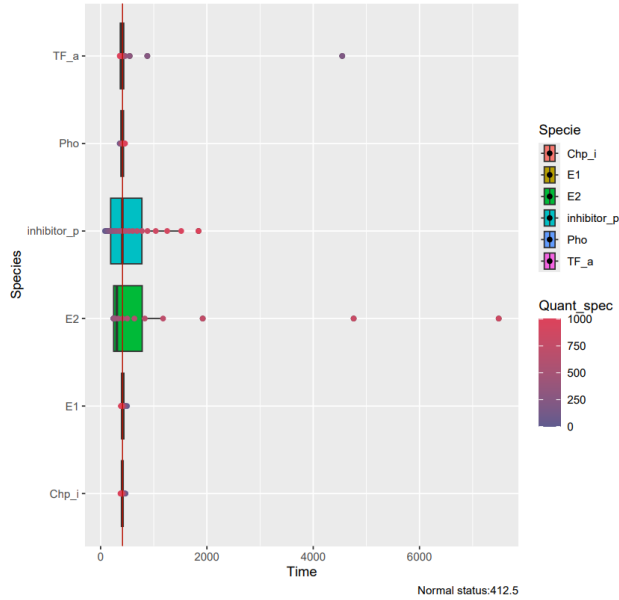


(d)

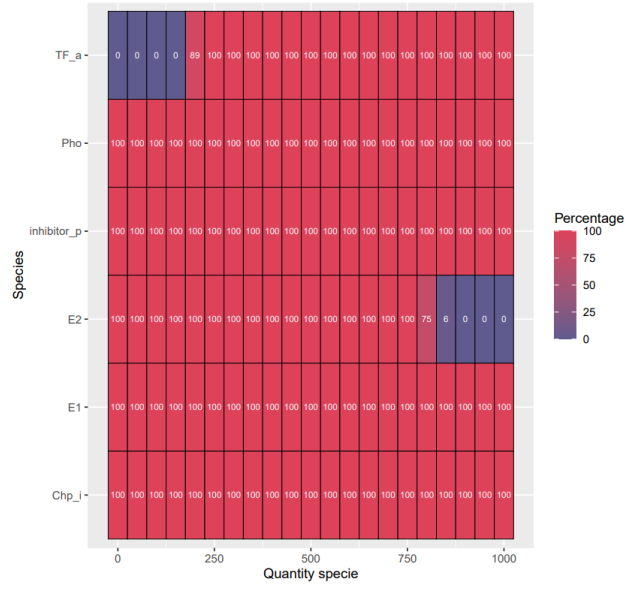


## B<sup>I</sup> A Species

(a)

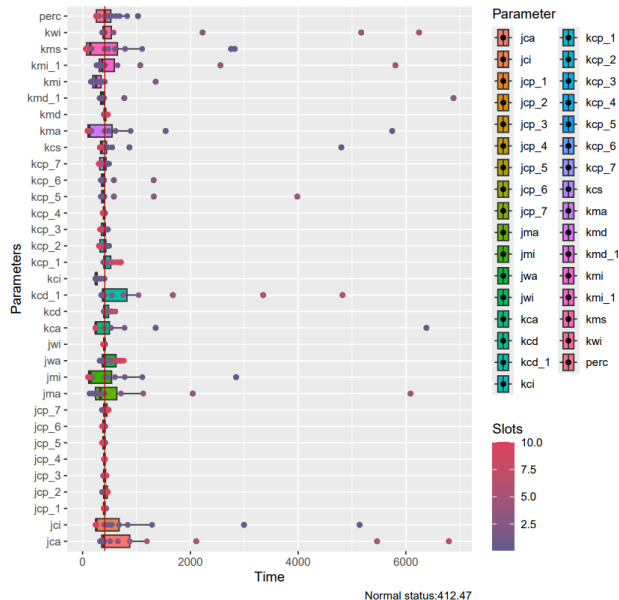


(b)

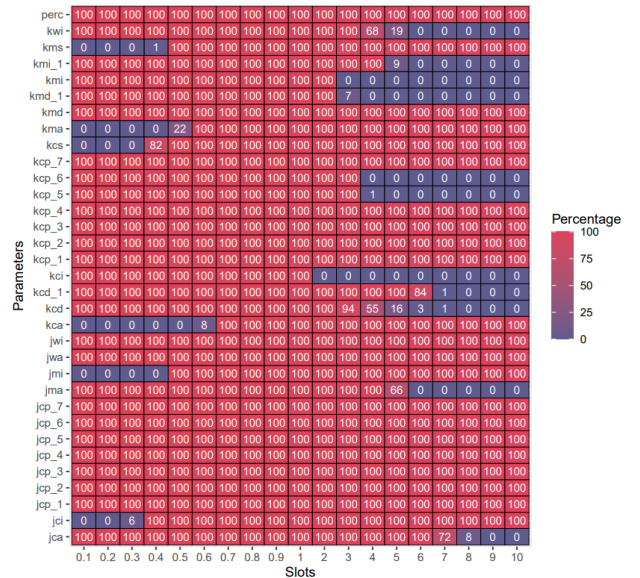


## B<sup>I</sup> A Parameters

(c)



(d)



# ***Ringraziamenti***

*Desidero ringraziare inazitutto il Professor Alessandro Romanel, relatore di questa tesi e mentore di questi due anni di magistrale. Sempre disponibile, coinvolto e attento a questo progetto oltre che sempre presente per dubbi e domande di varia natura.*

*Ringrazio i miei genitori, che nonstante non sappiano ancora precisamente in cosa mi laurei, sono sempre stati il sostegno piu' grande che ho avuto, lasciandomi compelta liberta' nelle mie scelte, supportando tutte le mie decisioni e avendomi dimostrato un amore incodizionato. Se sono la persona che sono oggi e' principalmente merito vostro.*

*Un grazie sincero a Mattia, Simone, Riccardo, Luca, Alessandro, Francesco, Massimiliano, Alberto, Valerio, Claudia, Sara, Silvia e Martino. Nonostante vi abbia incontrati in periodi diversi della mia vita, siete stati e sarete sempre parte imporanti di questa. Vi ringrazio sempre per il supporto che avete dimostrato e la vostra presenza incodizionata.*

*Ringrazio anche i miei zii Fabio e Carla, che anche se involontariamente sono stati parte integranti nella mia passione riguardante la scienza e la ricerca.*

*Ringrazio anche Andrea, Nicola e Chiara, amici e colleghi di questo percorso.*

*Infine un ringraziamento speciale va a Gloria, per avermi supportato e sopportato in questi due anni di alti e di bassi, per avermi spronato quando non ero sicuro di riuscire e avermi fatto entrare nel suo mondo. Ringrazio anche Paola e Andrea per avermi accolto nella vostra splendida famiglia.*